Aligned Carbon Nanotubes as Porous Materials for Selective Gas Adsorption

Dissertation

Mahshid Rahimi

Darmstadt, 2016 — D 17

TECHNISCHE
UNIVERSITÄT
DARMSTADT

Aligned Carbon Nanotubes as Porous Materials for Selective Gas Adsorption

Vom Fachbereich Chemie

der Technischen Universität Darmstadt

zur Erlangung des akademischen Grades eines

Doktor rerum naturalium (Dr. rer. nat.)

genehmigte

Dissertation

vorgelegt von:

Mahshid Rahimi, M.Sc. of Physics
aus Isfahan, Iran

Referent:	Prof. Dr. Florian Müller-Plathe
Korreferent:	Prof. Dr. Nico van Der Vegt
Tag der Einreichung:	19.10.2015
Tag der mündliche Prüfung:	18.01.2016

Darmstadt 2016

D 17

Zusammenfassung

Kohlendioxid und Schwefeldioxid sind als umweltschädliche Komponenten in Rauch und Abgasen enthalten. Daher ist das Auffinden neuer Lösungen für die Abscheidung und Speicherung dieser Stoffe von äußerster Wichtigkeit.

Wir haben groß-kanonische Monte Carlo Simulationen durchgeführt, um die Adsorption von Kohlendioxid und Schwefeldioxid in vertikalen Anordnungen von Kohlenstoffnanoröhrchen (CNT) verschiedener Rohrdurchmesser und unterschiedlicher Abstände zu verstehen. Solche Kohlenstoffnanoröhrchen sind seit kurzem experimentell verfügbar; sie sind nicht nur vielversprechend als Sorptionsmaterialien, sondern dienen auch wegen ihrer Reproduzierbarkeit und Regelmäßigkeit als ideale Modellsysteme für die Untersuchung der Gasadsorption in Materialien, die auf Kohlenstoff basieren.

Um die Sorptionskapazität des Materials zu optimieren, wurden die geometrischen Eigenschaften von CNT Systemen variiert. Wir untersuchten die Änderung der Adsorption, für positive und negativ Beladungen der Nanoröhren. Die is von Interesse, da elektisch kontaktisch Röhren ein mögliches Funktionsmaterial für elektrische Adsorptionsanlagegeräte sind.

Die Adsorptionsisothermen haben gezeigt, dass die entfernung zwischen den Röhren das Adsorptionsverhalten stärker beeinflußt, als ihr Durchmesser. Die höchste Adsorption für eine vorgegebene entfernung zwischen den CNT Molekulen hängt stark vom angewandten Druck ab. Für niedrigere Drücke zeigten die systeme mit kurzen CNT-Abständen eine hohe Adsorption. Wenn der Druck ansteigt, vergrößert sich auch der CNT-Abstand, der die Adsorption maximiert. Außerdem kann die Optimierung der CNT-Abstände die Adsorption bis zu ~40 % vergrößern. Dieser wert hängt aber sowohl von System und Druck ab. Dies ist in Übereinstimmung mit den Experimenten und zeigt die Wichtigkeit nur Optimierung der Geometrie.

Das Laden der Röhren mit 0,04 Elektronen pro Atom erhöht die Adsorption von Kohlendioxid bis p=1,88 bar bis zu 35% während die Zugabe der gleichen Menge an negativer Ladung die Adsorption verringert. Diese Zunahme / Abnahme ist durch die Wechselwirkungsenergie zwischen den Kohlendioxid-Molekulen und Nanoröhren bestimmt.

Das Trennverhalten binärer Mischungen in Kohlenstoffnanoröhren wurde mit gross-kanonischen Monte Carlo Simulationen untersucht. Die Ergebnisse zeigen, dass die Selektivität jedes Systems von der Entfernung der Nanoröhren und der Art der Adsorbatmoleküle abhängt. Die höchste Selektivität wird für die SO_2-N_2, *etc* Mischung beobachtet, gefolgt von der von CO_2-N_2 und schließlich von SO_2-CO_2. Außerdem ist die Selektivität für eine binere SO_2-CO_2 Mischung

nichtlinear von CNT-Abstand abhängig. Die höchste Selektivität über den gesamten untersuchten Druckbereich zeigen dicht gepackte CO_2-N_2 und SO_2-N_2 Nanoröhren.

Das Adsorptionsverhalten von SO_2-haltigen Materialien kann nicht durch eine Adsorptiontheorie für ideale Systeme vorhergesagt wurden. Die starke Wechselwirkung zwischen Schwefeldioxid und den Nanoröhren führt zu einer hohen Dichte und damit zu einem Verhalten des Gases, das zu weit vom Verhalten idealer Gase entfernt ist.

Die vorgestellten Simulationsergebnisse und ihre Übereinstimmung mit den experimentellen Befunden zeigen, dass gross-kanonische Monte-Carlo-Simulationen die Anzahl experimenteller für Studien reduzieren können. Weiterhin helfen die Ergebnisse, den Mechanismus und die molekularen Grundlagen der Adsorption und das Trennverhalten von Gasen auf Adsorptionsmitteln zu verstehen. Außerdem sind CNT-Verbindungen ein vielversprechendes Material für die Adsorption und Trennung von schädlichen Gasen, sie haben auch das Potenzial für eine elektrische Wechseladsorption, um sehr kleinen Geräten.

Abstract

Carbon dioxide and sulfur dioxide are environmentally noxious components of flue and exhaust gases. Hence, new solutions for carbon dioxide and sulfur dioxide sequestration and storage are highly important. We used grand-canonical Monte Carlo simulations to understand the adsorption of carbon dioxide and sulfur dioxide in bundles of regular parallel arrays of carbon nanotubes of different tube diameters and different intertube distances. Such carbon nanotube arrays have recently become available experimentally; they are not only promising as sorption materials but, because of their reproducibility and regularity, serve also as ideal model systems for the study of gas adsorption in carbon-based materials. The geometrical properties of the nanotube arrays were varied in order to optimize the sorption capacity of the material. We also investigated how the adsorption changes when the nanotube arrays are positively or negatively charged, as electrically contacted carbon nanotube arrays are a possible functional material for electric swing adsorption devices.

The adsorption isotherms showed that the intertube distance plays a more important role than the nanotube diameter. The highest adsorption among the intertube distance of carbon nanotubes depends strongly on applied pressure. For lower pressures, the lower intertube distances show higher adsorption. As the pressure increases, the intertube distance that maximizes the adsorption shifts to a higher value. Moreover, optimizing the intertube distance can increase the adsorption up to ~40 %, depending on the system and pressure. This is in agreement with experiments and shows the importance of the geometry optimization.

Charging the carbon nanotubes with +0.04 *e* per atom of carbon increases the adsorption of carbon dioxide by up to 35% at p=1.88 bar while adding the same amount of negative charge to the carbon nanotubes causes the adsorption to decrease. This increase/decrease is due to the change in the potential energy for the interaction between the individual carbon dioxide molecules and the nanotube.

The separation behavior of binary mixtures in carbon nanotubes is investigated using grand-canonical Monte Carlo simulations. The results show that the quantity and quality of the selectivity for each system depend on the intertube distance of nanotubes and the type of the adsorbate molecules. The main reason for having different selectivities is the difference between the strength of interactions between the nanotubes and the individual molecules of one gas compared to the other one. This difference is the highest for the SO_2-N_2 mixture, followed by CO_2-N_2 and finally SO_2-CO_2. Selectivity also follows the same order with SO_2-N_2 being the best in terms of selectivity. Furthermore, for a binary mixture of SO_2-CO_2, the selectivity towards sulfur dioxide is characterized as a nonlinear behavior as a function of intertube distance. On the other

hand for CO_2-N_2 and SO_2-N_2, the close-packed nanotubes show the highest selectivity over the entire pressure range studied. The ideal adsorbed solution theory cannot predict the adsorption of the systems containing sulfur dioxide. The strong interaction between sulfur dioxide and nanotube leads to a high density and causes the gas behavior to be far from ideal.

The presented simulation results and their agreement with experiments show that grand-canonical Monte Carlo simulation can be used as a pre-screening method for experiments. Furthermore, the results help to understand the mechanism and molecular origin of adsorption and separation behavior of gases on adsorbents. Moreover, they show the carbon nanotube arrays as a promising material for adsorption and separation of harmful gases and also as a potential technique for electrical swing adsorption that can be applied in very small adsorption/release devices and gas pumps.

Table of Contents

1 Introduction

From 2000 to 2010 emissions of greenhouse gases were the highest in history. Consumption of fossil fuels like coal, petroleum and natural gas contributes more than 80% of this drastic rise. The anthropogenic increase of greenhouse gases is blamed as the main reason for the changes in the climate system such as the temperature increment of atmosphere and oceans, reduction of snow and ice and rise of sea level. Carbon-dioxide (CO_2) emission is reported to be in charge of 78% increase of greenhouse gases in the atmosphere. Beside the greenhouse gases, combustion of fossil fuels emits some other harmful gases, among them sulfur-dioxide (SO_2) contributes significantly in air pollution. There is an urgent need for strategies to reduce the global atmospheric concentrations of SO_2 and CO_2. Among many options which are being considered, adsorption and separation is the central strategy.[1–4]

1.1 Adsorption and Adsorbents

Adsorption is the binding of molecules of a gas or liquid to a solid surface, which leads to an increase in the density of fluid in the interface. Porous solid materials are the heart of an adsorption process because of their high surface area or high micro-pore volume. The adsorption ability of porous materials for adsorption have been known since the eighteenth century. However, the practical application of them is a more recent development. Besides its high surface area or micro-pore volume, a porous material with a high adsorption capacity, should have relatively large pore network; it is necessary for the transport of molecules from its surface to its interior. The majority of the materials, which are commonly used in the gas adsorption, satisfy these two criteria. Some of the important adsorbents are: zeolites, metal organic frameworks (MOFs), activated carbon, and carbon nanotubes (CNTs).

Zeolites, commonly used as a commercial adsorbent,[5] are one of the most reported adsorbents in the patent and literature.[6] Because of their micro porous structure with a uniform pore dimension,[7] zeolites have been reported to provide high CO_2 adsorption capacity.[8] However, they are typically used at high pressure. Moreover, the presence of water in the gas reduces considerably their adsorption capacity.[9,10]

Due to their geometrically and crystallographically well-defined framework structures, MOFs are an important class of adsorbents.[11] The structure and properties of MOFs can be well-designed and systematically tuned. The high surface area to weight ratio of MOFs, is another crucial property contributing to their high gas adsorptivity.[12] Adjustable pore sizes, large surface areas, and controllable surface properties pose MOFs as promising adsorbents for gas storage

and separation.[13,14] However, MOFs exhibit a high sensitivity to chemical degradation in the presence of air and water, and thus, limiting their practical application.[4]

Since their discovery in 1991 by Iijima,[15] CNTs have been in the centre of attention due to their unique structure, extraordinary mechanical, electrical and thermal properties.[16] In 1997, Dillon and coworkers[17] showed for the first time that hydrogen can be condensed to high density inside narrow single-walled carbon nanotubes (SWCNTs). Therefore they suggested CNTs as a potential medium for gas storage with high density. Since then, CNTs are identified as promising carbon-based adsorbents because of their hollow cylindrical geometry, light mass density, large specific area and well-defined adsorption sites.[16,18–20] Carbon nanotubes are widely used for storing various gases such as H_2, N_2, CO_2, SO_2, alkanes and noble gases.[21,22]

Many comparative studies of CNTs with other gas adsorbents has shown that CNTs have a better performance including gas adsorption and selectivity. An experimental study showed that purified SWCNT can adsorb almost twice the volume of CO_2 compared to activated carbon.[23] Lu *et al.*[24] performed a comparative experimental study of CO_2 storage in granular activated carbon, zeolites and CNTs. The surface of these adsorbents was modified by the 3-aminopropyl-triethoxysilane. Under the same conditions, CNTs show the highest CO_2 adsorption capacity, followed by zeolites and then granular activated carbon. Furthermore, the CNT adsorption capacity in this work is higher than that of many carbon and silica adsorbents. The diffusivities of light gases (H_2 and CH_4) in carbon nanotubes and two zeolites with comparable pore sizes were studied by molecular dynamic simulation.[25] The diffusivity in carbon nanotubes was found to be orders of magnitude faster than the diffusivity in zeolites. A grand-canonical Monte Carlo (GCMC) study for the adsorption behavior of equimolar CO_2 and CH_4 mixture in CNTs, showed that CNTs demonstrate higher selectivity for CO_2 than those reported in the literature for activated carbons, zeolites and MOFs.[26]

1.2 Optimization of Pore Size of CNTs

The unique structure of CNT is one of the main reasons for its high gas uptake. Hence, it is expected that the geometrical properties of the CNTs like chirality, tube diameter and intertube distance play important roles in their adsorption capacity. These properties have been the subject of many works.[27–30] As was shown by several molecular simulations, chirality is not an essential factor on adsorption.[27–29]

The studies on tube diameter optimization do not give a straightforward result. Liu *et al.* used GCMC simulations to study CO_2 adsorption on SWCNTs with two different diameters, 1.36 and 2.03 nm, at 300 K. They found that the SWCNTs with larger diameter can have higher adsorption

capacity. The same method was used to investigate the adsorption of different gases ($CO_2/CH_4/N_2/H_2/CO$) on hexagonally ordered carbon nanopipes at 298 K.[30] The results showed that increasing pore diameter from 3 to 6 nm, enhances pure gases adsorption, especially for CO_2. Many other works also confirm that increasing the tube diameter leads to higher adsorption. On the other hand, Kowalczyk *et al.*[29] used the GCMC technique to find an optimal SWCNT for CO_2 adsorption at 298K. They used SWCNTs of diameters varying from 0.93 nm to 14 nm and different chirality. They reported that there is an obvious dependence between CO_2 storage and the tube diameter. It was concluded that the optimum pore size depends on the operating storage pressure. For instance, the optimal diameter for maximum adsorption capacity at 1.5 MPa is 3.8 nm. Nevertheless, at a pressure of 3.5 MPa, a nanotube with higher diameter (4.8 nm) maximizes the CO_2 storage. Despite these results, a recent experimental work[31] investigated CO_2 and N_2 adsorption in parallel-aligned arrays of double-walled carbon nanotubes (DWCNTs); their inner diameters were 5 nm and 8 nm. It was found that gas adsorption in DWCNT bundles increases with decreasing CNT diameter.

There is an uncertainty about the most efficient nanotube diameter which maximizes adsorption. Some authors claimed that gas adsorption could increase with nanotube diameter, while some others showed the opposite. Unlike these two groups, a third group argued that the optimal CNT radius for maximum adsorption would depend on the external pressure. This uncertainty might be due to the fact that in some works only a limited number of nanotube diameters or pressure values had been considered. A systematic study using different diameter and pressure is required to validate one of the former results.

Carbon nanotubes are usually found as bundles or complicated aggregates because of the strong attractive van der Waals forces between the carbon atoms of neighboring nanotubes.[32,33] Bundles of CNTs show higher adsorption than disordered ones due to the well-defined inner and outer adsorption sites in such geometry.[34,35] Water assisted chemical vapor deposition method was used in several experimental works to synthesize aligned CNT arrays.[36,37]

Bundles of CNT form new possible sorption sites (figure 1), namely: inner (the volume within the tubes), grooves (where the two CNTs are in touch) and interstitial (the region surrounded by three CNT and three grooves). The new adsorption sites lead to higher adsorptive capacity in CNT bundles. As was founded in a density functional theory (DFT) work, the interstitials and grooves of SWCNT bundles exhibit a higher adsorption capacity than the individual nanotubes.

To study the adsorption locally, Bienfait *et al.*[38] used adsorption isotherms, isosteric heat of adsorption, and neutron diffraction measurements of hydrogen, methane, argon, oxygen on SWCNTs bundles. They showed that gas condensation happened first on grooves as well as

interstitial, and subsequently on the outer surface of the bundles. A combined study of molecular simulation and Raman spectroscopy investigated the contributions of different regions.[39] It was found that the groove regions play an important role on adsorption at low pressure until they were saturated. Another molecular study also showed that the adsorption energy in the grooves is the highest followed by that in the inner and finally in the outer surface.[40]

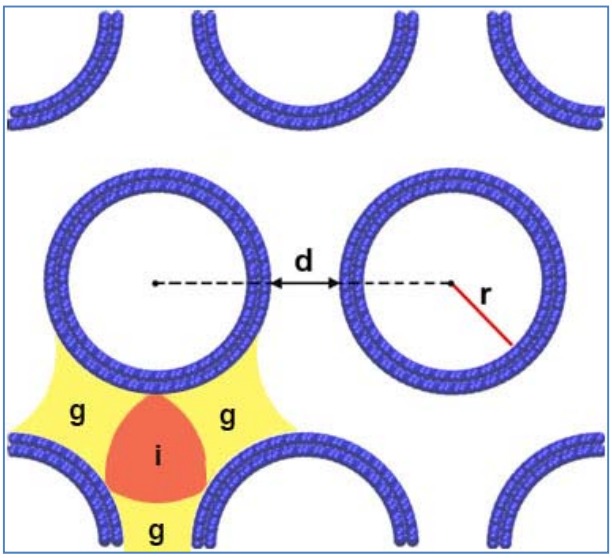

Figure 1: Schematic arrangement of double walled carbon nanotubes as used in this work, with internal radius *r* and intertube(surface-to-surface) distance *d*. Interstitial and groove regions are represented by symbol *i* and *g*, respectively.

Although the intertube distance is tunable,[41] and many works confirmed that the interstitial regions and grooves are important adsorption sites,[42–45] not much is known about the optimal intertube distance for the highest adsorption capacity of CNT bundles. In the former studies, the intertube distance has been always fixed such that the CNTs are in touch. Furthermore, for a fixed intertube distance, the curvature of the CNT as well as the intertube space volume change with changing the diameter. Thus, the optimal intertube distance might not be unique for different diameters and would depend on the diameter size.

1.3 Adsorption Behavior of Non-Pristine CNTs

Pure CNTs are not the only promising materials for gas adsorption since functionalization can alter the charge distribution of CNTs[46,47] leading to a better adsorption. Functionalization can be achieved by different experimental methods such as oxidative damage by strong acids[48,49] and plasma treatments.[50,51] Babu *et al.*[31] used oxygen plasma treating to graft C–O functional groups onto the CNT surface. They found out that at low pressure regimes, plasma functionalized

carbon nanotubes exhibit better adsorption characteristics. Another experimental work demonstrated that amine-functionalized multi-walled CNTs have higher adsorption capacity for the CO_2 capture.[52]

Enhancement of adsorption can be achieved not only by functionalization, but also by doping the CNT surface with metal atoms. The improvement of adsorption properties is caused by changes of the charge distribution of CNTs.[53] The viability of metal doping of CNTs has been demonstrated experimentaly.[54,55] Chen *et al.*[56] measured hydrogen adsorption on lithium- and potassium-doped carbon nanotubes for the first time. They reported that Li- and K-doped CNTs could obtain a hydrogen storage of 20 weight% and 14 weight% at 473–673K and at room temperature, respectively. These values are much higher than hydrogen storage capacities in pure CNT which is only 0.4 weight% under similar conditions. Similar trend was reported by some later studies.[57,58] The enhancement of hydrogen adsorption on Li-doped CNTs was investigated theoretically using density functional theory (DFT).[59] The most stable configuration for a lithium impurity was found to be on the center of a hexagon between three different sites: on top of a carbon, on top of a C-C bond, on top of the centre of hexagonal ring. This result was found in similar works for nanotube and graphene.[60–62] Moreover, it was concluded that the charge density of the CNT wall near the Li impurity increases due to the charge transfer from the Li to the surface. Therefore, the adsorption energy of a Li doped CNT is twice more than that of pure nanotube.

An alternative way to perturb charge distribution of CNT is to replace one of the carbons of CNT with another atom (called doping proper).[63] Experiments have shown the possibility of chemical doping of CNTs.[64] Paura *et al.*[65] studied the electronic structure of the CO_2 molecule interacting with pristine and cobalt-doped SWCNTs with several diameters and chiralities. For pristine SWCNTs, they pointed out that the binding energy was almost the same in all cases, independent of the diameter and chirality. Unlike pristine SWCNTs, the binding energy depends on the chirality and the diameter of a cobalt-doped SWCNTs. The binding energy of zigzag chirality is higher than that of armchair chirality. For armchair chirality, a direct relationship and for zigzag chirality an inverse relationship between the binding energy and the diameter of tubes is observed. Moreover, cobalt-doped SWNTs shows a greater binding energy relative to pristine ones.

Increasing or decreasing adsorption in CNTs upon functionalization and doping suggests that the charge distribution has a key role on adsorption. Beside, graphitic or CNT-based materials are electrically conductive and can be charged and discharged easily.[66] Consequently, Electric Swing Adsorption (ESA) has been suggested as a promising method for gas storage in carbon-

base sorbents.[67,68] This technology can cause rapid adsorption and desorption of $CO_2$by applying and removing electrical charges on the sorbent. It has been shown that femtosecond laser pulses can be used for charging the surface of dielectrics, semiconductors and metals.[69] Using charge injection and electric force microscopy (EFM) experiments, Zdrojek and coworkers[70] studied electrostatic properties of individually separated SWCNTs, DWCNTs, and multi-walled CNTs. They observed charge patterns along the CNTs and concluded that they caused by the charge storage in the CNT and in the oxide layers along the CNT. Other researchers suggested that the procedure for having charged CNT is mounting the CNT array electrically insulated from the container, so the container walls can be the oppositely charged plate of a capacitor. A DFT calculation[71] explained electronic structures of charged single-walled CNTs in detail. Simonyon and coworkers[72] used GCMC to explore the adsorption of molecular hydrogen gas on charged SWCNTs. They found that charging a SWCNT (0.1 *e* per carbon) increases adsorption by ~10%–20% and 15%–30% for T=298 K and 77 K, respectively, relative to the uncharged tubes. Additionally at 77K, the negatively charged nanotubes show higher adsorption than positively charged tubes because the quadrupole moment of hydrogen is positive, nevertheless at 298K, there is no difference between these two cases. The adsorption of CO_2 exhibits a stronger dependence on extra charge in CNTs because of the higher quadrupole moment of a CO_2 molecule. However, CO_2 adsorption in charged CNTs has not been investigated in the earlier studies. Understanding the mechanism of CO_2 adsorption on charged and uncharged CNTs can contribute to the discussion as to whether gas adsorption and desorption could technically be driven by charging and discharging the CNT array.

1.4 Multi-Component Adsorption and Separation

In most practical applications, we deal with a mixture of different gases adsorbing on CNT. Therefore, it is not adequate to focus solely on single-component adsorption. A GCMC study[73] focused on the adsorption of CO_2/CH_4 mixtures in different nanopore models, including pristine mesoporous carbons, carbon foams, CNTs, and nanopore models modified with hydrophilic carboxylic groups. Modified CNTs are found to have the highest selectivity toward CO_2 among all the models tested. Using the same method, Wang and coworkers[74] calculated capture of sulfur gases from binary mixtures in SWCNT bundles with different tube diameters but fixed intertube distance. It was reported that among the considered diameters, the CNTs with a diameter of 0.81 nm showed the highest selectivity for H_2S-CH_4, H_2S-CO_2, and SO_2-N_2 binary mixtures. The optimized pore size for separation of SO_2-CO_2 mixture was 1.09 nm. Furthermore, they observed an inverse relationship between selectivity and temperature. As it has been explained in part 1.2, close-packed CNT bundles were always the subject of earlier works, while we believe the

intertube distance has an important influence on adsorption and separation. Thus, it is important to find the optimum intertube distance which maximizes the adsorption.

For multi-component systems, the description of adsorption equilibria can be quite difficult. The Ideal Adsorbed Solution Theory (IAST) developed by Myers and Prausnitz[75] is a method to calculate the adsorption of multi-component equilibria based on single-component adsorption isotherms. Many groups confirmed the agreement of IAST and GCMC simulation for the adsorption of binary mixtures of $CO_2/CH_4/H_2/N_2$on different materials, like MOFs and CNTs.[76–79] Challa *et al*. used GCMC technique and IAST to explore adsorption isotherms of hydrogen isotopes in carbon nanotubes. They observed a direct relationship between selectivity in the nanotubes and interstices and pressure until the nanotube is saturated. The IAST predictions were in line with the simulation results up to moderate loadings. The same method was employed in a later work to study the adsorption and selectivity of light linear alkanes on closed nanotube bundles.[44] The agreement between IAST and simulation for the adsorption of alkanes mixture was confirmed. Peng *et al*.[30] compared IAST prediction of CO_2 and CH_4 adsorption in ordered carbon nanopipes with experimental results; they observed a good agreement. Among all multi-component adsorption studies, the number of studies considering SO_2 are very limited. It would be helpful for experimental studies to know if IAST can be used for the adsorption of mixtures containing SO_2 in bundles of CNTs.

1.5 Problems Addressed in the Thesis

My thesis is structured as follows. In the second chapter, we used a combination of experiments and GCMC simulations to understand the adsorption of CO_2 onto bundles of aligned DWCNTs of diameter of 5 nm at 303 K. In order to investigate adsorption in different pore types and regions and also to compare with the experiments, we considered three limiting cases: a) *outer*, the CNTs were assumed to be completely closed, and adsorption could only take place on their outside regions; b) *inner* only, adsorption occured only within the tubes; c) *unrestricted*, adsorption may take place in all regions. This corresponded to the limiting case of all CNTs being open. We used the adsorption results of these three cases to predict the amount of closed CNTs in the experiments. Furthermore, we addressed the effect of intertube distance on the adsorption mechanism of CO_2 onto DWCNTs for a fixed diameter. The third chapter presents the effect of having charge in CNTs on the adsorption performance. We used Zigzag and armchair SWCNTs of diameter 3 nm, with different intertube distances, from 0 to 2 nm. We explored the adsorption and orientational ordering of CO_2 molecules on parallel bundles of charged as well as uncharged CNTs using both GCMC and molecular dynamic methods. In the fourth chapter, the effect of intertube distance and diameter were studied simultaneously. CO_2 adsorption onto

bundles of DWCNT with inner diameters of 1, 3, 8 nm and intertube distance of 0-15 nm was studied to observe if the curvature has any effects on the optimal intertube distance found in the second chapter. The role of intertube distance and diameter was compared to find the most effective one. In addition, the effects of intertube distance and diameter were investigated for the adsorption of SO_2 in similar DWCNTs and results were compared with CO_2 results. In the last chapter, we studied the adsorption and separation of binary mixtures in bundles of DWCNTs. We studied the adsorption isotherms of mixtures of CO_2-SO_2, SO_2-N_2 and CO_2-N_2in 3-mm diameter DWCNTs. The results were compared to IAST predictions in order to see the accuracy of the IAST for different mixtures.

Chapter two and four of this thesis resulted from a close collaboration with the working group of Prof. Jörg Schneider (Eduard-Zintl-Institut für Anorganische Chemie, Technische Universität Darmstadt). The experimental sections of these chapters (*i.e.* 2.3, 4.2, 4.4.1) were done by Deepu J. Babu, a PhD student in the working group of Prof. Jörg Schneider, but they cannot left out the presentation as it would otherwise be incomplete.

References

1 J. Rouquerol, F. Rouquerol, P. Llewellyn, G. Maurin and K. S. W. Sing, *Adsorption by Powders and Porous Solids: Principles, Methodology and Applications*, Academic Press, London, 2014.

2 D. M. Ruthven, *Principles of Adsorption and Adsorption Processes*, John Wiley & Sons, New York, 1984.

3 D. D. Do, *Adsorption Analysis: Equilibria and Kinetics*, London, 1998, vol. 2.

4 D. M. D'Alessandro, B. Smit and J. R. Long, *Angew. Chem. Int. Ed. Engl.*, 2010, **49**, 6058–82.

5 S. I. Garcés, J. Villarroel-Rocha, K. Sapag, S. A. Korili and A. Gil, *Ind. Eng. Chem. Res.*, 2013, **52**, 6785–6793.

6 S. Choi, J. H. Drese and C. W. Jones, *ChemSusChem*, 2009, **2**, 796–854.

7 *Introduction to Zeolite Science and Practice*, Elsevier, 1991.

8 A. L. C. Zhijian Liang, Marc Marshall, *Energy & Fuels*, 2009, **23**, 2785–2789.

9 P. J. E. Harlick and A. Sayari, *Ind. Eng. Chem. Res.*, 2006, **45**, 3248–3255.

10 K. T. Chue, J. N. Kim, Y. J. Yoo, S. H. Cho and R. T. Yang, *Ind. Eng. Chem. Res.*, 1995, **34**, 591–598.

11 J.-R. Li, R. J. Kuppler and H.-C. Zhou, *Chem. Soc. Rev.*, 2009, **38**, 1477–504.

12 R. Q. Snurr, J. T. Hupp and S. T. Nguyen, *AIChE J.*, 2004, **50**, 1090–1095.

13 R. E. Morris and P. S. Wheatley, *Angew. Chem. Int. Ed. Engl.*, 2008, **47**, 4966–81.

14 O. M. Yaghi, G. Li and H. Li, *Nature*, 1995, **378**, 703–706.

15 S. Iijima, *Nature*, 1991, **354**, 56–58.

16 M. J. O'Connell, *Carbon Nanotubes: Properties and Applications*, CRC Taylor & Francis, Boca Raton, FL, 2006.

17 A. C. Dillon, K. M. Jones, T. A. Bekkedahl, C. H. Kiang, D. S. Bethune and M. J. Heben, *Nature*, 1997, **386**, 377–379.

18 J. M. D. T. Eduardo J. Bottani, *Adsorption by Carbons: Novel Carbon Adsorbents*, Elsevier, 2011.

19 A. V Eletskii, *Physics-Uspekhi*, 2004, **47**, 1119–1154.

20 X. Ren, C. Chen, M. Nagatsu and X. Wang, *Chem. Eng. J.*, 2011, **170**, 395–410.

21 F. L. Darkrim, P. Malbrunot and G. P. Tartaglia, *Int. J. Hydrogen Energy*, 2002, **27**, 193–202.

22 J. Zhao, A. Buldum, J. Han and J. P. Lu, *Nanotechnology*, 2002, **13**, 195–200.

23 M. Cinke, J. Li, C. W. Bauschlicher, A. Ricca and M. Meyyappan, *Chem. Phys. Lett.*, 2003, **376**, 761–766.

24 C. Lu, H. Bai, B. Wu, F. Su and J. F. Hwang, *Energy & Fuels*, 2008, **22**, 3050–3056.

25 A. I. Skoulidas, D. M. Ackerman, J. K. Johnson and D. S. Sholl, *Phys. Rev. Lett.*, 2002, **89**, 185901.

26 L. Huang, L. Zhang, Q. Shao, L. Lu, X. Lu, S. Jiang and W. Shen, *J. Phys. Chem. C*, 2007, **111**, 11912–11920.

27 L. Liu and S. K. Bhatia, *J. Phys. Chem. C*, 2013.

28 H. Cheng, A. C. Cooper, G. P. Pez, M. K. Kostov, P. Piotrowski and S. J. Stuart, *J. Phys. Chem. B*, 2005, **109**, 3780–6.

29 P. Kowalczyk, S. Furmaniak, P. a. Gauden and A. P. Terzyk, *J. Phys. Chem. C*, 2010, **114**, 21465–21473.

30 X. Peng, D. Cao and W. Wang, *Chem. Eng. Sci.*, 2011, **66**, 2266–2276.

31 D. J. Babu, M. Lange, G. Cherkashinin, A. Issanin, R. Staudt and J. J. Schneider, *Carbon*, 2013, **61**, 616–623.

32 J. Zhao, A. Buldum, J. Han and J. P. Lu, *Nanotechnology*, 2001, **13**, 195–200.

33 S. Agnihotri, J. P. B. Mota, M. Rostam-Abadi and M. J. Rood, *Carbon*, 2006, **44**, 2376–2383.

34 A. Cao, H. Zhu, X. Zhang, X. Li, D. Ruan, C. Xu, B. Wei, J. Liang and D. Wu, *Chem. Phys. Lett.*, 2001, **342**, 510–514.

35 D. Zilli, P. R. Bonelli and A. L. Cukierman, *Nanotechnology*, 2006, **17**, 5136–5141.

36 D. J. Babu, M. Lange, G. Cherkashinin, A. Issanin, R. Staudt and J. J. Schneider, *Carbon*, 2013, **61**, 616–623.

37 R. Joshi, J. Engstler, L. Houben, M. Bar Sadan, A. Weidenkaff, P. Mandaliev, A. Issanin and J. J. Schneider, *ChemCatChem*, 2010, **2**, 1069–1073.

38 M. Bienfait, P. Zeppenfeld, N. Dupont-Pavlovsky, M. Muris, M. Johnson, T. Wilson, M. DePies and O. Vilches, *Phys. Rev. B*, 2004, **70**, 035410.

39 S. Agnihotri, J. P. B. Mota, M. Rostam-Abadi and M. J. Rood, *Langmuir*, 2005, **21**, 896–904.

40 D. D. Do, H. D. Do, A. Wongkoblap and D. Nicholson, *Phys. Chem. Chem. Phys.*, 2008, **10**, 7293–303.

41 D. N. Futaba, K. Hata, T. Yamada, T. Hiraoka, Y. Hayamizu, Y. Kakudate, O. Tanaike, H. Hatori, M. Yumura and S. Iijima, *Nat. Mater.*, 2006, **5**, 987–94.

42 W. Shi and J. Johnson, *Phys. Rev. Lett.*, 2003, **91**, 015504.

43 F. J. A. L. Cruz, I. A. A. C. Esteves, S. Agnihotri and J. P. B. Mota, *J. Phys. Chem. C*, 2011, **115**, 2622–2629.

44 J. J. Cannon, T. J. H. Vlugt, D. Dubbeldam, S. Maruyama and J. Shiomi, *J. Phys. Chem. B*, 2012, **116**, 9812–9.

45 F. Cruz and J. Mota, *Phys. Rev. B*, 2009, **79**, 165426.

46 J. Beheshtian, A. A. Peyghan and Z. Bagheri, *J. Mol. Model.*, 2013, **19**, 391–6.

47 F. OuYang, B. Huang, Z. Li, J. Xiao, H. Wang and H. Xu, *J. Phys. Chem. C*, 2008, **112**, 12003–12007.

48 J. Chen, *Science*, 1998, **282**, 95–98.

49 K. Esumi, M. Ishigami, A. Nakajima, K. Sawada and H. Honda, *Carbon*, 1996, **34**, 279–281.

50 D. J. Babu, S. Yadav, T. Heinlein, G. Cherkashinin and J. J. Schneider, *J. Phys. Chem. C*, 2014, **118**, 12028–12034.

51 A. Felten, C. Bittencourt, J. J. Pireaux, G. Van Lier and J. C. Charlier, *J. Appl. Phys.*, 2005, **98**, 074308.

52 Q. Liu, Y. Shi, S. Zheng, L. Ning, Q. Ye, M. Tao and Y. He, *J. Energy Chem.*, 2014, **23**, 111–118.

53 A. M. Rao, P. C. Eklund, S. Bandow, A. Thess and R. E. Smalley, 1997, **388**, 257–259.

54 R. S. Lee, H. J. Kim, J. E. Fischer, A. Thess and R. E. Smalley, *Nature*, 1997, **388**, 255–257.

55 V. Z. Mordkovich, M. Baxendale, R. P. H. Chang and S. Yoshimura, *Synth. Met.*, 1997, **86**, 2049–2050.

56 P. Chen, *Science*, 1999, **285**, 91–93.

57 R. T. Yang, *Carbon*, 2000, **38**, 623–626.

58 F. E. Pinkerton, B. G. Wicke, C. H. Olk, G. G. Tibbetts, G. P. Meisner, M. S. Meyer and J. F. Herbst, *J. Phys. Chem. B*, 2000, **104**, 9460–9467.

59 I. Cabria, M. J. López and J. A. Alonso, *J. Chem. Phys.*, 2005, **123**, 204721.

60 J.-J. Chen, W.-W. Li, X.-L. Li and H.-Q. Yu, *Environ. Sci. Technol.*, 2012, **46**, 10341–8.

61 P. Dubot and P. Cenedese, *Phys. Rev. B*, 2001, **63**, 241402.

62 E.-C. Lee, Y.-S. Kim, Y.-G. Jin and K. J. Chang, *Phys. Rev. B*, 2002, **66**, 073415.

63 Z. Zhou, X. Gao, J. Yan and D. Song, *Carbon*, 2006, **44**, 939–947.

64 K. Gong, F. Du, Z. Xia, M. Durstock and L. Dai, *Science*, 2009, **323**, 760–4.

65 E. N. C. Paura, W. F. da Cunha, P. H. de Oliveira Neto, G. M. e Silva, J. B. L. Martins and R. Gargano, *J. Phys. Chem. A*, 2013, **117**, 2854–61.

66 C. A. Grande and A. E. Rodrigues, *Int. J. Greenh. Gas Control*, 2008, **2**, 194–202.

67 C. A. Grande, R. P. L. Ribeiro, E. L. G. Oliveira and A. E. Rodrigues, *Energy Procedia*, 2009, **1**, 1219–1225.

68 S.-H. Moon and J.-W. Shim, *J. Colloid Interface Sci.*, 2006, **298**, 523–8.

69 R. Stoian, A. Rosenfeld, D. Ashkenasi, I. V. Hertel, N. M. Bulgakova and E. E. B. Campbell, *Phys. Rev. Lett.*, 2002, **88**, 097603.

70 M. Zdrojek, T. Mélin, H. Diesinger, D. Stiévenard, W. Gebicki and L. Adamowicz, *J. Appl. Phys.*, 2006, **100**, 114326.

71 J. Luo, L.-M. Peng, Z. Xue and J. Wu, *Phys. Rev. B*, 2002, **66**, 115415.

72 V. V. Simonyan, P. Diep and J. K. Johnson, *J. Chem. Phys.*, 1999, **111**, 9778.

73 L. Lu, S. Wang, E. A. Müller, W. Cao, Y. Zhu, X. Lu and G. Jackson, *Fluid Phase Equilib.*, 2014, **362**, 227–234.

74 W. Wang, X. Peng and D. Cao, *Environ. Sci. Technol.*, 2011, **45**, 4832–8.

75 A. L. Myers and J. M. Prausnitz, *AIChE J.*, 1965, **11**, 121–127.

76 X. Peng, X. Cheng and D. Cao, *J. Mater. Chem.*, 2011, **21**, 11259–11270.

77 R. Babarao, Z. Hu, J. Jiang, S. Chempath and S. I. Sandler, *Langmuir*, 2007, **23**, 659–66.

78 P. Kowalczyk, *Phys. Chem. Chem. Phys.*, 2012, **14**, 2784–90.

79 D. W. Hand, S. Loper, M. Ari and J. C. Crittenden, *Environ. Sci. Technol.*, 1985, **19**, 1037–43.

THE JOURNAL OF PHYSICAL CHEMISTRY C

Article

pubs.acs.org/JPCC

Understanding Carbon Dioxide Adsorption in Carbon Nanotube Arrays: Molecular Simulation and Adsorption Measurements

Mahshid Rahimi,[†] Jayant K. Singh,*[,†,‡] Deepu J. Babu,[†] Jörg J. Schneider,[†] and Florian Müller-Plathe*[,†]

[†]Eduard-Zintl-Institut für Anorganische und Physikalische Chemie, Technische Universität Darmstadt, Petersenstr. 20, D-64287 Darmstadt, Germany

[‡]Department of Chemical Engineering, Indian Institute of Technology Kanpur, Kanpur 208016, India

ABSTRACT: Grand-canonical Monte Carlo simulations and adsorption experiments are conducted to understand the adsorption of CO_2 onto bundles of 3D aligned double-walled carbon-nanotubes of diameter 5 nm at 303 K. The simulation of partial adsorption isotherms, i.e., only inner tube volume, only interstices between tubes, and unrestricted, allows a breakdown of the experimental adsorption isotherms into contributions of different regions. The results are compatible with microscopic observations of the majority of the inner tube volumes being accessible for CO_2. Further, the unrestricted adsorption isotherm is quantitatively equivalent to the sum of inner and outer adsorption for the pressure range considered in this work, $p < 40$ bar, indicating no significant interference between inner and outer regions. The intertube distance, which is varied from 0 to 15 nm, dramatically affects the isosteric heat of adsorption and adsorption capacity. Excess adsorption is found to display a nonlinear behavior with d, for unrestricted and outer cases. For low pressures ($p \leq 14$ bar), maximum adsorption occurs at $d = 0.5$ nm. However, for higher pressures, $14 < p < 40$ bar, the adsorption peaks at $d = 1$ nm. The Freundlich isotherm is found to fit the experimental and simulation data. The adsorption sequence changes with the intertube distance for the unrestricted case. At $d \leq 0.5$ nm, adsorption proceeds with increasing loading in the following order: grooves and inner surface adsorption → fill interstitial region → fill inner region. However, at higher distances, $d > 0.5$ nm, the sequence changes the following: inner surface adsorption + partial outer surface adsorption → complete outer surface adsorption → fill interstitial, groove, inner adsorption. The change in mechanism of adsorption is clearly reflected in the behavior of the heat of adsorption, where we observed a crossover behavior at around $d = 0.5$ nm.

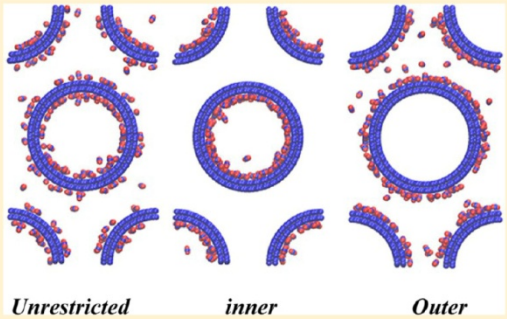

1. INTRODUCTION

Increasing atmospheric carbon dioxide is considered as a globally alarming environmental issue.[1] It is found to have a key role in the recent rise of global temperature as summarized by Marcott and co-workers[2] based on reconstruction of more than 11 000 years of earth temperature across the globe. Hence, the quest for an immediate solution for carbon-dioxide sequestration and storage is warranted. Many options are being considered. Among them are geological sites such as unused oil fields and coal mines. In addition to storage, separating carbon dioxide from other gaseous content is of challenge, too.

In order to understand the mechanism of CO_2 adsorption, numerous investigations have been done to date using various porous materials, which is summarized in recent reviews.[3] Among adsorbents, carbon nanotubes (CNTs) and bundles of them are currently considered as potential media for selective adsorption. Cinke and co-workers[3] showed that purified single-walled carbon nanotubes (SWCNT) adsorbs almost twice the volume of CO_2 compared to activated carbon. SWNT or multiwalled CNT (MWCNT) can be synthesized and fine-tuned as per the requirement.[4−6] CNTs also offer themselves as models for ideal pores for the investigation of adsorption and selectivity of gaseous components. For instance, Huang and co-workers[7] studied adsorption of a CO_2−CH_4 mixture in CNTs of diameters varying from 0.678 to 1.356 nm using molecular simulation and found CNTs to demonstrate a higher selectivity toward CO_2 than toward other materials. Skoulidas and co-workers[8] studied the adsorption and transport diffusion of CO_2 in SWNTs using molecular simulations, which were found to be in good agreement with the experiments. It is well-known that synthesis and processing conditions affect the morphology of CNTs, and CNTs usually are found as bundles or complicated aggregates.[9] CNT bundles are known to exhibit a high adsorptive capacity mainly due to different possible regions or sites of adsorption in such geometry. For example, a triangular SWNT array has been studied for its adsorption capacity for methane storage and found to meet the requirement of DOE energy criteria.[10] Recently, Kowalczyk et al[11] have studied the adsorption of CO_2 in SWNT bundles using Monte Carlo simulations. The authors conclude that

Received: April 12, 2013
Revised: June 10, 2013
Published: June 13, 2013

adsorption is indifferent to the chirality of the nanotubes. Further, they observed that the optimum size of the nanotube varies with external pressure. The authors, however, did not study the effect of intertube distance on the adsorption isotherm and isosteric heat of adsorption. Further, the mechanism of adsorption of CO_2 with variable intertube distance has not been addressed. Some work, however, on the adsorption mechanism of organic molecules onto CNT bundles[12−14] has been done using Monte Carlo simulations. In particular, Cruz et al.[13] studied the adsorption of light alkanes and alkenes on SWNT bundles. The authors observed, based on very low pressure data, that for closed-packed bundles the adsorption is first dependent on the diameter of the tube. Further, the authors state that for CNTs beyond 1.47 nm diameter, adsorption starts in the grooves, where two CNTs touch, and only after filling the corresponding volume it proceeds to other surface regions of the CNT. The observations of the authors were still based on SWCNTs of less than 2 nm diameter. However, it is not known if such behavior is also found for double or multiwalled CNT bundles with more than 2 nm diameter. Furthermore, not much work has been done to understand the effect of pore size and intertube distance on the adsorption of CO_2 in MWNT bundles. For large scale commercial application of CNT arrays for the adsorption of CO_2 and other gases as compared to other porous media, a study on the effect of different bundle arrangements on the adsorption mechanism is necessary. In this work, using a combination of experiments and simulations, we address the effect of intertube distance and tube diameter on the adsorption mechanism of CO_2 onto 3D vertically aligned CNT bundles containing double walled nanotubes (DWCNTs).

2. MODEL AND METHOD

Figure 1 shows a schematic description of the DWCNT arrangement used in this work. The DWCNTs are arranged on a hexagonal lattice. In order to analyze the effect of porosity of the system, the intertubular distance (d; i.e, the surface-to-surface distance along the vector joining the axes of neighboring DWCNTs) is varied. We define d such that d = 0 represents the case of touching DWCNTs (i.e., the distance between the outer layers of the adjacent tubes for the case of d = 0 is 0.34 nm). In this work, we have considered seven values of d viz., d = 0, 0.2, 0.5, 1.0, 4.0, 2, and 15 nm. The effect of pore size is also analyzed in order to compare with the experiments, by considering internal diameter $(2r)$ = 5.0 nm. The system is set up using orthorhombic periodic boundary conditions with two DWCNTs in the simulation cell. The cell length in the direction of the CNT axes is 24.78 nm; the cell lengths perpendicular to the CNT axes are adjusted to the required intertube distance d.

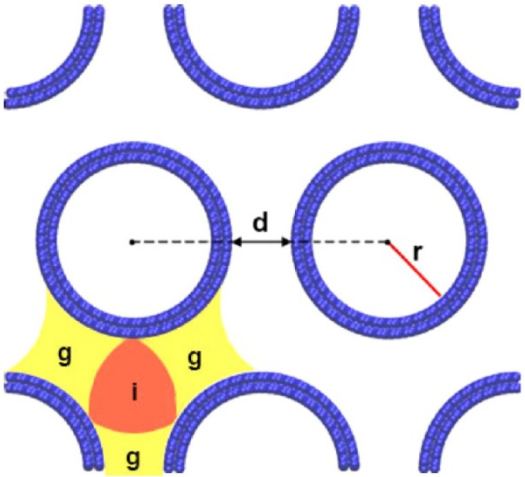

Figure 1. Schematic arrangement of double walled CNTs as used in this work, with internal radius r and intertube (surface-to-surface) distance d. Interstitial and groove regions are represented by symbol i and g, respectively.

A carbon nanotube is modeled as a rigid structure with the Lennard-Jones potential as in AMBER96 force field (ε = 0.36 kJ/mol, σ = 0.34 nm).[15] This model has also been used to understand the fast transport of water in CNT.[16] Carbon particles are considered to be neutral. Carbon-dioxide is modeled using the 3-site rigid potential of Harris and Yung,[17] which contains three centers with Lennard-Jones interactions and partial charges. It has been derived for the simulation of vapor−liquid phase equilibria. The CO_2 Lennard-Jones parameters are $\sigma_{c\text{-}c}$ = 0.2757 nm, $\varepsilon_{c\text{-}c}$ = 0.23388 kJ/mol, $\sigma_{o\text{-}o}$ = 0.3033 nm, $\varepsilon_{o\text{-}o}$ = 0.66837 kJ/mol, q_o = −0.3256e, q_c = 0.6512e, $l_{c\text{-}o}$ = 1.149 Å. The Lennard-Jones interactions between unlike atoms are approximated using the Lorentz−Berthelot rules. Lennard-Jones and Coulombic interactions, based on center-of-mass of molecules, are truncated at 1 nm. Long range corrections are not considered in this work.

Grand-canonical Monte Carlo (GCMC) simulations were carried out to investigate the adsorption of CO_2 onto double walled nanotube bundle. GCMC is performed at constant chemical potential μ, volume V, and temperature T. The temperature is fixed at 303 K. In order to generate the adsorption isotherm, simulations were conducted at different chemical potentials to span the region from low to high pressure. Three MC moves are employed, namely displacement, addition/removal, and rotation, with relative trial probabilities: 0.2, 0.7, and 0.1, respectively. For each simulation run, 1×10^7 Monte Carlo steps are used for both the equilibration and production periods. In order to compare with the experimental data, the absolute adsorption amount (N_{ad}: absolute number of CO_2 molecules in the simulation cell) is converted to the absolute excess adsorption N^{ex} by discounting the "sorption" of bulk fluid into the available volume:

$$N^{ex} = N_{ad} - \rho_b V_{free} \quad (1)$$

where the bulk density ρ_b is obtained from independent GCMC simulations of the bulk fluid at the same thermodynamic conditions. V_{free} is the volume available for fluid molecules. Various methods for obtaining the free volume[10,18,19] exist. In this work, we have used the geometric approach by Mahdizadeh et al.[10] together with their choice of parameters. The excess adsorption is reported in the specific form (in mmol per gram of adsorbent) as n^{ex}.

The strength of force between the adsorbent and fluid molecules is reflected in the isosteric heat of adsorption, q_{st}, which can be defined approximately as[20]

$$q_{st} \approx RT - \left(\frac{\partial U_{ad}}{\partial N_{ad}}\right)_{T,V} \quad (2)$$

dx.doi.org/10.1021/jp403624c | J. Phys. Chem. C 2013, 117, 13492−13501

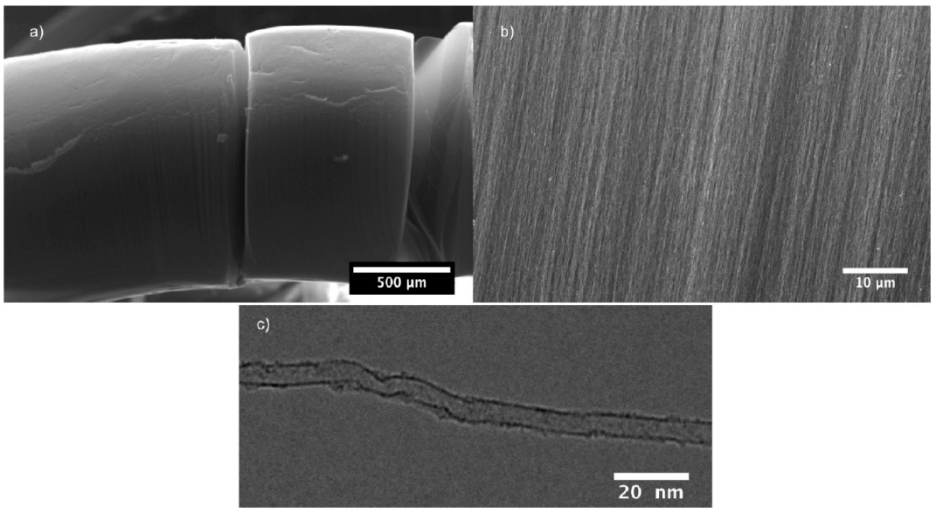

Figure 2. (a) SEM image of 3D aligned CNT block structure, (b) magnified image demonstrating the vertical alignment of the CNTs within such an array, and (c) TEM image of an individual double walled CNT (~ 5 nm inner diameter) unhinged from a CNT block by ultrasonification.

where U_{ad} is the intermolecular energy of the adsorbed phase. The partial derivative in eq 2 is calculated using fluctuation theory. Equation 2 can be written as

$$q_{st} = RT - \frac{\langle U_{ad}N_{ad}\rangle - \langle U_{ad}\rangle\langle N_{ad}\rangle}{\langle N_{ad}{}^2\rangle - \langle N_{ad}\rangle^2} \quad (3)$$

3. EXPERIMENTAL DETAILS

3D vertically aligned CNTs were synthesized by water assisted chemical vapor deposition method (WACVD). 10−12 nm of Al was deposited onto a B-doped ⟨100⟩ Si/SiO_2 (600 nm of SiO_2) substrate by thermal evaporation. Al along with a 0.6−1.2 nm layer of sputtered Fe served as catalyst for the CNT growth. CNTs were synthesized in an upscaled 3 in. CVD reactor to meet the requirements of 50−100 mg of CNT sample for each adsorption measurement. CNTs were grown at 850 °C in the presence of ppm quantities of water for 15 min. WACVD method produces vertically aligned 3D CNTs with high purity in a controlled manner.[21,22] These 3D CNT arrays with the flexibility in tuning the diameter and the intertube distance are ideal model structures for investigating the gas adsorption characteristics on carbon materials. Further details of the procedure may be found elsewhere.[23]

N_2 adsorption measurements were made in a Quantachrome Autosorb. Prior to the measurement, 20−30 mg of sample was heated to 573 K under vacuum conditions for 12 h. Pore size distributions were calculated from the desorption branch of the N_2 adsorption isotherm at 77 K, using the nonlinear density functional theory (NLDFT)[24,25] approach assuming a slit/cylindrical pore structure. The multipoint BET method[26] was used for calculating the surface area. High pressure CO_2 adsorption studies were carried out with a magnetic suspension balance (Rubotherm) that can be operated up to 200 bar. The aligned 3D CNT samples (50 mg) were placed in a stainless steel sample holder, which was evacuated to 10^{-3} mbar at 423 K for 12 h until a constant mass was obtained. The gas was dosed into the chamber at an elevated pressure and equilibrium was achieved in less than 30 min, characterized by constant weight and pressure. A helium buoyancy correction was made for each sample. A detailed description of the experiment can be found elsewhere.[27] High pressure CO_2 adsorption measurements were carried out at three different temperatures (20, 30, and 40 °C), and the heat of adsorption was calculated using the Clausius-Clapeyron equation.

4. RESULTS AND DISCUSSION

Figure 2a shows a low magnification image of a 3D aligned CNT structure, obtained using WACD method, depicting the bundled structure of the CNTs used in the study. The CNTs are organized over macro sized dimensions in a dense and compact arrangement with an average height of 800 μm. The individual CNTs in the block structures are held together by van der Waals forces which act alongside the overall length of the tubes and are mainly responsible for positioning of the

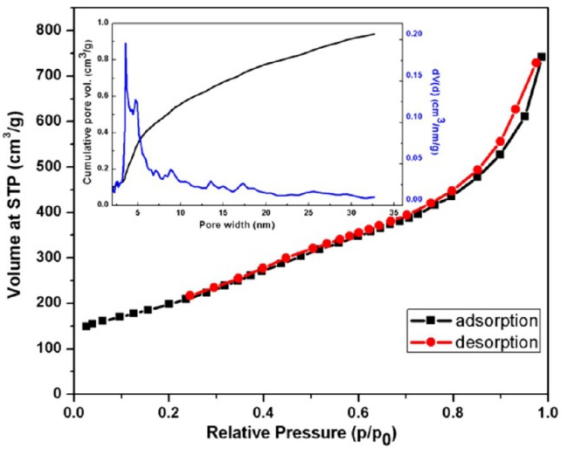

Figure 3. Nitrogen adsorption−desorption isotherm at 77 K for the as-prepared 3D aligned CNT sample, p_0 = 1 bar. The inset shows the pore size distribution using nonlinear density function theory[25,26] as measured using the Quantachrome Autosorb.

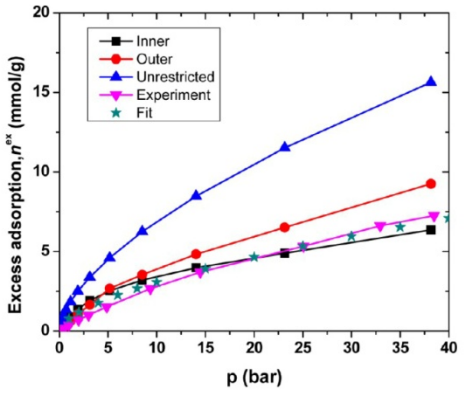

Figure 4. Excess adsorption amount of CO_2 in double-walled carbon nanotube arrays with r = 2.5 nm and d = 15 nm, for different modes of adsorption. T = 303 K.

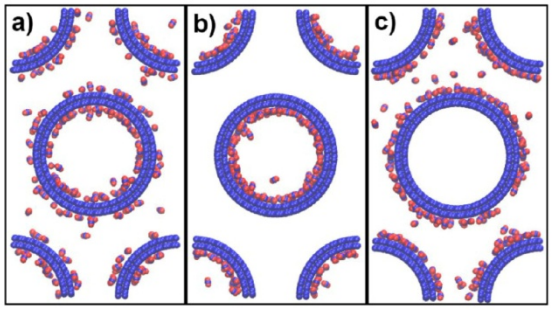

Figure 5. Snapshot of adsorption at loading of ~2.5 mmol/g, T = 303 K, r = 2.5 nm, d = 2 nm for cases: (a) unrestricted, (b) inner, and (c) outer.

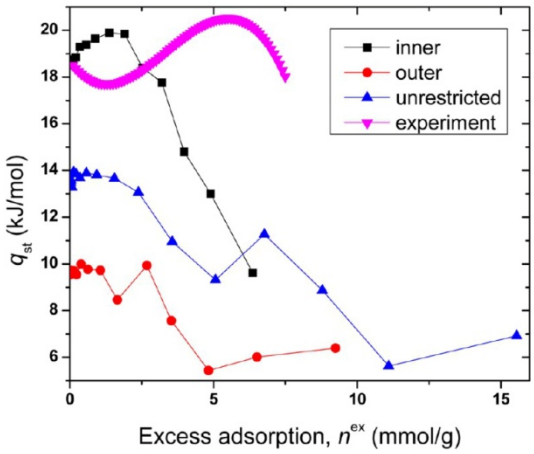

Figure 6. Isosteric heat of adsorption for different modes of adsorption of CO_2 in double-walled carbon nanotube arrays with r = 5.0 nm and d = 15 nm at T = 303 K.

tubes and thus the tube distance. Due to their large aspect ratio, the CNTs may distort locally along the individual tube length. However, their overall alignment in the bundled CNT structure remains intact. Figure 2b shows a high magnification image of such a structure revealing an inside view of the dense highly

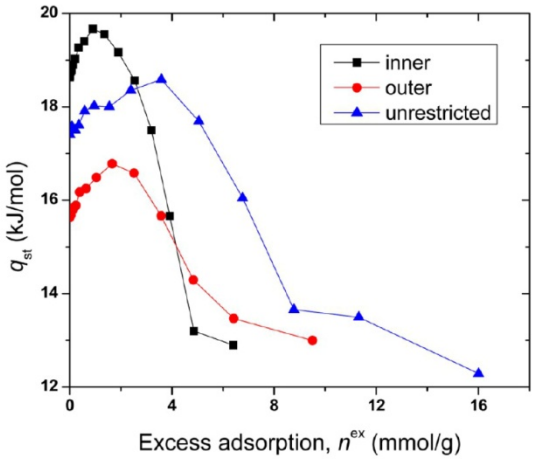

Figure 7. Isosteric heat of adsorption for different modes of adsorption of CO_2 in double-walled carbon nanotube arrays with r = 2.5 nm and d = 2 nm at T = 303 K.

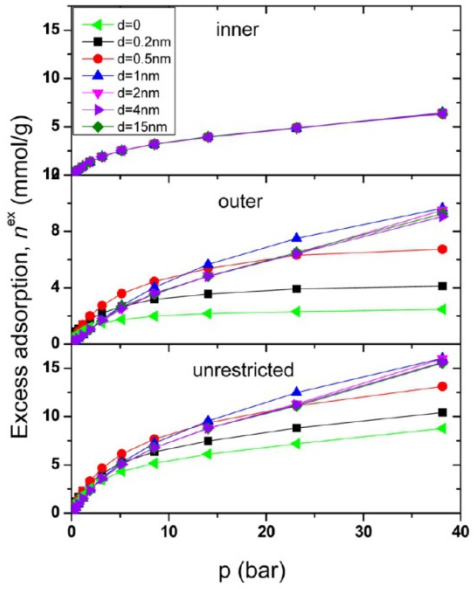

Figure 8. Excess adsorption isotherm of CO_2 in double-walled carbon nanotube arrays with radius, r = 2.5 nm. Intertube distance, d, is varied from 0 to 15 nm.

parallel vertically aligned CNT arrangement. As seen from the TEM image in Figure 2c, the CNTs are usually double-walled with an average inner diameter of 5 nm. Widespread methods for obtaining CNTs often incorporate catalyst particles and produces CNTs that are randomly oriented. Necessary purification steps of such CNT materials inevitably leads to the uncontrolled addition of functional groups or formation of defects on their surface. This seriously alters the adsorption behavior of CNTs in an uncontrolled manner.[28] However, the as-prepared CNTs obtained by WACVD are catalyst free (see Figure 2) and show a high degree of purity. Hence no further purifications were carried out.

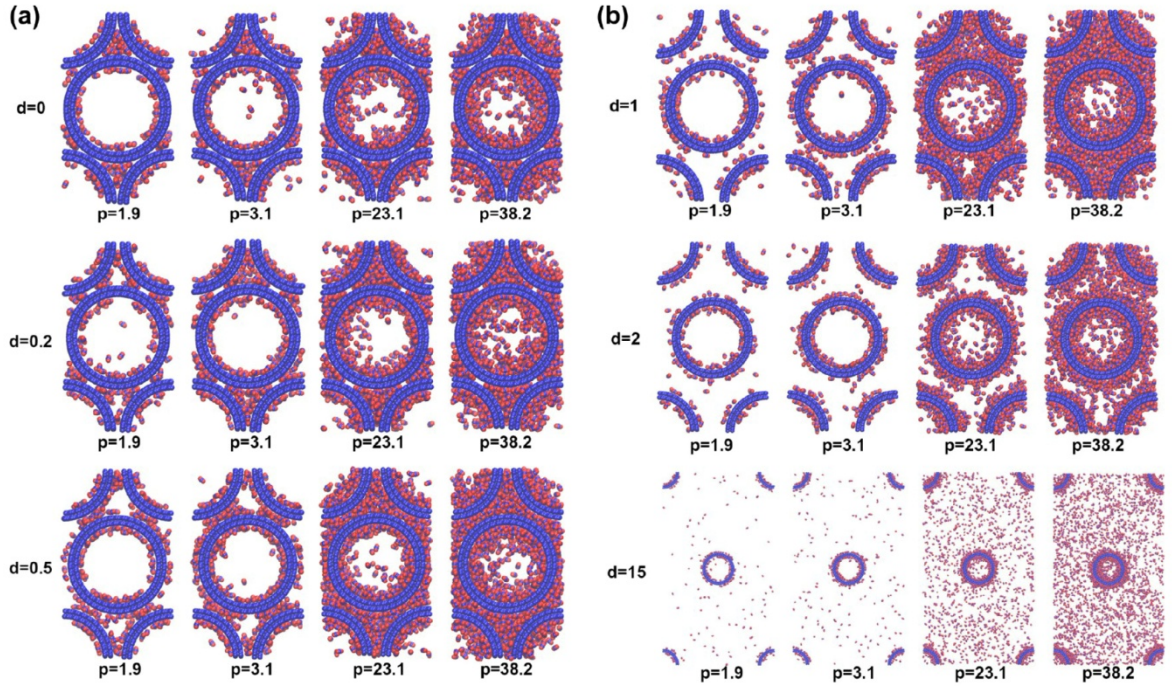

Figure 9. Snapshots of carbon-dioxide molecules in double-walled carbon nanotube arrays for unrestricted adsorption: (a) rows from top to bottom: d (nm) = 0, 0.2, and 0.5 (b): rows from top to bottom: d (nm) = 1, 2, and 15. Columns from left to right correspond to p (bar) = 1.9, 3.1, 23.1, and 38.2.

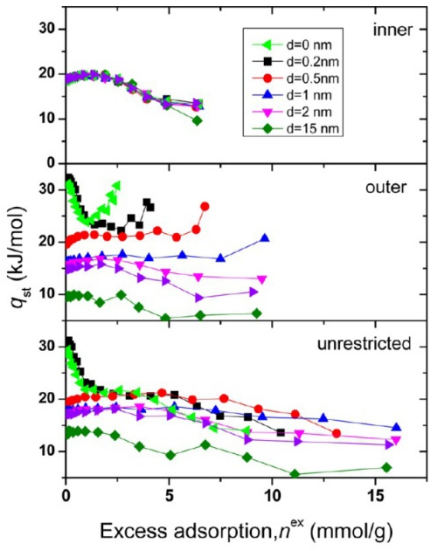

Figure 10. Isosteric heat of adsorption of CO_2 in double-walled carbon nanotube arrays with radius, r = 2.5 nm. Intertube distance, d, is varied from 0 to 15 nm.

The N_2 adsorption isotherm for the CNTs at 77 K (Figure 3) shows a type II behavior at lower relative pressure (p/p_0 < 0.5, p_0 = 1 bar) and a type IV isotherm at higher relative pressures, which is typical for CNTs.[29−31] The pore size distribution determined using NLDFT in the pore width range 1−40 nm revealed a split peak between 4 and 6 nm. It corresponds roughly to the inner CNT diameter of 5 nm, measured by TEM. The intertube distance, though, is not very clear from the pore size distribution. However, for vertically aligned CNT arrays with still larger tubes of internal diameter 8 nm, we have observed a second peak in the range of 13−15 nm which is the typical intertube spacing value reported in the literature for WACVD[5] (figure not shown). The prepared 5 nm CNTs have a specific surface area of 720 m^2/g as measured by the multipoint BET method. Due to the uncertainities associated with the pore size distribution calculations for nanoporous materials[32] like carbon nanotubes, the internal pore size diameter was selected based on the experimental TEM study.

Various strategies have been used in the past to explain the experimental observations by simulation. Some authors have assumed nonideal packing of the tubes with larger interstitial pores together with a distribution of nanotube diameters within a bundle.[33,34] Other authors have considered a certain percentage of the nanotubes to be open, allowing gas adsorption on the inside, to improve the agreement between simulation and experiment.[10] In our simulation set-ups, we consider three limiting cases with an aim to investigate the adsorption in different pore types and regions and also to compare with the experiments: (a) outer, the CNTs are assumed to be completely closed, and adsorption can only take place on their outside in the interstitial and groove regions (see Figure 1); (b) inner only, adsorption occurs only within the tubes and the interstitial and groove regions are assumed to be inaccessible; (c) unrestricted, adsorption may take place in all regions. This corresponds to the limiting case of all CNTs being open.

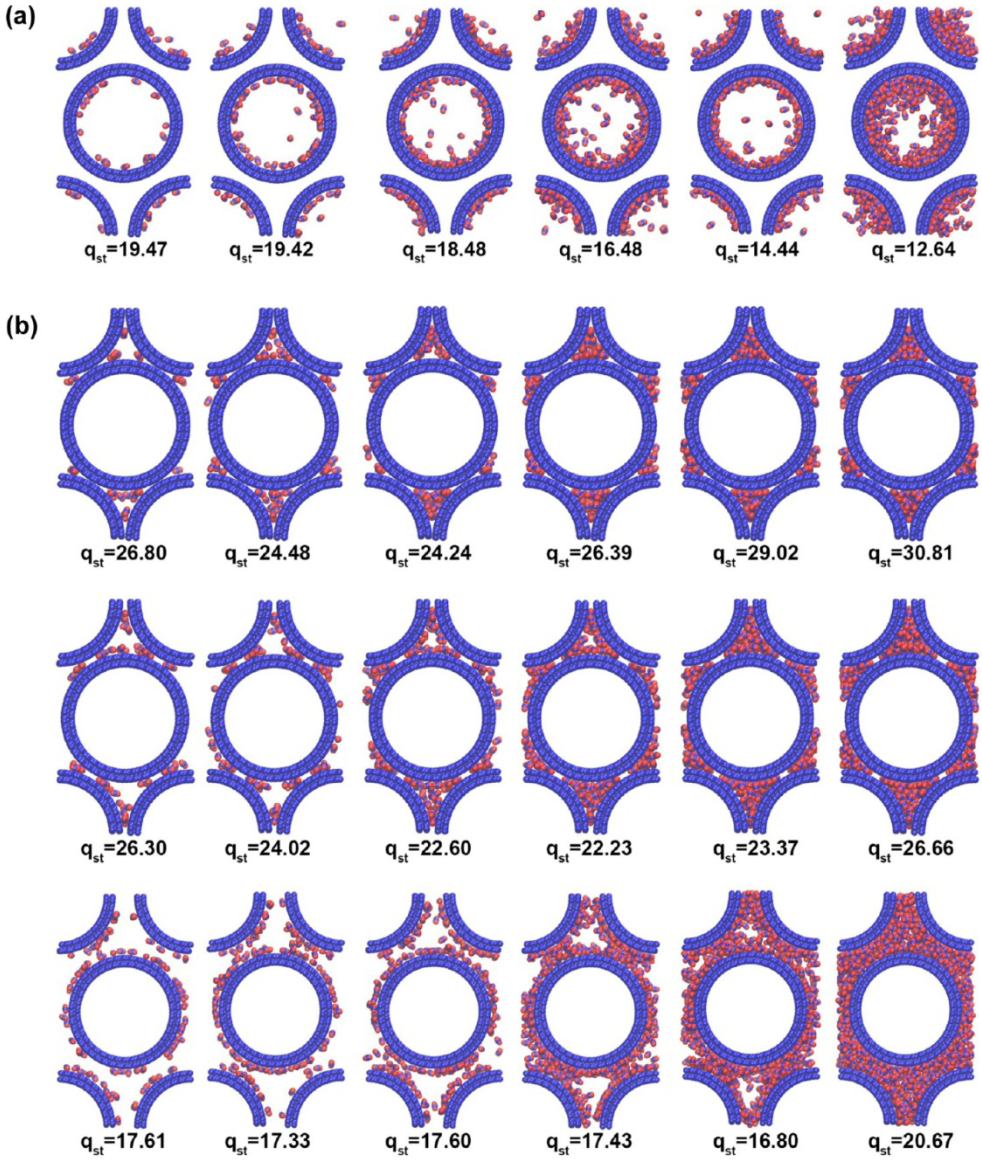

Figure 11. Snapshots of carbon-dioxide molecules in double-walled carbon nanotube arrays for adsorption modes at different q_{st} values. (a) Inner adsorption, d = 0.5 nm. (b) Outer adsorption, rows from top to bottom correspond to d = 0.0, 0.2, and 1.0 nm. q_{st} values are displayed at the bottom of the snapshots.

The measured excess adsorption isotherm for a bundle of 5-nm-diameter double-walled CNTs is presented in Figure 4 along with the simulation data for the three adsorption modes. At a low pressure range, as studied in this work (p < 40 bar), unrestricted adsorption is simply a sum of adsorptions for inner and outer cases. It is first noted that the experiment is of the same order as all simulation scenarios. The deviation in the adsorbed amount is less than a factor of 2−3 in all cases. Boltzmann inversion translates this into a difference of the free energy of adsorption of less than 0.7−1.0 k_BT, which is at the accuracy limit of force-fields without special adaptation. It is also evident, however, that the experimental data is not in precise agreement with any specific simulation scenario. There is also a qualitative difference. The experimental isotherm is linear, for p < 15 bar), which is in contrast to the behavior seen in Monte Carlo simulations for the inner and the unrestricted cases. On the other hand, the linear behavior of the experimental curve is qualitatively in line with that observed for the outer adsorption data obtained from simulations. However, the quantitative difference between the experiments and interstitial isotherms from simulations is still significant. It is clear though that the idealized scenario of open vertically aligned CNTs is far from real. One needs to take into account that a certain percentage of CNTs is closed, and intertube spacing, d, may vary. However, for the current analysis, we start

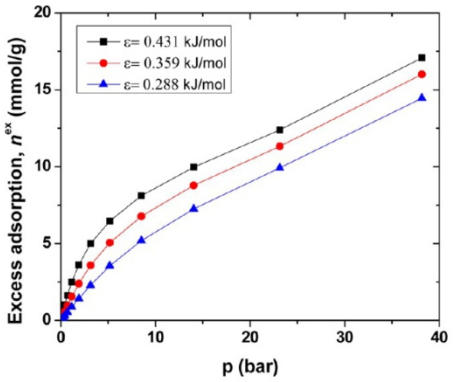

Figure 12. Excess adsorption amount of CO_2 in double-walled carbon nanotube arrays with r = 2.5 nm and d = 2 nm for unrestricted adsorption and different values of the Lennard-Jones energy parameter ε of the CNT carbon, T = 303 K.

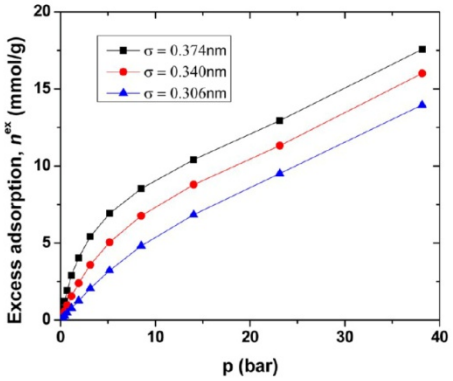

Figure 13. Excess adsorption amount of CO_2 in double-walled carbon nanotube arrays with r = 2.5 nm and d = 2 nm for unrestricted adsorption and different values of the Lennard-Jones energy parameter σ of the CNT carbon, T = 303 K.

with the typical value of d = 15 nm. We first fit the data from the experiment with the following equation:

$$n^{ex} = c(\alpha n^{ex}_{inner} + (1 - \alpha)n^{ex}_{outer})$$

where n^{ex}_{inner} and n^{ex}_{outer} are excess adsorptions for the inner and outer cases, respectively. The values of α and c, from the fit, are 0.58 and 0.89, respectively. The data from the fit are also included in Figure 4. Based on these fitted parameters, the surface area of the porous sample used in our simulation is ~650 m^2/g, which is slightly lower than the experimental value of 720 m^2/g. The fitting results indicate that the majority of the carbon nanotubes is open and their inner volume is available for adsorption. A recent study on single-walled CNTs found 44% of the tubes open.[12] Furthermore, not all of the outer tube walls are accessible for adsorption, for example due to DWCNTs touching. The factor c in the fit absorbs all experimental and simulational uncertainties and adjusts the overall agreement. The raw isotherms generated from the simulation globally overestimate experiment by ~10%; the fact that c is close to 1 gives some confidence to the modeling strategy. The above analysis does not change much if we use the data for d = 2 nm. Variations in the intertube distance beyond $d \geq 2$ nm do not change the above analysis. However, lower values of d have, in general, significant effect on the adsorption isotherm, which is analyzed in a subsequent section. Further, uncertainties in the force field parameters may have some effects, as also reflected by c, which we also discuss in a later section.

It is evident that in case of open CNTs for a given loading, fewer CO_2 molecules adsorb on the inner surface compared to the case of outer adsorption. (That is to say, the displayed excess isotherm is smaller for unrestricted than for outer adsorption, whereas the opposite is of course true for the absolute number of adsorbed molecules, cf. section 2.) This is also evident from the snapshots of adsorption at a given loading for different cases, Figure 5.

Although the agreement of the adsorption isotherms is good as reflected in Figure 4, the isosteric heat of adsorption q_{st} data calculated for our idealized CNT geometry agrees less well with experiment (see Figure 6). The simulated q_{st} obtained for an intertube distance d = 15 nm is considerably lower, in general, than in experiment. To assess a possible dependence of q_{st} on the intertube distance, we have also calculated q_{st} for d = 2 nm (Figure 7) keeping the same inner tube diameter $2r$ = 5 nm. Decreasing d dramatically affects the heat of adsorption: e.g. for unrestricted adsorption, the heat of adsorption increases by almost 50−100%, when d is lowered from 15 to 2 nm. This is a strong indication that the mean value of d in the experiments is either significantly lower than the assumed 15 nm, or that the q_{st} varies strongly and nonlinearly with d, such that small-d arrangements contribute disproportionately to the overall q_{st}, which may be the reason behind the different curvature of the experimental data. This is discussed in more detail in the next section.

Effect of Intertube Distance on the CO_2 Adsorption Mechanism. Figure 8 presents the adsorption isotherm for intertube distances d = 0−15 nm. As expected, the inner adsorption isotherm is indifferent to the value of d. For the outer case (i.e., when pores are closed) the adsorption isotherms are not much different at lower pressure. At low d values, isotherms saturate at a very low pressure as seen for d = 0−0.5 nm. However, the saturation value increases significantly, by about 200%, from d = 0 to 0.5 nm. Further increase in d increases the adsorption amount, and the saturation point is shifted to a higher pressure value. We notice that d does not affect the outer adsorption profile linearly as seen for d = 2.0 and 4.0 and 15 which are fairly similar. However, the distance d = 1.0 nm exhibits an interesting behavior. The corresponding excess adsorption amount of CO_2 is the largest for all the d values studied, for $p \geq 14$ bar. In the low pressure region, $p <$ 14 bar, it is the intertube distance of d = 0.5 which displays the largest excess adsorption of CO_2. The behavior of the unrestricted adsorption resembles that of the outer adsorption.

To illustrate the adsorption mechanism, Figure 9a presents snapshots at different pressures for the unrestricted case, for $d <$ 1 nm. At d = 0, the adsorption is mainly due to contributions from interstitial and inner adsorptions. The interstitial region is saturated within $p \approx 4$ bar, and subsequent adsorption takes place mainly in the inner region. Hence, the adsorption isotherm is dominated by the inner adsorption characteristic. At d = 0.2 nm, adsorption at low pressure is mainly contributed by the grooves, interstitial regions and inner surface adsorptions. With increasing pressure, first the grooves and the interstitial region are filled followed by inner region, where multilayer adsorption is visible. At d = 0.5 nm, clearly groove region is filled up first followed by interstitial and inner regions with

increasing pressure, respectively. When d is increased to 1.0 nm and beyond (see Figure 9 b), adsorption is initiated at the surface, preferentially at the inner surface. Hence, at low pressures there is mainly inner adsorption. Moreover, groove and interstitial regions are no more attractive for preferential adsorption due to the large surface-to-surface distance, which decreases the effective attraction of fluid molecules in that region. We observed the following sequence of adsorption for the unrestricted case: groove + inner surface adsorption → interstitial region → inner adsorption, for $d \leq 0.5$ nm. At higher $d > 0.5$ nm, we have the following: inner surface adsorption + partial outer surface adsorption → outer surface adsorption → interstitial + groove + inner adsorption. This is not entirely in agreement with the prediction of Cruz et al.,[13] whose assessment was limited to the case of closed packed arrangement. However, in the case of $d < 0.5$ nm, the adsorption mechanism of hydrocarbons in carbon-nanotube bundles is similar to that seen for CO_2. With an increase in pressure, the excess adsorption increases with increase in the d value until $d = 1.0$ nm; subsequently, it is seen to decrease. For example, we notice that at $p = 40$ bar, the $d = 15$ nm case has lower excess adsorption than that of $d = 1.0$ nm (see Figure 8), which has a maximum excess adsorption amount. This clearly indicates that d plays an important role in the storage of CO_2, as it can be tuned to obtain an increase in adsorption by a factor of 2 within a pressure range of 15−40 bar.

Now, we turn our attention to the effect of intertube distance on the isosteric heat of adsorption, which is shown in Figure 10. In the case of inner adsorption, the behavior is similar for all values of d. q_{st} first increases until a loading of ∼1.9 mmol/g, and subsequently decreases with further loading. The increasing regime corresponds to the stage where particles cover the surface with increasing loading, indicative of increasing adsorption energy with surface coverage. Further increase in loading, beyond a critical loading value, decreases the q_{st}, indicative of the filling of second or higher adsorption layers, as can also be seen in Figure 11a for $d = 0.5$. In case of outer adsorption, the behavior is opposite. Here, we observe q_{st} to strongly depend on d. At low $d = 0$−0.2 nm, q_{st} is to seen to drop with increasing loading first. This is mainly due to filling of the groove regions (see Figure 11b), which have a high carbon density. Once the outer surface in the interstitial groove region is wetted, the q_{st} increases with further increasing in loading. Such behavior is prominent where interstitial volume is extremely small as for $d = 0$−0.2 nm. Beyond a certain loading (which in this case is ∼1 and 3 mmol/g for $d = 0$ and 0.2 nm, respectively) q_{st} starts increasing again. As seen from Figure 11b, the increase in q_{st} corresponds to the regime where complete filling of the interstitial and groove regimes is seen. The opposite behavior is observed for $d > 0.2$ nm, where q_{st} first increases with increasing loading until a certain loading, followed by decrease in the q_{st} values. The effect of loading on the rise in q_{st}, however, diminishes with increasing d. The overall difference in the behavior of $d < 0.5$ and $d \geq 0.5$, is mainly due to different mechanisms of adsorption. The role of interstitial and groove regions diminishes with increase in d. Figure 11b also presents snapshots for different loading at $d = 1.0$ nm, where, adsorption starts at the outer surface uniformly. With increase in pressure or loading, we observed second layer deposition followed by the filling of the interstitial and groove regions. Figure 10c plots the isosteric heat of adsorption for the unrestricted case. Similar to the case of open pores, we have a decreasing q_{st} for $d = 0$ and 0.2 nm and an increasing q_{st} for $d >$ 0.2 nm. However, q_{st} does not increase with increasing loading for $d = 0$ and 0.2 nm. In case of $d > 0.5$ nm, the unrestricted adsorption is more or less similar to the outer adsorption.

The experimental q_{st} curvature (cf. Figure 6) has a decreasing trend, at low loadings, which based on the above analysis is possible only for low d value. Hence, the presence of small intertube distances cannot be ignored. However, pore size distribution and TEM analysis do not indicate lower values of d. Nevertheless, considering the fit to the experimental adsorption isotherm, we speculate that DWCNTs are not perfectly aligned, and intertube distances below 0.5 nm may be present locally, which disproportionally contribute to the q_{st}. Furthermore, we speculate that defects of the order of 0.2−0.5 nm are possibly present, and they may substantially influence the isosteric heat of adsorption.

Influence of Force-Field Parameters. In order to estimate the uncertainty of the present results due the choice of force field parameters, we have repeated the isotherm calculations with the Lennard-Jones interactions between CNTs and CO_2 changed. We have considered two cases viz., ±10% change in energy ε and size parameter σ of the CNT carbon atoms at a time, leaving the CO_2 force-field parameters unchanged. These changes are drastic. For example, reducing the Lennard-Jones σ of carbon (0.34 nm, derived from graphite interlayer spacing) by 10%, one arrives at a typical diameter of an oxygen atom. Because of the Lorentz−Berthelot mixing rules, the actual interaction potentials between CNT and CO_2 are affected by approximately 5%. Figures 12 and 13 present illustrative adsorption isotherms for the case of unrestricted adsorption ($d = 2$ nm), which clearly indicate that adsorption increases or decreases with either ε or σ. The effect is larger at low pressures, where a 10% change of either ε or σ shifts the adsorption by about 100%. At large pressures, the influence is more like 25%. Thus, possible errors or uncertainties in the dispersion parameters for the solid−fluid interaction, which are much smaller than the extreme cases investigated here, can visibly affect the adsorption. The alteration, however, stays well below a factor of 2. We are therefore confident that the main conclusions of this work (e.g., the fraction of open CNTs, or the influence of the intertube distance) would remain unchanged with a different force-field choice.

■ CONCLUSION

In this work, we have used a combination of molecular simulations and experiments to understand the adsorption mechanism of carbon-dioxide in 3D aligned CNT bundles of variable intertube spacing. Our analysis is compatible with a majority (order of 58%) of the CNTs in experimental 5-nm bundles being open and available for adsorption. Intertube spacing d is found to have a strong effect on the isosteric heat of adsorption q_{st}. A crossover of its behavior is seen in between $d = 0.2$ and 0.5 nm for the case of closed pores. At low $d = 0$ to 0.2 nm, q_{st} first decreases and later increase with loading. The opposite behavior is seen for larger d. The difference in q_{st} behavior is mainly due to a change of adsorption mechanism with d, which is not evident in the adsorption isotherm. Intertube spacing also affects the excess adsorption. For low pressures, $p \leq 14$ bar, maximum adsorption is found for $d = 0.5$ nm. However, at $14 < p < 40$ bar, excess adsorption is found to peak at $d = 1$ nm. In addition, the intertube distance also influences the mechanism and the sequence of adsorption of CO_2 in CNT bundles. At small intertube distances ($d \leq 0.5$ nm), adsorption for the unrestricted case, proceeds from the

groove regions (.i.e. where two CNTs touch) in the following sequence: adsorption in grooves and on inner surface → fill interstitial region → fill inner region. For d > 0.5 nm, the adsorption sequence changes: inner surface adsorption + partial outer surface adsorption → complete outer surface adsorption → fill interstitial, groove and inner regions. A force field parameter sensitivity analysis suggests that the conclusions are invariant to small changes in the force field.

AUTHOR INFORMATION

Corresponding Author

*E-mail: jayantks@iitk.ac.in; f.mueller-plathe@theo.chemie.tu-darmstadt.de.

Notes

The authors declare no competing financial interest.

ACKNOWLEDGMENTS

J.K.S. thanks Parul Katiyar for providing a code for generating carbon nanotube structures and assembly. J.K.S. also thank Alexander von Humboldt Foundation for financial support. We also thank Enrico Riccardi for stimulating discussion. This work was supported by the Priority Programme 1570 *Porous media with well-defined pore structure in chemical engineering: Modelling, application, synthesis* of Deutsche Forschungsgemeinschaft. Part of our experimental work (TEM) is supported by the ERC-TU1 project of Ernst-Ruska Centre (ERC), Jülich, and TU Darmstadt.

REFERENCES

(1) White, C. M.; Smith, D. H.; Jones, K. L.; Goodman, A. L.; Jikich, S. A.; LacCount, R. B.; DuBose, S. B.; Ozdemir, E.; Morsi, B. I.; Schroeder, K. T. Sequestration of Carbon Dioxide in Coal with Enhanced Coalbed Methane RecoverysA Review. *Energy Fuels* **2005**, *19*, 659−725.

(2) Marcott, S. A.; Shakun, J. D.; Clark, P. U.; Mix, A. C. A Reconstruction of Regional and Global Temperature for the Past 11,300 Years. *Science* **2013**, *339*, 1198−1201.

(3) Cinke, M.; Li, J.; Bauschlicher, C. W.; Ricca, A.; Meyyappan, M. CO2 Adsorption in Single-Walled Carbon Nanotubes. *Chem. Phys. Lett.* **2003**, *376*, 761−766.

(4) Futaba, D. N.; Hata, K.; Namai, T.; Yamada, T.; Mizuno, K.; Hayamizu, Y.; Yumura, M.; Iijima, S. 84% Catalyst Activity of Water-Assisted Growth of Single Walled Carbon Nanotube Forest Characterization by a Statistical and Macroscopic Approach. *J. Phys. Chem. B* **2006**, *110*, 8035−8038.

(5) Futaba, D. N.; Hata, K.; Yamada, T.; Hiraoka, T.; Hayamizu, Y.; Kakudate, Y.; Tanaike, O.; Hatori, H.; Yumura, M.; Iijima, S. Shape-Engineerable and Highly Densely Packed Single-Walled Carbon Nanotubes and Their Application as Super-Capacitor Electrodes. *Nat. Mater.* **2006**, *5*, 987−994.

(6) Yamada, T.; Namai, T.; Hata, K.; Futaba, D. N.; Mizuno, K.; Fan, J.; Yudasaka, M.; Yumura, M.; Iijima, S. Size-Selective Growth of Double-Walled Carbon Nanotube Forests from Engineered Iron Catalysts. *Nat. Nanotechnol.* **2006**, *1*, 131−136.

(7) Huang, L.; Zhang, L.; Shao, Q.; Lu, L.; Lu, X.; Jiang, S.; Shen, W. Simulations of Binary Mixture Adsorption of Carbon Dioxide and Methane in Carbon Nanotubes: Temperature, Pressure, and Pore Size Effects. *J. Phys. Chem. C* **2007**, *111*, 11912−11920.

(8) Skoulidas, A. I.; Sholl, D. S.; Johnson, J. K. Adsorption and Diffusion of Carbon Dioxide and Nitrogen through Single-Walled Carbon Nanotube Membranes. *J. Chem. Phys.* **2006**, *124*, 054708−054715.

(9) Einarsson, E.; Shiozawa, H.; Kramberger, C.; Rummeli, M. H.; Gruneis, A.; Pichler, T.; Maruyama, S. Revealing the Small Bundle Internal Structure. *J. Phys. Chem. C* **2007**, *111*, 17861−17864.

(10) Mahdizadeh, S. J.; Tayyari, S. F. Influence of Temperature, Pressure, Nanotube's Diameter and Intertube Distance on Methane Adsorption in Homogeneous Armchair Open-Ended SWCNT Triangular Arrays. *Theor. Chem. Acc.* **2011**, *128*, 231−240.

(11) Kowalczyk, P.; Furmaniak, S.; Gauden, P. A.; Terzyk, A. P. Optimal Single-Walled Carbon Nanotube Vessels for Short-Term Reversible Storage of Carbon Dioxide at Ambient Temperatures. *J. Phys. Chem. C* **2010**, *114*, 21465−21473.

(12) Cruz, J. A. L. F.; Esteves, I. A. A. C.; Agnihotri, S.; Mota, J. P. B. Adsorption Equilibria of Light Organics on Single-Walled Carbon Nanotube Heterogeneous Bundles: Thermodynamics Aspects. *J. Phys. Chem. C* **2011**, *115*, 2622−2629.

(13) Cruz, J. A. L. F.; Esteves, I. A. A. C.; Mota, J. P. B. Adsorption of Light Alkanes and Alkenes onto Single-Walled Carbon Nanotube Bundles: Langmuirian Analysis and Molecular Simulations. *Colloids Surf., A* **2010**, *357*, 43−52.

(14) Cruz, J. A. L. F.; Esteves, I. A. A. C.; Mota, J. P. B.; Agnihotri, S.; Müller, E. A. A Molecular Simulation Study of Propane and Propylene Adsorption onto Single-Walled Carbon Nanotube Bundles. *J. Nanosci. Nanotechnol.* **2011**, *10* (4), 2537−2546.

(15) Cornell, W. D.; Cieplak, P.; Bayly, C. I.; Gould, I. R.; Merz, K. M.; Ferguson, D. M.; Spellmeyer, D. C.; Fox, T.; Caldwell, J. W.; Kollman, P. A. A Second Generation Force Field for the Simulation of Proteins, Nucleic Acids, and Organic Molecules. *J. Am. Chem. Soc.* **1995**, *117*, 5179−5197.

(16) Hummer, G.; Rasaiah, J. C.; Noworyta, J. P. Water Conduction Through the Hydrophobic Channel of a Carbon Nanotube. *Nature* **2001**, *414*, 188−190.

(17) Harris, J. G.; Yung, K. H. Carbon Dioxide's Liquid-Vapor Coexistence Curve And Critical Properties as Predicted by a Simple Molecular Model. *J. Phys. Chem.* **1995**, *99* (31), 12021−12024.

(18) Do, D. D.; Do, H. D. Modeling of Adsorption on Nongraphitized Carbon Surface: GCMC Simulation Studies and Comparison with Experimental Data. *J. Phys. Chem. B* **2006**, *110*, 17531−17538.

(19) Liua, Z.; Horikawa, T.; Do, D. D.; Nicholson, D. Packing Effects on Argon and Methanol Adsorption Inside Graphitic Cylindrical and Slit Pores: A GCMC Simulation Study. *J. Colloid Interface Sci.* **2012**, *368*, 474−487.

(20) Babarao, R.; Hu, Z.; Jiang, J.; Chempath, S.; Sandler, S. I. Storage and Separation of CO2 and CH4 in Silicate, C168 Schwarzite and IRMOF-1: A Comparative Study from Monte Carlo Simulation. *Langmuir* **2007**, *23* (2), 659−666.

(21) Hata, K.; Futaba, D. N.; Mizuno, K.; Namai, T.; Yumura, M.; Iijima, S. Water-Assisted Highly Efficient Synthesis of Impurity-Free Single-Walled Carbon Nanotubes. *Science* **2004**, *306*, 1362−1364.

(22) Ci, L.; Vajtai, R.; Ajayan, P. M. Vertically Aligned Large-Diameter Double-Walled Carbon Nanotube Arrays Having Ultralow Density. *J. Phys. Chem. C* **2007**, *111*, 9077−9080.

(23) Joshi, R.; Engstler, J.; Houben, L.; Bar Sadan, M.; Weidenkaff, A.; Mandaliev, P.; Issanin, A.; Schneider, J. J. Catalyst Composition, Morphology and Reaction Pathway in the Growth of "Super-Long" Carbon Nanotubes. *ChemCatChem* **2010**, *2* (9), 1069−1073.

(24) Ravikovitch, P. I.; Vishnyakov, A.; Russo, R.; Neimark, A. V. Unified Approach to Pore Size Characterization of Microporous Carbonaceous Materials from N2, Ar, and CO2 Adsorption Isotherms. *Langmuir* **2000**, *16* (6), 2311−2320.

(25) Ravikovitch, P. I.; Neimark, A. V. Density Functional Theory Model of Adsorption on Amorphous and Microporous Silica Materials. *Langmuir* **2006**, *22*, 11171−11179.

(26) Brunauer, S.; Emmett, P. H.; Teller, E. Adsorption of Gases in Multimolecular Layers. *J. Am. Chem. Soc.* **1938**, *60*, 309−319.

(27) Keller, J. U.; Staudt, R. *Gas Adsorption Equilibria: Experimental Methods and Adsorptive Isotherms*; Springer: New York, 2005.

(28) Ren, X.; Chen, C.; Nagatsu, M.; Wang, X. Carbon Nanotubes as Adsorbents in Environmental Pollution Management: A Review. *Chem. Eng. J.* **2011**, *170*, 395−410.

(29) Yang, Q.-H.; P-X., H.; Bai, S.; Wang, M.-Z.; Cheng, H.-M. Adsorption and Capillarity of Nitrogen in Aggregated Multi-Walled Carbon Nanotubes. *Chem. Phys. Lett.* **2001**, *345*, 18−24.
(30) Li, Z.; Pan, Z.; Dai, S. Nitrogen Adsorption Characterization of Aligned Multiwalled Carbon Nanotubes and Their Acid Modification. *J. Colloid Interface Sci.* **2004**, *277*, 35−42.
(31) Inoue, S.; Ichikuni, N.; Suzuki, T.; Uematsu, T.; K., K. Capillary Condensation of N2 on Multiwall Carbon Nanotubes. *J. Phys. Chem. B* **1998**, *102*, 4689−4692.
(32) Thommes, M. Physical Adsorption Characterization of Nanoporous Materials. *Chemie Ingenieur Technik* **2010**, *82*, 1059−1073.
(33) Talapatra, S.; Migone, A. D. Adsorption of Methane on Bundles of Closed-Ended Single-Wall Carbon Nanotubes. *Phys. Rev. B* **2002**, *65*, 045416−045422.
(34) Johnson, M. R.; Rols, S.; Wass, P.; Muris, M.; Bienfait, M.; Zeppenfeld, P.; Dupont-Pavlovsky, N. Neutron Diffraction and Numerical Modelling Investigation of Methane Adsorption on Bundles of Carbon Nanotubes. *Chem. Phys.* **2003**, *293*, 217−230.

THE JOURNAL OF PHYSICAL CHEMISTRY C

Article

pubs.acs.org/JPCC

CO_2 Adsorption on Charged Carbon Nanotube Arrays: A Possible Functional Material for Electric Swing Adsorption

Mahshid Rahimi,*[,†] Jayant K. Singh,[†,‡] and Florian Müller-Plathe[†]

[†]Technische Universität Darmstadt, Eduard-Zintl-Institut für Anorganische und Physikalische Chemie and Center of Smart Interfaces, Alarich-Weiss-Str. 4, D-64287 Darmstadt, Germany

[‡]Department of Chemical Engineering, Indian Institute of Technology Kanpur, Kanpur 208016, India

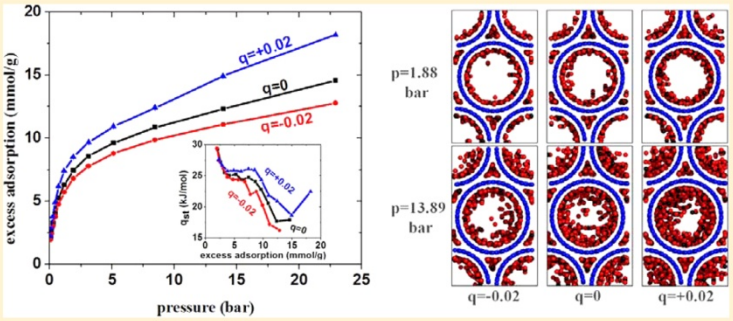

ABSTRACT: The adsorption and orientational ordering of carbon dioxide molecules on parallel bundles of charged as well as uncharged carbon nanotubes were investigated at 300 K using grand canonical Monte Carlo and molecular dynamics. Zigzag and armchair single-walled carbon nanotubes of radius ∼1.5 nm and different intertube distances between 0 and 2 nm were used. A fixed charge of 0.01−0.04*e* was placed on each carbon to investigate the effect of charge. Adding a positive charge to the carbon nanotubes causes a significant increase in adsorption (up to 35% at a pressure of 1.88 bar), while the gas adsorption decreases by up to 15% on negatively charged carbon nanotubes. The increase or decrease of adsorption upon charging is attributed to the change in potential energy for the interaction between the individual carbon dioxide molecule and the nanotube. The higher adsorption on positively charged nanotubes leads to thicker adsorbed layers and a lower orientational order of the adsorbed molecules.

1. INTRODUCTION

Global warming is one of the important environmental concerns of our age. The anthropogenic increase of greenhouse gases in the atmosphere is blamed as its main reason. Among all greenhouse gases, the predominant one is CO_2 since it causes about 60% of global warming.[1] A reduction of CO_2 emissions to the atmosphere is therefore an objective declared by governments and industry alike.[2,3] One contribution to an overall strategy is CO_2 adsorption and separation using various materials[4] like zeolites,[5] activated carbon,[6] metal−organic frameworks (MOFs),[7,8] and carbon nanotubes (CNTs).[9]

In 1997, Dillon and co-workers[10] showed for the first time CNTs as a potential medium for gas storage with high density. Since then, CNTs have been tried for storing different gases like H_2, SO_2, NO_2, CH_4, and CO_2. Key properties of the CNTs are, among others, their large specific area and their well-defined adsorption sites.[11] The geometrical parameters of CNTs have been considered in many works. Kowalczyk et al.[12] used the grand canonical Monte Carlo (GCMC) technique to find an optimal CNT for CO_2 adsorption at 298 K and reported that its optimum size depends on the storage pressure. Furthermore, they showed that chirality does not have a strong effect on CO_2 adsorption, while there is an obvious dependence on the tube diameter. A similar dependence of the adsorption on chirality and tube diameter has been found for H_2 adsorption by molecular dynamics (MD) calculations.[13] Bundles of CNTs are known to adsorb gases better than isolated tubes, because between the CNTs new possible sorption sites are formed, which have higher adsorptivity than the CNT walls. Zhao et al.[14] used density functional theory (DFT) to study adsorption of various gases on single-walled CNTs and bundles of them. They observed a better adsorption on interstitial (region limited by three CNTs) and groove sites (region between two opposite CNT surfaces; for an image, see Figure 1 in ref 15, for example) of the bundles than that on individual tubes. Do et al.[15] used Monte Carlo integration to calculate Henry constant and isosteric heat of adsorption in single-walled and double-walled CNT bundles. They showed that the amount of adsorption in bundles of double-walled CNT is lower than that in single-walled CNT bundles. Recently

Received: March 25, 2015
Revised: June 5, 2015
Published: June 8, 2015

DOI: 10.1021/acs.jpcc.5b02874
J. Phys. Chem. C 2015, 119, 15232−15239

Babu and co-workers[16] experimentally investigated CO_2 and N_2 adsorption in parallel-aligned arrays of double-walled CNT with the inner diameter of 5 and 8 nm. They found that with decreasing CNT diameter, the gas adsorption in CNT bundles increases. Bienfait et al.[9] used adsorption isotherms, isosteric heat of adsorption, and neutron diffraction measurements of different gases to study the adsorption locally. They showed that grooves are the best sites for adsorption. This result was confirmed theoretically by GCMC studies.[17] Moreover, in this GCMC study, it was indicated that intertube distance does not linearly affect the CO_2 adsorption. At low pressure ($p < 14$ bar), intertube distance of 0.5 nm shows the maximum adsorption. Further increase in pressure changes the optimum intertube distance to 1 nm.

Pure CNTs are not the only promising material for gas adsorption since doping with metal atoms can alter the charge distribution of CNTs[18] and lead to a better adsorption. Deng and co-workers[19] used GCMC simulations to show that Li-doped single-walled CNTs can store hydrogen up to 6.5 mass % H_2 at 50 bar at room temperature. Chen and co-workers[20] analyzed charge distribution of gas molecules adsorbed on Li-doped graphene nanostructures using DFT. They analyzed three different sites (on top of a carbon, on top of a C−C bond, on top of the center of a hexagonal ring) and found Li on top of the center of hexagonal ring as a stable configuration. In the stable configuration, they showed that Li^+ cations polarize CH_4 and also caused charge transfer from CO_2 and H_2S to the substrate. Thus, it enhances the adsorption interaction. Replacing one of the carbons of a CNT with another atom, which is called doping proper, is another way to perturb charge distribution of the CNT. Recently, a DFT investigation of the electronic structure of CO_2 interacting with pristine and cobalt-doped single-walled CNTs[21] claimed that doping with cobalt increases the binding energy specifically in zigzag CNTs. Zhou et al. used DFT calculations to study the effect on hydrogen adsorption of integrating B and N in single-walled CNTs.[22] The electron density distribution for pure, B-doped, and N-doped single-walled CNTs shows that doping with B produces an electron-deficient six-membered ring structure while doping with N produces an electron-rich six-membered ring structure. Nevertheless, in both cases the adsorption energy decreases.

Increasing or decreasing adsorption in CNTs upon doping suggests that the charge distribution has a key role in adsorption. Consequently, electric swing adsorption (ESA) for CO_2 capture with carbon-base sorbents has been suggested, because graphitic or CNT-based materials are electrically conductive and can thus be charged and discharged easily.[23] This technology can apply and remove electrical charges on the sorbent, causing rapid adsorption and desorption of CO_2. A recent review summarized the fundamentals of ESA.[24] Stoian and co-workers[25] used femtosecond laser pulses for charging the surface of dielectrics, semiconductors, and metals. Zdrojek and co-workers[26] studied charge injection experiments on CNTs using electric force microscopy (EFM). They stated that charge storage in the CNT and in the oxide layers along the CNT is the reason for observed charge patterns. The other suggested procedure for producing charged CNTs is mounting the CNT array electrically insulated from the container, so container walls can be the oppositely charged plate of a capacitor. However, studies on charged CNTs are still limited. Electronic structures of charged single-walled CNTs have been studied in detail using DFT.[27] Simonyon and co-workers[28] used GCMC to explore hydrogen adsorption on charged single-walled CNTs. They observed that extra charge on the CNTs generally increases adsorption. In addition, at 77 K, negatively charged CNTs adsorb H_2 more than positively charged CNTs, but at 298 K, there is no difference between these two cases.

In this work, we study the effect of negative and positive extra charge in parallel-aligned bundles of single-walled CNTs on the magnitude of CO_2 adsorption. In addition, we investigate the mechanism by which CNT charge enhances or decreases CO_2 adsorption and the structure arising in the adsorbed gas layers. With this investigation we wish to contribute to the discussion as to whether these CNT arrays, which are already very good functional materials for CO_2 sequestration, can be further improved by electrically contacting them so that they can be easily charged and discharged as required.

2. METHOD AND MODEL

Bundles of single-walled CNTs were arranged in a hexagonal lattice so that two CNTs were in the periodic simulation box (Figure 1). Armchair and zigzag CNTs, (22, 22) and (38, 0),

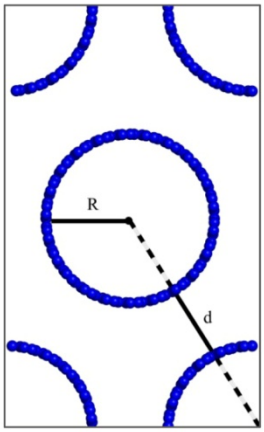

Figure 1. A schematic view of the simulation box as used in this work with radius of R and intertube distance of d.

with a radius of R = 1.492 and 1.488 nm and a length of 4.19 and 5.12 nm (with period continuation) were studied. The C−C bond length was taken to be 0.142 nm, and the intertube distances (surface-to-surface) were varied from d = 0 to 2 nm. In total, there were 3520 and 3648 C atoms for armchair and zigzag configurations, respectively. For charged CNTs, a fixed amount of charge was place on all carbon atoms in the CNT (q = ±0 to 0.04e per carbon atom).

The CNTs were considered as rigid structures with a Lennard-Jones potential as in the AMBER96 force field (ε = 0.36 kJ/mol, σ = 0.34 nm).[29] This model has been used in similar work.[17,30] Carbon dioxide was modeled by the EPM2 model of Harris and Yung, which describes it as a three-site rigid molecule with Lennard-Jones interactions and partial charges (σ_{C-C} = 0.2757 nm, ε_{C-C} = 0.23388 kJ/mol, σ_{O-O} = 0.3033 nm, ε_{O-O} = 0.66837 kJ/mol, q_O = −0.3256e, q_C = 0.6512e, l_{C-O} = 1.149 Å).[31] The Lorentz−Berthelot mixing rules were used to calculate the cross-action parameter of the Lennard-Jones potential. The smooth particle-mesh Ewald (SPME)[32] method was used for the electrostatic interactions.

CO_2 adsorption isotherms were simulated by the grand-canonical Monte Carlo (GCMC) method where the temper-

DOI: 10.1021/acs.jpcc.5b02874
J. Phys. Chem. C 2015, 119, 15232−15239

ature T, the chemical potential μ, and the volume V are held constant during the simulation. The chemical potential was converted to a pressure by considering CO_2 as an ideal gas. Our interest has been mainly to see the change in the adsorption behavior due to the charge; more accurate chemical potential would not change the qualitative picture at high pressure. Several simulations with different chemical potential were performed to cover the pressure region between 0.1 and 22.9 bar. The relative probabilities for the three MC moves were displacement 0.2, rotation 0.1, and molecule insertion/removal 0.7. During the equilibration, the maximum allowed displacement and rotation of the molecules was adjusted so that half of the trial moves were accepted. For each simulation run, 2×10^7 Monte Carlo steps were used, the first 10^7 steps for equilibration and the rest for production. The simulation output is the average of the total number of CO_2 molecules in the simulation box, which is called *absolute* adsorption N_{ad}. Depending on the system, average values ranged between 30 molecules (0.1 bar) and 1300 molecules (23 bar). The value measured in experiment is the *excess* adsorption, N_{ex}, which can be obtained from the absolute adsorption by

$$N_{ex} = N_{ad} - \rho_b V_{free} \quad (1)$$

The bulk number density, ρ_b, is obtained by simulating the bulk fluid at the same thermodynamic conditions. The free volume V_{free} is the volume not occupied by carbon nanotubes. It is calculated from the geometry of the CNT bundles, as described by Mahdizadeh et al.[33] In the discussions and in the figures, the raw excess adsorption of eq 1 has been converted into the customarily used unit, mmol CO_2 per gram of carbon nanotube.

The derivative of the adsorption energy with respect to the absolute adsorption, which is called isosteric heat of adsorption, q_{st}, reflects the strength of adsorbent−adsorbate interaction[34] and can be calculated approximately as[35]

$$q_{st} \approx RT - \left(\frac{\partial U_{ad}}{\partial N_{ad}}\right)_{T,V} \quad (2)$$

where U_{ad} is the intermolecular energy of the system. With this sign convention, a higher value of q_{st} signifies stronger adsorption. Using fluctuation theory, eq 2 can be brought into the form used here

$$q_{st} \approx RT - \frac{\langle U_{ad}N_{ad}\rangle - \langle U_{ad}\rangle\langle N_{ad}\rangle}{\langle N_{ad}^2\rangle - \langle N_{ad}\rangle^2} \quad (3)$$

In order to observe the density profile and orientational ordering of CO_2, we performed molecular dynamics (MD) simulations with the same force field and at the same thermodynamic conditions using configurations of the MC simulations as input: A configuration near the end of the MC run was chosen, which happened to have a number of CO_2 molecules equal to the average of the GCMC production run. The MD simulations were then carried out in the NVT ensemble using DL-POLY package.[36] The number of CO_2 molecules varied between 287 and 680 for the different systems. In addition to the pre-equilibration by MC, the MD simulations were further equilibrated for 3 ns, before data were collected for 7 ns. The temperature is controlled by Nose−Hoover thermostat with relaxation constant of 0.1 ps. A time step of 1 fs was used, and all data were saved every 1000 fs for analysis. In both MC and MD simulations, the temperature was fixed at T = 300 K, the cutoff distance for the Lennard-Jones interactions was r_c = 1.0 nm and orthorhombic periodic boundary conditions were applied in all directions.

3. RESULT AND DISCUSSION

3.1. Effect of Carbon Nanotube Charge. The excess adsorption isotherms for parallel bundles of 3 nm diameter single-walled CNTs, of both zigzag and armchair configurations, intertube distance of d = 0, and charges per C atom of q = 0, −0.02e and 0.02e are given in Figure 2. As expected, in all three armchair systems (shown by lines in Figure 2), the CO_2 excess adsorption increases with the pressure. Moreover, positive charges on the CNTs lead to a significant increase of the CO_2 excess adsorption in the whole pressure region (+15% at p = 1.88 bar and +22% at p = 13.89 bar). In contrast, negative charges decrease the CO_2 excess adsorption (−8% at p = 1.88 bar and −10% at p = 13.89 bar). All curves can be fitted by Freundlich isotherms and show multilayer adsorption for the three systems. Isosteric heats of adsorption of the three systems as a function of excess adsorption are shown in Figure 3. For all three systems, q_{st} decreases initially (< ∼ 4 mmol/g) with increasing the excess adsorption, then it remains almost constant and finally decreases again (>7.5 mmol/g). The initial decrease is due to the fact that in the grooves region high carbon density causes strong interaction between CO_2 and CNT. Thus, the grooves which are the favorable sites for the

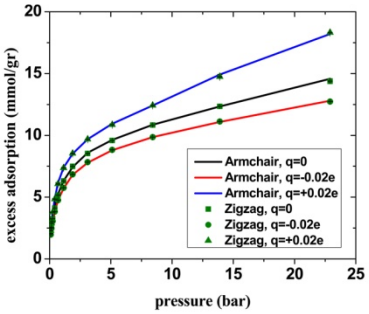

Figure 2. Excess adsorption isotherms of CO_2 in single-walled carbon nanotube arrays, zigzag and armchair, with tube radius $R \approx 1.5$ nm and intertube distance d = 0 nm, for different extra charges q = 0, −0.02e, and +0.02e. T = 300 K. Error bars are smaller than the symbols.

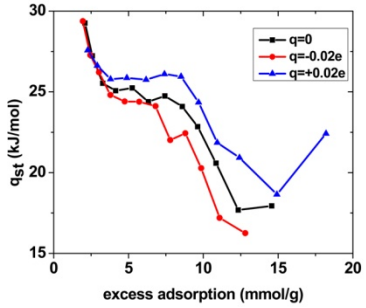

Figure 3. Isosteric heat of adsorption of CO_2 in single-walled carbon nanotube arrays, armchair, with tube radius $R \approx 1.5$ nm and intertube distance d = 0 nm for different extra charge q = 0, −0.02e, and 0.02e. T = 300 K.

DOI: 10.1021/acs.jpcc.5b02874
J. Phys. Chem. C 2015, 119, 15232−15239

adsorption are occupied first. When they have been filled q_{st} shows a plateau, which means that less favorable surface sites of equal energy are filling. The final decrease shows that a second adsorption layer is forming. For the pressure range studied in this work, q_{st} of positively charged CNTs is larger than neutral CNTs; and negatively charged CNTs have the lowest heat of adsorption. Thus, the adsorbent−adsorbate interaction is strongest on positively charged CNTs. Figure 4 presents

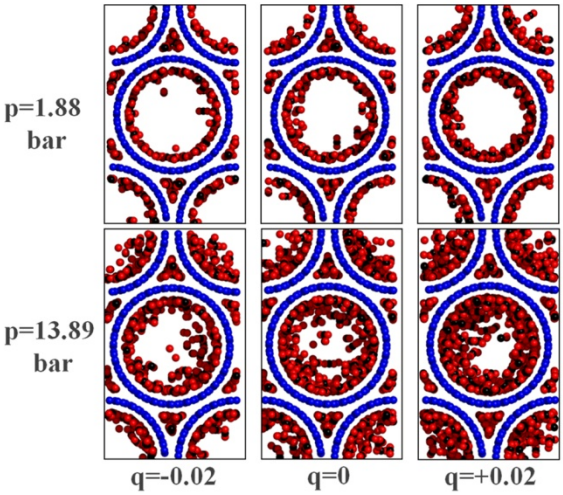

Figure 4. Snapshots of adsorption at p = 1.88 bar (top) and p = 13.89 bar (bottom), T = 300 K, tube radius $R \approx$ 1.5 nm, and intertube distance d = 0 nm for systems (a) $q = -0.02e$, (b) $q = 0$, and (c) $q = +0.02e$.

snapshots of armchair systems with d = 0 at p = 1.88 bar and p = 13.89 bar and different charge states. They show that the number of CO_2 outside the CNTs (the interstitial volume between the CNTs) is indifferent to the charge. In contrast, inside the CNTs, the first CO_2 layer is completely formed for all three charge states at p = 1.88 bar, but it becomes thicker from negative to positive charge. At p = 13.89, the thickening of the first layer from negative to positive charge is also visible. In addition, there are only traces of a second layer being formed for $q = -0.02e$, whereas the second layer is completely formed for $q = +0.02e$.

In previous studies,[13,12] it was shown that tube chirality does not affect gas adsorption on uncharged CNTs. To check whether chirality is inconsequential also for adsorption on charged nanotubes, the excess adsorption on zigzag CNTs with similar diameter as the armchair tube was studied, while keeping all other system parameters the same. The corresponding excess adsorption isotherms are shown by symbols in Figure 2. They fall right on top the armchair curves and show that chirality does not play any role on CO_2 adsorption. The isotherms show the same dependence on the charge status of the CNTs.

In order to study the effect of CNT charge in more detail, we started from an uncharged armchair system at a pressure p = 1.88 bar and increased the extra positive and negative charge to $\pm 0.04e$. Figure 5 shows the excess adsorption as a function of CNT charge. The curve can be fitted very well with the following equation:

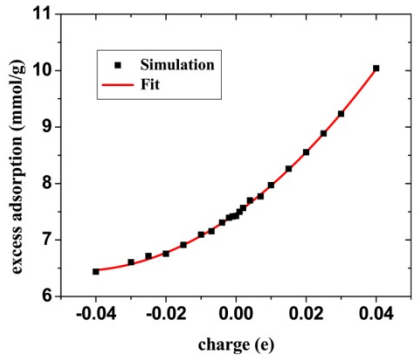

Figure 5. Excess adsorption of CO_2 in single-walled armchair carbon nanotube arrays as a function of nanotube charge; d = 0 nm, p = 1.88 bar, and T = 300 K.

$$N_{ex} = A_1 q^2 + A_2 q + A_3 \quad (4)$$

where A_1, A_2, and A_3 are fitting parameters with values of 485.96 ± 12.52 mmol/ge^2, 44.50 ± 0.31 mmol/ge, and 7.47 ± 0.01 mmol/g, respectively. At a fixed pressure, positive charging of the CNT increases the adsorption by up to 35%. On the other hand, negative charging of the CNT reduces the adsorption by up to 15%. Thus, adsorption and desorption can be modulated by the CNT charge, while keeping the pressure constant.

3.2. Structure of the Adsorbed Layer at Different Charge States. To find the molecular explanation of the increased/decreased CO_2 adsorption on positively/negatively charged CNTs, we used MD calculations. The density profile of the armchair system at the three charge states and two different pressures, p = 1.88 and 13.89 bar is presented in Figure 6. Outside the CNT, the density increases with pressure, whereas it is indifferent to the charge, confirming the qualitative observations in the snapshots of Figure 4. The indifference to charge is owed to the outer, intertube volume being small and,

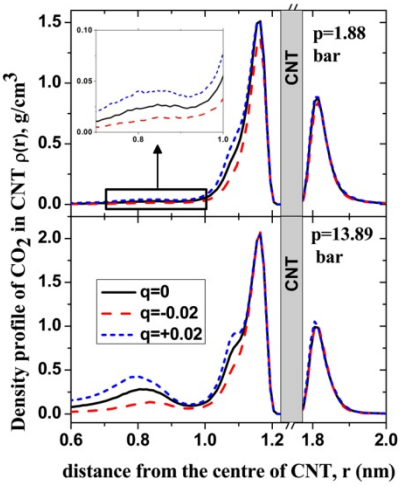

Figure 6. Density profile for single-walled carbon nanotube, armchair, with tube radius $R \approx$ 1.5 nm and intertube distance d = 0 nm, at fixed pressure (top, p = 1.88 bar; bottom, 13.89 bar), for different extra charge q = 0, −0.02e, and 0.02e. T = 300 K.

DOI: 10.1021/acs.jpcc.5b02874
J. Phys. Chem. C 2015, 119, 15232−15239

hence, becoming saturated soon. Inside the neutral CNT at p = 1.88 bar, one layer of CO_2 is formed. At the low pressure, however, the first layer is incomplete, and consequently, the second layer is not formed. For the positively charged CNTs, the maximum density in the first layer is almost equal to that of the neutral CNTs. However, it is thicker for the positive than that for the uncharged system. Besides, a second layer starts to appear, although the first layer is still not saturated. Most of the additional CO_2 is, thus, accommodated by thickening of the first layer. The reverse is observed for the negatively charged CNTs: not only is the first layer thinner than for the neutral system, but also the maximum value of the density is 9% lower. In addition, like in the uncharged system, there is no significant second layer. Hence, negatively charged CNT bundles have the lowest adsorption. At p = 13.89 bar, the difference between the thicknesses of the first CO_2 layers of the three charge states increases. At this higher pressure, a second CO_2 layer develops inside the CNT. Its maximum density decreases from positive to neutral to negative CNTs. In the positively charged systems, the second layer of CO_2 is fully formed, while in negatively charged system it is just beginning to grow (cf. Figure 4). The density profiles of the corresponding zigzag systems are identical confirming that tube chirality has no effect on the structure of the adsorbed layers. Figure 7 represents the density

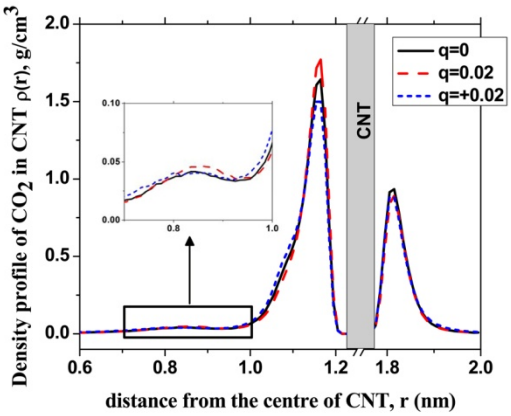

Figure 7. Density profile for single-walled carbon nanotube, armchair, with tube radius $R \approx 1.5$ nm and intertube distance d = 0 nm, for different extra charge q = 0, −0.02e, and 0.02e and different pressure at a constant N_{ex} = 8.5 mmol/g. T = 300 K.

profiles of three systems with different charge state, whose pressures have been selected in a way that N_{ex} = 8.5 mmol/g, that is, the number of CO_2 molecules are equal. Outside the CNT, the density is again indifferent to the charge state. Inside the CNT, the negatively charged CNT has the highest maximum value of the density followed by neutral and positively charged CNTs. The difference in the thickness of first layers exist; however it is less than in Figure 6.

The orientation and alignment of CO_2 molecules and their dependence on pressure and CNT charge is measured by three angle distributions: the angle between the molecular axes of neighboring CO_2 molecules α, the angle between the molecular axis of a CO_2 molecule and the surface normal of the carbon nanotube θ, and the angle between the molecular axis of a CO_2 molecule and the axis of the CNT φ. The first two orientations are characterized by the second Legendre polynomial (equation with β):

$$P_2 = \left\langle \frac{3}{2}\cos^2\beta - \frac{1}{2} \right\rangle \quad (5)$$

where β is angle α or θ. When P_2 = −0.5, all vectors are perpendicular, while P_2 = 1 means that all vectors are parallel. A random distribution of orientations leads to P_2 = 0. Figure 8

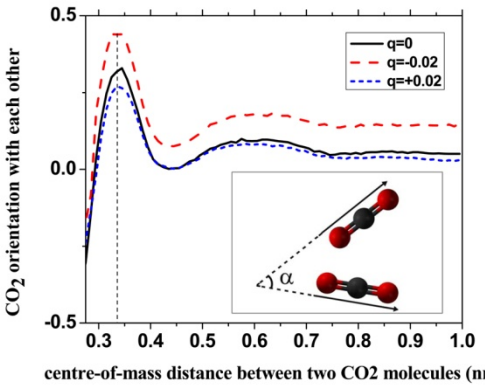

Figure 8. Mutual orientation of CO_2 molecules with respect to each other in the first layer (distance from CNT axis is from r = 1.0 nm to r = 1.3 nm) on the inside of armchair CNTs: second Legendre polynomial of the cosine of the angle α between their molecular axes P_2, as a function of their distance; intertube distance d = 0 nm, p = 1.88 bar, and T = 300 K.

presents the mutual orientation of CO_2 molecules P_2, in the first layer inside an armchair CNT (from r = 1.0 nm to r = 1.3 nm in the notation of Figures 6 and 7) at p = 1.88 bar. At very short distances, P_2 is negative, but it is positive everywhere else with a maximum at a distance of 0.34 nm. The mutual orientation of molecules is therefore predominantly parallel. The height of the maximum decreases from 0.43 for negatively charged CNTs to 0.32 for neutral CNTs and 0.26 for positively charged CNTs. This trend continues at all distances: the negative CNT induces more intermolecular alignment than the neutral or the positive CNT. We believe that the differences in the degree of alignment depend on the CNT charge indirectly through the thickness of the adsorbed layer. The negative CNT has the lowest adsorption and the thinnest adsorbed layer. In a thin layer, molecules are forced flat onto the surface and, because of the common orientation with respect to the surface, they also are more highly oriented with respect to one another.

The hypothesis that layer thickness (and thus molecule confinement) is the mechanism to create orientation among the adsorbed CO_2 molecules also shows in their orientation angle with respect to the CNT surface normal θ. The second Legendre polynomial of its distribution for an armchair CNT is shown in Figure 9. It is first observed, that in all charge states, the distributions of the first layer inside and outside of the CNT are symmetric. Second, within the first and second layer inside the CNT (density peaks at ∼1.05−1.2 nm and ∼0.7−0.9 nm, cf. Figure 6) as well as on the outside (∼1.8−1.9 nm), P_2 is negative and indicates the favorable orientation for CO_2 molecules to be perpendicular to the surface normal. Only around the density minima between the layers, for example between 0.9 and 1.05 nm, is P_2 positive. This means that the

DOI: 10.1021/acs.jpcc.5b02874
J. Phys. Chem. C 2015, 119, 15232−15239

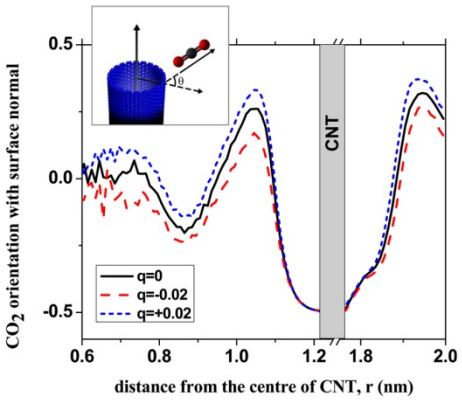

Figure 9. Orientation of CO_2 molecules with respect to the surface of armchair CNTs. Second Legendre polynomial of the cosine of the angle between the molecular axis and the surface normal θ, P_2; intertube distance d = 0 nm, p = 1.88 bar, and T = 300 K.

few molecules residing here, tend to orient parallel to the surface normal. Third, at all distances, P_2 is highest for positively and lowest for negatively charged CNTs. The negative charge causes a lower CO_2 adsorption, thinner layers and more confinement, forcing the CO_2 molecules to lie flat on the CNT surface, in line with the arguments above. Fourthly, the orientation distributions of CO_2 on zigzag CNTs are very similar those on armchair CNTs.

The orientation of CO_2 molecules in the first layer (from r = 1.0 nm to r = 1.3 nm) inside the armchair CNTs relative to the CNT axis is illustrated in Figure 10. There are visible

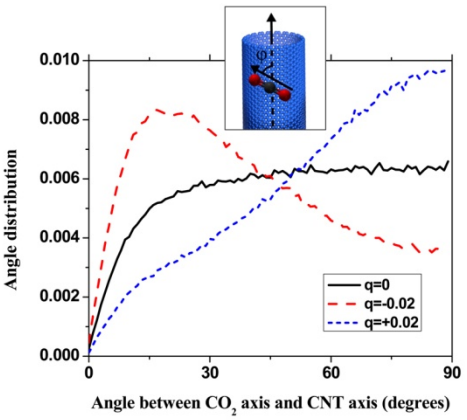

Figure 10. Orientation of CO_2 molecules with respect to the CNT axis in the first layer (distance from CNT axis is from r = 1.0 nm to r = 1.3 nm) inside the armchair CNT: Second Legendre polynomial of the cosine of the angle ϕ between the molecular axes and the CNT axis; intertube distance d = 0 nm, p = 1.88 bar, and T = 300 K.

differences. Molecules inside positive CNTs prefer to be perpendicular to the CNT axis, whereas inside a negative CNT, there is a maximum for near-parallel orientation (~15°). Inside a neutral tube, the CO_2 orientation is nearly uniform between 20° and 90°. To investigate the reason, we optimized the position and orientation of one single CO_2 molecule inside negative, neutral, and positive CNTs. For this purpose, we used conjugate gradients minimization combined with MD: the energy is minimized by 10 conjugate gradient steps, interlaced with 100 MD steps at low temperature (at 25 K). The cycle of alternating minimization and MD continues for a total MD time of 3 ns. The energy-minimized angles are 0.0°, 50.9°, and 80.0° and the minimum energies are −22.94, −22.88, and −24.96 kJ/mol for negative, neutral, and positive CNTs, respectively (Figure 11). The optimum angles are not the same for individual molecules as for dense layers (Figure 10). Probably, the mutual orientation of CO_2 molecules has a more important role than their orientation with respect to the carbons of the CNT surface. The lowest single-molecule optimum energy belongs to positively charged CNTs. This is the underlying reason that this system shows the maximum adsorption in three studied systems. The optimized energies of negatively charged and uncharged systems are almost the same. We finally note that the angle distributions in the first layer of zigzag systems closely resemble those of armchair systems (not shown).

3.3. Effect of Intertube Distance. We repeated the grand-canonical MC calculations for armchair systems with q = 0, −0.02e, and 0.02e for intertube distances d = 0−2 nm. The CO_2 excess adsorption isotherms are shown in Figure 12. For all intertube distances, the same sequence as for d = 0 is observed: the excess adsorption decreases from positive to neutral and to negative nanotubes.

The effect of intertube distance is almost the same in charged and uncharged CNTs. At low pressures (p < 8 bar), the adsorption increases significantly from d = 0 to 0.5 nm, but it does not have a linear behavior. Further increase of d reduces the adsorption again. Therefore, at low pressures, there is a maximum of adsorption at d = 0.5 nm. Increasing the pressure shifts the optimum d because more space needs to be filled before saturation. The shift, however, depends on the CNT charge. It is $p \approx 8$, 9, and 10 bar for positive, uncharged, and negative CNTs, respectively. This is because the system with higher adsorption saturates before the others. At high pressures (p > 10 bar), the CNT array with intertube distances of d = 1 nm shows the maximum adsorption. Further increase of d reduces the adsorption again.

Comparing the adsorption on neutral nanotubes in this work, with our previous work[17] on the effect of the intertube distance on CO_2 adsorption in arrays of neutral double-wall CNTs with a radius of r = 2.5 nm, we observe the same optimum values for the intertube distance at low and high pressures.

4. CONCLUSION

In this work, we used a combination of molecular dynamics and grand canonical Monte Carlo to understand the mechanism of CO_2 adsorption on charged and uncharged carbon nanotube arrays. Parallel bundles of armchair and zigzag single-wall CNTs with a constant radius of $R \approx$ 1.5 nm but different intertube distances of d = 0−2 nm were considered. To observe the charge effect, a fixed charge between 0.01e and 0.04e was placed on each carbon atom of the CNTs. The adsorption increases significantly when the CNTs have a positive charge, while a negative charge causes the adsorption to decrease compared with neutral CNT arrays. Furthermore, the adsorption is indifferent to the tube chirality in both charged and uncharged states. We have also clarified the structure of the adsorbed layers at different pressures and charge states and found that the higher adsorption on positive CNTs corresponds to thicker adsorption layers at the same pressure, which in turn cause

DOI: 10.1021/acs.jpcc.5b02874
J. Phys. Chem. C 2015, 119, 15232−15239

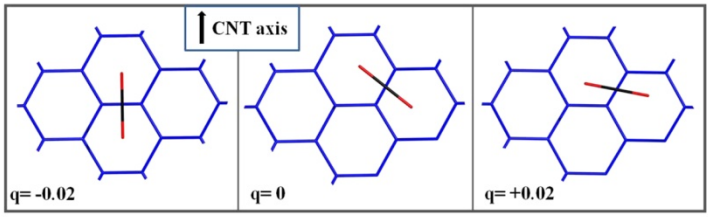

Figure 11. Location and orientation of a single CO_2 on the inside of an armchair nanotube after energy minimization.

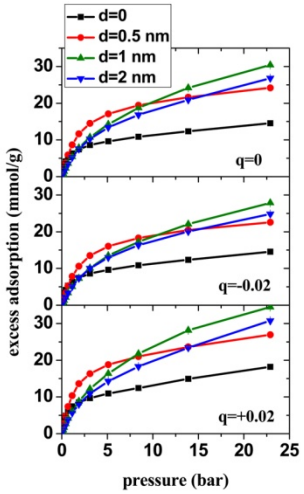

Figure 12. Excess adsorption isotherm of CO_2 in single-walled armchair CNT arrays with tube radius $R \approx 1.5$ nm. The intertube distance, d, is varied from 0 to 2 nm. $T = 300$ K.

more orientational disorder among the adsorbed CO_2 molecules.

These results have possible technological implications. Charging the CNT positively to a charge per carbon atom of $+0.04e$, at constant pressure of 1.88 bar, increases the excess adsorption by one-third; charging it negatively to $q = -0.04e$ reduces it by about 1/6. The existence of this charge effect on adsorption is beyond doubt, although its magnitude may depend on simulation details. This indicates that gas adsorption and desorption could technically be driven by charging and discharging the CNT array. Similar gas loadings could be achieved as by changing the pressure, which could open the way to very small adsorption/release devices and gas pumps.

AUTHOR INFORMATION

Corresponding Author

*E-mail: f.mueller-plathe@theo.chemie.tu-darmstadt.de. Phone: +49 6151 166 524.

Notes

The authors declare no competing financial interest.

ACKNOWLEDGMENTS

M.R. thanks Mohammad Rahimi and Evangelos Voyiatzis for valuable comments and discussion. This work was supported by the Priority Programme 1570 *Porous media with well-defined pore structure in chemical engineering: Modelling, application, synthesis* of Deutsche Forschungsgemeinschaft.

REFERENCES

(1) Yamasaki, A. An Overview of CO_2 Mitigation Options for Global Warming-Emphasizing CO_2 Sequestration Options. *J. Chem. Eng. Jpn.* **2003**, *36*, 361−375.

(2) White, C. M.; Smith, D. H.; Jones, K. L.; Goodman, A. L.; Jikich, S. A.; LaCount, R. B.; DuBose, S. B.; Ozdemir, E.; Morsi, B. I.; Schroeder, K. T. Sequestration of Carbon Dioxide in Coal with Enhanced Coalbed Methane Recovery—A Review. *Energy Fuels* **2005**, *19*, 659−724.

(3) D'Alessandro, D. M.; Smit, B.; Long, J. R. Carbon Dioxide Capture: Prospects for New Materials. *Angew. Chem., Int. Ed.* **2010**, *49*, 6058−6082.

(4) Hedin, N.; Chen, L.; Laaksonen, A. Sorbents for CO(2) Capture from Flue Gas–Aspects from Materials and Theoretical Chemistry. *Nanoscale* **2010**, *2*, 1819−1841.

(5) Sun, W.; Lin, L.-C.; Peng, X.; Smit, B. Computational Screening of Porous Metal-Organic Frameworks and Zeolites for the Removal of SO_2 and NO_X from Flue Gases. *AIChE J.* **2014**, *60*, 2314−2323.

(6) Zhou, X.; Yi, H.; Tang, X.; Deng, H.; Liu, H. Thermodynamics for the Adsorption of SO_2, NO and CO_2 from Flue Gas on Activated Carbon Fiber. *Chem. Eng. J.* **2012**, *200−202*, 399−404.

(7) Abid, H. R.; Ang, H. M.; Wang, S. Effects of Ammonium Hydroxide on the Structure and Gas Adsorption of Nanosized Zr-MOFs (UiO-66). *Nanoscale* **2012**, *4*, 3089−3094.

(8) Peng, X.; Cheng, X.; Cao, D. Computer Simulations for the Adsorption and Separation of $CO_2/CH_4/H_2/N_2$ Gases by UMCM-1 and UMCM-2 Metal Organic Frameworks. *J. Mater. Chem.* **2011**, *21*, 11259−11270.

(9) Bienfait, M.; Zeppenfeld, P.; Dupont-Pavlovsky, N.; Muris, M.; Johnson, M.; Wilson, T.; DePies, M.; Vilches, O. Thermodynamics and Structure of Hydrogen, Methane, Argon, Oxygen, and Carbon Dioxide Adsorbed on Single-Wall Carbon Nanotube Bundles. *Phys. Rev. B* **2004**, *70*, No. 035410.

(10) Dillon, A. C.; Jones, K. M.; Bekkedahl, T. A.; Kiang, C. H.; Bethune, D. S.; Heben, M. J. Storage of Hydrogen in Single-Walled Carbon Nanotubes. *Nature* **1997**, *386*, 377−379.

(11) Ren, X.; Chen, C.; Nagatsu, M.; Wang, X. Carbon Nanotubes as Adsorbents in Environmental Pollution Management: A Review. *Chem. Eng. J.* **2011**, *170*, 395−410.

(12) Kowalczyk, P.; Furmaniak, S.; Gauden, P. A.; Terzyk, A. P. Optimal Single-Walled Carbon Nanotube Vessels for Short-Term Reversible Storage of Carbon Dioxide at Ambient Temperatures. *J. Phys. Chem. C* **2010**, *114*, 21465−21473.

(13) Cheng, H.; Cooper, A. C.; Pez, G. P.; Kostov, M. K.; Piotrowski, P.; Stuart, S. J. Molecular Dynamics Simulations on the Effects of Diameter and Chirality on Hydrogen Adsorption in Single Walled Carbon Nanotubes. *J. Phys. Chem. B* **2005**, *109*, 3780−3786.

(14) Zhao, J.; Buldum, A.; Han, J.; Lu, J. P. Gas Molecule Adsorption in Carbon Nanotubes and Nanotube Bundles. *Nanotechnology* **2002**, *13*, 195−200.

(15) Do, D. D.; Do, H. D.; Wongkoblap, A.; Nicholson, D. Henry Constant and Isosteric Heat at Zero-Loading for Gas Adsorption in Carbon Nanotubes. *Phys. Chem. Chem. Phys.* **2008**, *10*, 7293−7303.

(16) Babu, D. J.; Lange, M.; Cherkashinin, G.; Issanin, A.; Staudt, R.; Schneider, J. J. Gas Adsorption Studies of CO_2 and N_2 in Spatially Aligned Double-Walled Carbon Nanotube Arrays. *Carbon* **2013**, *61*, 616−623.

DOI: 10.1021/acs.jpcc.5b02874
J. Phys. Chem. C 2015, 119, 15232−15239

(17) Rahimi, M.; Singh, J. K.; Babu, D. J.; Schneider, J. J.; Müller-Plathe, F. Understanding Carbon Dioxide Adsorption in Carbon Nanotube Arrays: Molecular Simulation and Adsorption Measurements. *J. Phys. Chem. C* **2013**, *117*, 13492−13501.
(18) Lee, R. S.; Kim, H. J.; Fischer, J. E.; Thess, A.; Smalley, R. E. Conductivity Enhancement in Single-Walled Carbon Nanotube Bundles Doped with K and Br. *Nature* **1997**, *388*, 255−257.
(19) Deng, W.-Q.; Xu, X.; Goddard, W. New Alkali Doped Pillared Carbon Materials Designed to Achieve Practical Reversible Hydrogen Storage for Transportation. *Phys. Rev. Lett.* **2004**, *92*, No. 166103.
(20) Chen, J.-J.; Li, W.-W.; Li, X.-L.; Yu, H.-Q. Improving Biogas Separation and Methane Storage with Multilayer Graphene Nanostructure via Layer Spacing Optimization and Lithium Doping: A Molecular Simulation Investigation. *Environ. Sci. Technol.* **2012**, *46*, 10341−10348.
(21) Paura, E. N. C.; da Cunha, W. F.; de Oliveira Neto, P. H.; e Silva, G. M.; Martins, J. B. L.; Gargano, R. Vibrational and Electronic Structure Analysis of a Carbon Dioxide Interaction with Functionalized Single-Walled Carbon Nanotubes. *J. Phys. Chem. A* **2013**, *117*, 2854−2861.
(22) Zhou, Z.; Gao, X.; Yan, J.; Song, D. Doping Effects of B and N on Hydrogen Adsorption in Single-Walled Carbon Nanotubes through Density Functional Calculations. *Carbon* **2006**, *44*, 939−947.
(23) Grande, C. A.; Rodrigues, A. E. Electric Swing Adsorption for CO_2 Removal from Flue Gases. *Int. J. Greenhouse Gas Control* **2008**, *2*, 194−202.
(24) Ribeiro, R. P. P. L.; Grande, C. A.; Rodrigues, A. E. Electric Swing Adsorption for Gas Separation and Purification: A Review. *Sep. Sci. Technol.* **2014**, *49*, 1985−2002.
(25) Stoian, R.; Rosenfeld, A.; Ashkenasi, D.; Hertel, I. V.; Bulgakova, N. M.; Campbell, E. E. B. Surface Charging and Impulsive Ion Ejection during Ultrashort Pulsed Laser Ablation. *Phys. Rev. Lett.* **2002**, *88*, No. 097603.
(26) Zdrojek, M.; Mélin, T.; Diesinger, H.; Stiévenard, D.; Gebicki, W.; Adamowicz, L. Charging and Discharging Processes of Carbon Nanotubes Probed by Electrostatic Force Microscopy. *J. Appl. Phys.* **2006**, *100*, No. 114326.
(27) Luo, J.; Peng, L.-M.; Xue, Z.; Wu, J. Density-Functional-Theory Calculations of Charged Single-Walled Carbon Nanotubes. *Phys. Rev. B* **2002**, *66*, No. 115415.
(28) Simonyan, V. V.; Diep, P.; Johnson, J. K. Molecular Simulation of Hydrogen Adsorption in Charged Single-Walled Carbon Nanotubes. *J. Chem. Phys.* **1999**, *111*, 9778.
(29) Cornell, W. D.; Cieplak, P.; Bayly, C. I.; Gould, I. R.; Merz, K. M.; Ferguson, D. M.; Spellmeyer, D. C.; Fox, T.; Caldwell, J. W.; Kollman, P. A. A Second Generation Force Field for the Simulation of Proteins, Nucleic Acids, and Organic Molecules. *J. Am. Chem. Soc.* **1995**, *117*, 5179−5197.
(30) Hummer, G.; Rasaiah, J. C.; Noworyta, J. P. Water Conduction through the Hydrophobic Channel of a Carbon Nanotube. *Nature* **2001**, *414*, 188−190.
(31) Harris, J. G.; Yung, K. H. Carbon Dioxide's Liquid-Vapor Coexistence Curve and Critical Properties As Predicted by a Simple Molecular Model. *J. Phys. Chem.* **1995**, 12021−12024.
(32) Essmann, U.; Perera, L.; Berkowitz, M. L.; Darden, T.; Lee, H.; Pedersen, L. G. A Smooth Particle Mesh Ewald Method. *J. Chem. Phys.* **1995**, *103*, 8577.
(33) Mahdizadeh, S. J.; Tayyari, S. F. Influence of Temperature, Pressure, Nanotube's Diameter and Intertube Distance on Methane Adsorption in Homogeneous Armchair Open-Ended SWCNT Triangular Arrays. *Theor. Chem. Acc.* **2010**, *128*, 231−240.
(34) Jiang, J.; Sandler, S. I. Separation of CO_2 and N_2 by Adsorption in C168 Schwarzite: A Combination of Quantum Mechanics and Molecular Simulation Study. *J. Am. Chem. Soc.* **2005**, *127*, 11989−11997.
(35) Babarao, R.; Hu, Z.; Jiang, J.; Chempath, S.; Sandler, S. I. Storage and Separation of CO_2 and CH_4 in Silicalite, C168 Schwarzite, and IRMOF-1: A Comparative Study from Monte Carlo Simulation. *Langmuir* **2007**, *23*, 659−666.
(36) Todorov, I. T.; Smith, W.; Trachenko, K.; Dove, M. T. DL_POLY_3: New Dimensions in Molecular Dynamics Simulations via Massive Parallelism. *J. Mater. Chem.* **2006**, *16*, 1911−1918.

DOI: 10.1021/acs.jpcc.5b02874
J. Phys. Chem. C 2015, 119, 15232−15239

THE JOURNAL OF CHEMICAL PHYSICS **143**, 124701 (2015)

Double-walled carbon nanotube array for CO_2 and SO_2 adsorption

Mahshid Rahimi,[1,a),b)] Deepu J. Babu,[1,b)] Jayant K. Singh,[1,2] Yong-Biao Yang,[1] Jörg J. Schneider,[1,a)] and Florian Müller-Plathe[1]
[1]*Eduard-Zintl-Institut für Anorganische und Physikalische Chemie, Technische Universität Darmstadt, Alarich-Weiss-Str. 4, D-64287 Darmstadt, Germany*
[2]*Department of Chemical Engineering, Indian Institute of Technology Kanpur, Kanpur 208016, India*

(Received 26 March 2015; accepted 20 July 2015; published online 22 September 2015)

Grand-canonical Monte Carlo simulations and adsorption experiments are combined to find the optimized carbon nanotube (CNT) arrays for gas adsorption at low pressures and 303 K. Bundles of 3D aligned double-walled carbon nanotube (DWCNT) with inner diameter of 8 nm and different intertube distances were made experimentally. The experimental results show that decreasing intertube distance leads to a significant enhancement in carbon-dioxide (CO_2) adsorption capacity at 1 bar. The molecular simulation study on CO_2 adsorption onto bundles of 3D aligned DWCNT with inner diameters of 1, 3, and 8 nm and intertube distance of 0-15 nm shows that the intertube distance plays a more important role than the CNT diameter. The simulation results show that decreasing the intertube distance up to 1 nm increases the excess adsorption generally in all the studied systems at pressures $0 < p < 14$ bars (the increase can be up to ~40% depending on the system and pressure). This is in agreement with the experimental result. Further reduction in intertube distance leads to a decrease in the excess adsorption in the pressure range $9 < p < 14$ bars. However, at lower pressure, $0 < p < 9$ bars, intertube distance of 0.5 nm is found to have the highest excess adsorption. This result is indifferent to tube diameter. Furthermore, molecular simulations are conducted to obtain the optimal parameters, for the DWCNT bundle, for SO_2 adsorption, which are similar to those observed for CO_2 in the pressure range $0 < p < 3$ bars. © *2015 AIP Publishing LLC.* [http://dx.doi.org/10.1063/1.4929609]

I. INTRODUCTION

In the previous decade, carbon-dioxide (CO_2) emissions from the combustion of fossil fuels (coal, petroleum, and natural gas) accounts for 78% increase of greenhouse gases in the atmosphere.[1] Annual emissions of greenhouse gases, specially CO_2, are the main cause of the global warming.[2] Among other gases emitted from fossil fuel combustion, SO_2 contributes significantly in polluting the environment. It is one of the major reasons of acid rain formation.[3] The main strategy for a solution for these environmental concerns is to find a suitable material for capture and storage of these gases.

Carbon based materials are widely used for gas adsorption because of the preferential interaction that exists between gas molecules and carbon atoms.[4] Carbon nanotubes (CNTs) are an important class of carbon based materials. Due to their unique structure, CNTs have extraordinary mechanical, electrical, and thermal properties.[5] Recently, a new interest on them arose because of their potential as an adsorbent of flue gases. Their large specific area, light weight, well defined structure, and reproducibility are the properties that make them one of the most promising carbon based adsorbents.[6–8] Since CNTs are well-defined structures, optimizing their geometrical properties is very important to achieve the maximum possible amount of adsorption. Liu and co-workers[9] used grand-canonical Monte Carlo (GCMC) technique to study CO_2 adsorption on single-walled CNT (SWCNT) with different chiralities, and two different diameters, 1.36 and 2.03 nm, at 300 K. They found that the adsorption capacity of SWCNT could be enhanced by the increase in the SWCNT diameter while chirality is not an essential factor on adsorption. Using the same method to investigate different gases ($CO_2/CH_4/N_2/H_2/CO$) adsorption on hexagonally ordered carbon nanopipes at 298 K, Peng *et al.*[10] claimed that increasing pore diameter from 3 to 6 nm leads to an increase in pure gases adsorption, especially for CO_2. Kowalczyk *et al.*[11] studied the effect of SWCNT diameter on the CO_2 storage at 298 K using GCMC method. They claimed that the optimum diameter of CNT depends on the storage pressure.

Usually, CNTs form bundles or undergo complex aggregation, depending on the process of synthesis. Cao *et al.*[12] and Zilli *et al.*[13] experimentally showed that aligned CNTs have higher adsorption capacity. A combined study of molecular simulation and experiment of nitrogen adsorption was performed by Agnihotri *et al.*[14] to explain the high capacity of CNT bundles. They showed that CNT bundles exhibit different sites, namely, inner (the volume within the tubes), grooves (where the two CNTs are in touch), and interstitial (the region surrounded by three CNTs and three grooves). The groove regions play an important role on adsorption at low pressure till they are saturated. Cruz *et al.*[15] used GCMC to study light organic adsorption in the internal volume of SWCNT bundles and external adsorption sites separately at 300 K. In the case of external adsorption sites, they observed that the adsorption is

a)Author to whom correspondence should be addressed. Electronic addresses: mahshid.rahimi@theo.chemie.tu-darmstadt.de and joerg.schneider@ac.chemie.tu-darmstadt.de
b)M. Rahimi and D. J. Babu contributed equally to this work.

higher in grooves. Furthermore, they found that adsorption in grooves is in agreement with the Langmuir adsorption model.

Although many works confirmed that interstitial region and grooves are important adsorption sites,[16–20] not much is known about the optimal intertube distance for highest adsorption capacity of CNT bundles. Furthermore, the effect of curvature due to variable double-walled carbon nanotube (DWCNT) diameter, on the optimal intertube distance, was missing in the earlier works. In the present work, we study SO_2 and CO_2 adsorption onto DWCNT bundles with different diameters and intertube distances. The aim is to optimize diameter and intertube distance of DWCNT bundles for the maximum adsorption capacity at low pressures. Besides, a comparison is performed with the previous works of this group.[21,22]

II. EXPERIMENTAL DETAIL

Vertically aligned CNTs were synthesized by water assisted CVD method. In a typical synthesis, 10–13 nm of Al was deposited onto boron doped Si/SiO_2 (600 nm of SiO_2) substrate by thermal evaporation method. This was followed by the deposition of 1.2 nm of iron by sputtering. The substrate along with deposited catalyst was transferred to a 3 in. CVD quartz tube and was heated to 850 °C under a reducing atmosphere. Ethene was used as the carbon source and synthesis was carried out for 15 min in the presence of controlled ppm quantities of water. Further details can be found elsewhere.[23] Densification of CNT arrays was carried out by using ethanol (technical grade) or deionized water. CNT films were peeled off from the substrate and a few drops of ethanol or water were placed on top of these films. The liquid was left to evaporate overnight at room temperature.

CO_2 adsorption measurements were carried out using a TG setup (TG209F1 Iris, Netzsch GmbH). Gas inlet was controlled using a mass flow controller gas flow meter (Bronkhorst High-Tech B.V.). About 10 mg of CNTs was placed in a ceramic crucible and was heated to 300 °C under 50 SCCM of argon flow. After maintaining the sample at 300 °C for 2 h, it was cooled down to 35 °C and kept at this temperature for half an hour. The gas supply was then switched from argon to 50 SCCM of CO_2 for an hour. After the adsorption step, the sample was again heated to 300 °C in argon. A reference measurement, without the sample, was carried out before each measurement to account for buoyancy corrections. SEM measurements were carried out on a Philips XL30 FEG. N_2 adsorption measurements were performed on a quantachrome autosorb® system. About 30 mg of sample was used for each measurement and was evacuated overnight at a temperature of at least 250 °C. Specific surface areas were calculated using a multi-point BET method.

III. MODEL AND METHOD

Following our previous work, we arrange double-walled CNTs on a hexagonal lattice so that two CNTs are in a periodic simulation box (cf. Fig. 1 of Ref. 19). In order to study the effect of curvature and porosity of the system, armchair CNTs with the inner diameter of $2r$ = 1, 3, 8 nm, a length of 5 nm, and the intertube distances of d = 0 to 15 nm are used in this work. The total number of carbon atoms is between 3360 and 19 680, depending on the CNT diameter.

SO_2 and CO_2 molecules are modeled using a 3-site rigid model with Lennard-Jones potential, partial charges, and fixed angle.[24,25] We describe CNTs as rigid structure with Lennard-Jones potential as in AMBER96 force field.[26] The Lorentz-Berthelot combining rules are used to calculate the dissimilar non-bonded interactions. The electrostatic interactions are calculated by the smooth-particle-mesh Ewald (SPME) method.[27]

Excess adsorption isotherms of CO_2 and SO_2 are calculated using GCMC method at a constant chemical potential μ, volume V, and temperature T. In order to transform the chemical potential to pressure, CO_2 and SO_2 are considered as ideal gases since the fugacity coefficient of them is ~1 in the studied pressure range. Three Monte Carlo moves, displace, rotate, and insert/delete are implemented with the probability of 0.2, 0.1, and 0.7, respectively. For equilibration of the system, 10^7 Monte Carlo steps are used and then the simulation continues for another 10^7 steps to collect the data. The output of the simulation is the total number of gas molecules, N_{tot}, which varies between 80 and 3000 for CO_2 and between 85 and 3600 for SO_2 for different systems and pressures. Total number of gas molecules, N_{tot}, can be converted to excess adsorption (the value measured in experiment) by

$$N_{ex} = N_{tot} - \rho_b V_{free}, \tag{1}$$

where ρ_b is the bulk density and is calculated by simulating bulk fluid at the same condition. Free volume, V_{free}, is calculated using a 3-dimentional Monte Carlo integration as explained in the work of Greenfield and Theodorou.[28] The free volume in different system varies from 7.32 nm^3 to 2461.74 nm^3. We convert the unit of excess adsorption to a common unit for excess adsorption, mmol of gas per gram of adsorbent.

In an adsorption process, the isosteric heat of adsorption, q_{st}, which reflects the strength of adsorbent-adsorbate interaction,[29] is usually calculated by[30]

$$q_{st} \approx RT - \left(\frac{\partial U_{ad}}{\partial N_{ad}}\right)_{T,V}, \tag{2}$$

where R is the gas constant and U_{ad} is the intermolecular energy of the system. Using fluctuation theory, Eq. (2) can be written as

$$q_{st} \approx RT - \frac{\langle U_{ad}N_{ad}\rangle - \langle U_{ad}N_{ad}\rangle}{\langle N_{ad}{}^2\rangle - \langle N_{ad}{}^2\rangle}, \tag{3}$$

where the angle brackets denote the ensemble average.

IV. RESULTS AND DISCUSSION

A. Experimental results of CO_2 adsorption

In our previous works, we have carried out extensive characterization of the as-prepared aligned CNTs which are the sole material used in this study.[22,31,32] The as-synthesized double walled CNTs, containing a minor amount of multi-walled CNT (number of walls ≤4), have an average diameter of about 8 nm[22,31] and a height of 500 μm. Typical intertube distances (d) of the as-prepared vertically aligned structures

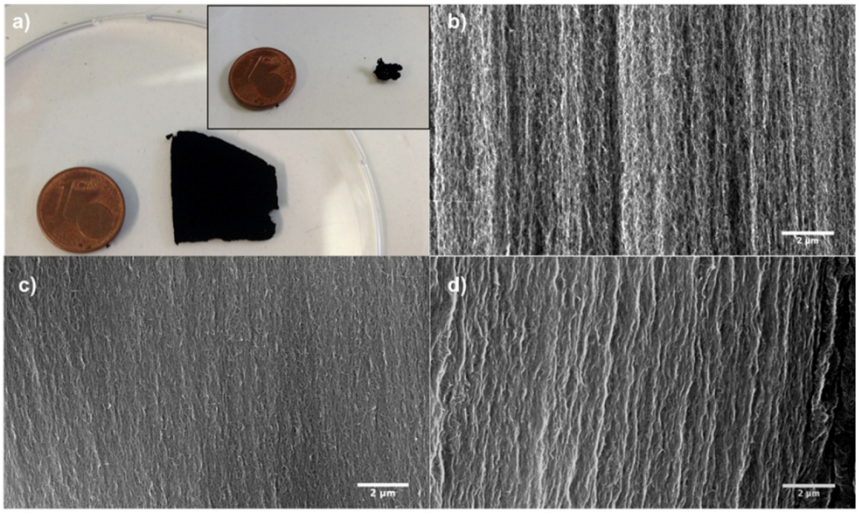

FIG. 1. (a) Photograph of the as-prepared vertically aligned CNT structure; inset shows the photograph of the same structure after ethanol evaporation. SEM images of (b) as-prepared vertically aligned CNT, (c) densified CNT by ethanol evaporation, (d) densified CNT architecture obtained by water evaporation (scale bar = 2μm).

are between 15 and 20 nm.[22] XPS measurements of the aligned CNTs indicated no peaks other than carbon (C1s), ruling out the presence of catalyst particles or functional groups in the as-prepared CNT.[22,31,32] Our previous CO_2 adsorption studies on these pristine CNT structures revealed an adsorption capacity of about 5.6 mg/g at 1 bar and 35 °C.[22] Theoretical calculations have shown that the interstitial sites are energetically favorable for adsorption and the adsorption capacity can be increased by optimizing the intertube distance.[21] To validate these results, all other parameters such as CNT diameter and specific surface area have to be kept constant and only the intertube distance should be varied. This can be realized by varying the bimetallic catalyst density. However, this invariably also leads to structural changes in CNT diameter as well as specific surface area.[33,34] Herein, we use the elastocapillary phenomenon[35] (also known as liquid induced collapse[36]) to increase the active surface area of the vertically aligned CNTs. When a liquid is introduced in the CNT arrays and allowed to evaporate, the resulting capillary and van der Waals forces effectively "zip" the nanotubes together, thereby densifying the structure. Futaba *et al.*[36] have shown that for aligned SWNT arrays, the intertube distance could be brought down from 15 nm to less than 1 nm without reducing the surface area. In the present study, we used ethanol and water for densification of vertically aligned CNT arrays. The CNT film crumbled upon evaporation and a considerable reduction in sample area is observed as shown in Fig. 1(a). Figs. 1(b)-1(d) show the SEM images of vertically aligned CNT structures before and after densification by elastocapillarity. The intervoid space between individual CNTs is considerably reduced after liquid evaporation. Though the macroscopic structure of the film is visibly distorted, the microscopic alignment is still intact to a certain degree. From SEM images, it is hard to discern differences between ethanol (Fig. 1(c)) and water (Fig. 1(d)) induced densified structures. However, CO_2 adsorption measurements revealed a significant difference between the two obtained CNT morphologies. Ethanol intercalated structures adsorbed about 7.5 mg/g of CO_2 at 1 bar/35 °C, whereas water intercalated CNT structures adsorbed 8.8 mg/g as shown in Fig. 2(a). This corresponds to an increase of 34% and 57% for ethanol and water intercalated

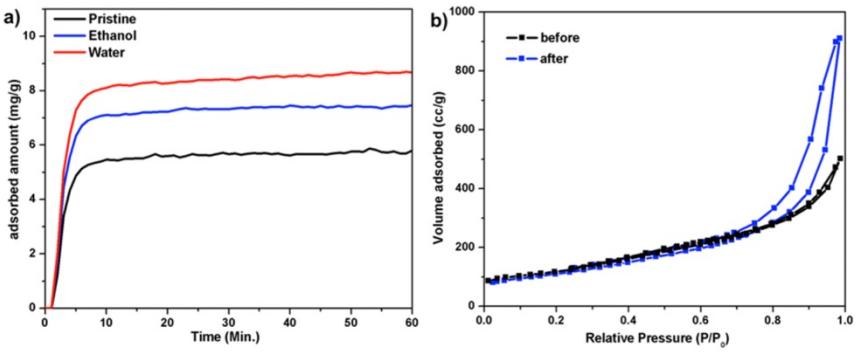

FIG. 2. (a) CO_2 adsorption at 1 bar and 35 °C for pristine and densified CNT structures. (b) N_2 adsorption isotherm on CNT structures before and after ethanol induced densification.

CNT architectures, respectively. De Volder and Hart[35] have shown that for a given material and geometry, the liquid induced compaction is proportional to the surface tension of the liquid. Water has a considerably higher surface tension of 71.99 m Nm^{-1} compared to 21.97 m Nm^{-1} of ethanol at 25 °C.[37] This may account for the better compaction and the observed enhancement in CO_2 adsorption for water intercalated structures.

N_2 adsorption measurements were carried out at 77 K before and after ethanol induced densification as shown in Fig. 2(b). No considerable changes in specific surface area are observed after the liquid induced collapse. Prior to densification, the CNT arrays had a BET specific surface area of about 423 m^2/g and after the evaporation of ethanol, the surface area decreased only slightly to 400 m^2/g. Similar observation regarding surface area was also made by Futaba *et al.* after densification of SWNT arrays.[36] From the N_2 adsorption isotherm, it can be observed that for the densified structure, the onset of capillary condensation (steep rise in adsorption) occurs at a lower pressure when compared to original structure. CO_2 adsorption on the densified structure clearly indicated an increase in the adsorption at 1 bar as shown in Fig. 2(a). In order to obtain the optimized value of the intertube distance, molecular simulation is used comprehensively to study the CO_2 adsorption on DWCNT bundles, which is described in detail in Sec. IV B.

B. Molecular simulation of CO_2 adsorption

Fig. 3 shows the CO_2 adsorption isotherms on DWCNT bundles with inner diameter $2r$ = 1 nm and intertube distance d = 0-15 nm at T = 303 K. By increasing d, the volume of the grooves increases leading to decrease in the adsorptivity of the carbon surface. Hence, the propensity for adsorption is higher at lower values of d. However, at low d, the groove volume is limited which saturates at a lower pressure, and at higher pressures, the amount of adsorption for the larger groove volume exceeds the amount seen for lower d values. Hence, the optimal intertube distance varies for a given pressure range depending on the above two opposite effects (increase in volume and decrease in carbon density). The system with $d = 0$ reaches the saturation value of ~2 mmol/g at a low pressure (p < 1 bar), due to its limited space in the intertube region. Increasing d to 0.5 nm increases the excess adsorption significantly (e.g., 125% at p = 1 bar and 250% at p = 4 bars). Nevertheless, the isotherm saturates at $p \sim 8$ bars and the adsorption amount remains almost constant (~9 mmol/g) at higher pressure. The excess adsorption of d = 1 nm is less than that of d = 0.5 nm in the low pressure range $0 < p < 9$ bars. This is primarily due to increase in the DWCNT surface-surface distance with increase in d leading to reduction in the carbon density in the grooves. This affects the effective interaction experienced by a gas molecule that decreases with increase in d. Hence, the saturation occurs at a higher pressure and this is the reason that d = 1 curve crosses d = 0.5 nm curve at $p \sim 9$ bars. Further increase in d to 2, 4, and 15 nm decreases the excess adsorption in the studied pressure range, so that these three cases show fairly similar curves. When d = 0.5 nm, the grooves have low volume but they have a very high adsorptivity due to the high carbon density in these regions. Thus, d = 0.5 nm shows the highest adsorption at low gas pressure; then, with increasing pressure, it saturates. By increasing d to 1 nm, the groove regions become larger but at the same time, larger space decreases the carbon density and the adsorptivity. Consequently, at low pressure, it shows lower adsorption than that of d = 0.5 nm but at higher pressure, where d = 0.5 nm saturates, adsorption for the case d = 1 nm becomes more than that of d = 0.5 nm.

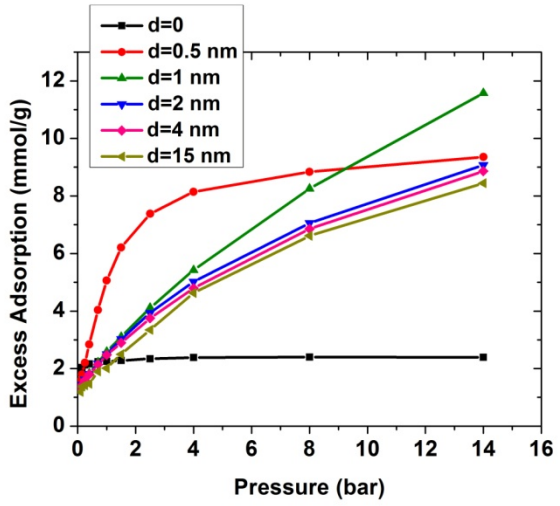

FIG. 3. Excess adsorption isotherms of CO_2 in double-walled carbon nanotube arrays, with inner tube diameter $2r$ = 1 nm and intertube distance d = 0-15 nm. T = 303 K. Error bars are smaller than the symbols.

In order to understand the adsorption behavior of CO_2 and SO_2 on the CNT bundles, Langmuir and Freundlich adsorption models are used in this work. The Langmuir adsorption model[38] can explain the monolayer adsorption behavior with the following equation:

$$N_{ex} = N_{ex}^{max} \frac{bp}{1 + bp}, \tag{4}$$

where b is the Langmuir constant, p is the pressure, and N_{ex}^{max} is the maximum CO_2 loading. Freundlich adsorption model[39] is another popular model, which relates excess adsorption to the pressure,

$$N_{ex} = Kp^n, \tag{5}$$

where K is Freundlich constant and shows the adsorption capacity, n is heterogeneity factor, and p is the pressure. The above models are fitted to the GCMC data of CO_2, and the results are summarized in Table I. The worst and best fits of the Langmuir model are for d = 0 nm and d = 0.5 nm, respectively (see Fig. S1 of the supplementary material[40]). As the intertube distance increases, the fit of the Langmuir model gets relatively inaccurate as reflected by R^2. On the other hand, worst fit for the Freundlich model is for d < 1.0 nm, whereas the fit is excellent for all intertube distances $d \geq 1$ nm (see Fig. S2 of the supplementary material[40]). Thus, for $d \geq 1$ nm, Freundlich isotherm fits much better than the Langmuir isotherm. Hence, it is clear that for higher intertube distance, $d \geq 1$ nm multilayer

TABLE I. Langmuir and Freundlich isotherm parameter obtained by fitting for CO_2 adsorption on double-walled CNT with $2r = 1$ nm and $d = 0$-15 nm. R^2 is the coefficient of determination of fitting.

	Langmuir model			Freundlich model		
d	N_{ex}^{max}	b	R^2	K	n	R^2
0	2.35 ± 0.02	45.43 ± 6.00	0.88	2.23 ± 0.01	0.04 ± 0.00	0.92
0.5	9.92 ± 0.22	1.10 ± 0.08	0.99	4.66 ± 0.31	0.31 ± 0.04	0.91
1	16.03 ± 2.36	0.15 ± 0.05	0.94	2.68 ± 0.13	0.55 ± 0.02	0.99
2	10.56 ± 1.21	0.29 ± 0.08	0.92	2.69 ± 0.08	0.46 ± 0.01	0.99
4	10.33 ± 1.26	0.28 ± 0.08	0.91	2.61 ± 0.09	0.46 ± 0.02	0.99
15	10.66 ± 1.34	0.22 ± 0.06	0.93	2.31 ± 0.11	0.49 ± 0.02	0.98

adsorption behavior is observed. The multilayer adsorption behavior of the system with $d > 1$ nm is also confirmed by the simulation snapshots (see Fig. S3 of the supplementary material[40]). The table clearly shows the remarkable effect of d on the adsorption capacity. Further, it is evident that $d = 1$ nm has the highest N_{ex}^{max} and n, i.e., $d = 1$ nm has the maximum capacity for CO_2 adsorption (62% and 52% more than $d = 0.5$ and 2 nm, respectively).

Figs. 4(a) and 4(b) present CO_2 adsorption on DWCNT with $2r = 3$, 8 nm and various intertube distances. The intertube distance of $d = 4$ and 15 nm is not included as adsorption behavior seen for them is akin to that seen for $d = 2$ nm. The effect of intertube distance is more or less the same for different diameters. The adsorption behavior is not much different from that of $2r = 1$ nm. At low pressure, $p < 9$ bars, $d = 0.5$ nm has the highest excess adsorption while at high pressure, $p > 9$ bars, the maximum excess adsorption belongs to $d = 1$ nm. The effect of intertube distance, however, reduces with increasing DWCNT diameter. For example, increasing d from 0 to 0.5 nm, at $p = 4$ bars, increases the excess adsorption by 250%, 79%, and 32% for $2r = 1$, 3, and 8 nm, respectively. The increased adsorption behavior for $d = 0.5$ nm is mainly attributed to the increased volume of the groove region. The relative volume available in the groove and interstitial regions decreases with increase in the diameter. Hence, the adsorption capacity also follows the same order.

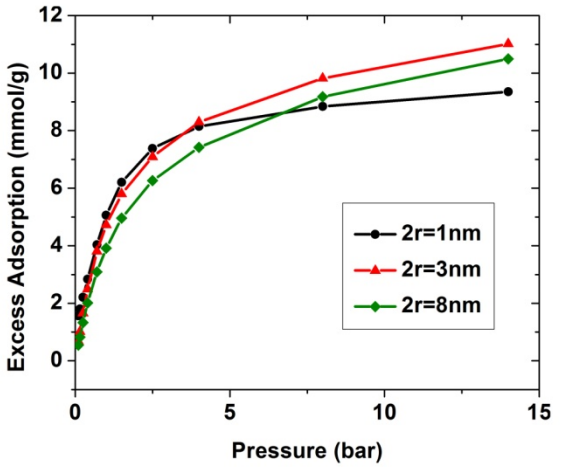

FIG. 5. Excess adsorption isotherms of CO_2 in double-walled carbon nanotube arrays, with intertube distance $d = 0.5$ nm and inner tube diameter $2r = 1$-8 nm. $T = 303$ K. Error bars are smaller than the symbols.

Fig. 5 shows the effect of inner diameter of DWCNT on CO_2 adsorption isotherm with a fixed intertube distance of $d = 0.5$ nm. At $p < 4$ bars, the excess adsorption of $2r = 1$ nm is slightly more than that of $2r = 3$ nm (the maximum difference is 0.4 mmol/g at $p = 1.5$ bars). The reason is probably the higher curvature of $2r = 1$ nm compared to that of $2r = 3$ nm. However, CO_2 adsorption on $2r = 1$ nm DWCNT saturates quickly with increasing pressure, $p \sim 4$ bars, due to its limited space. At $p > 4$ bars, $2r = 3$ nm displays the highest excess adsorption so that at $p = 14$ bars the excess adsorption of it is 1.66 mmol/g more than that of $d = 0$. Moreover, $2r = 3$ nm does not saturate within 14 bars. Further increase in the inner diameter decreases the excess adsorption marginally, as seen for $2r = 8$ nm in the pressure range studied in this work,

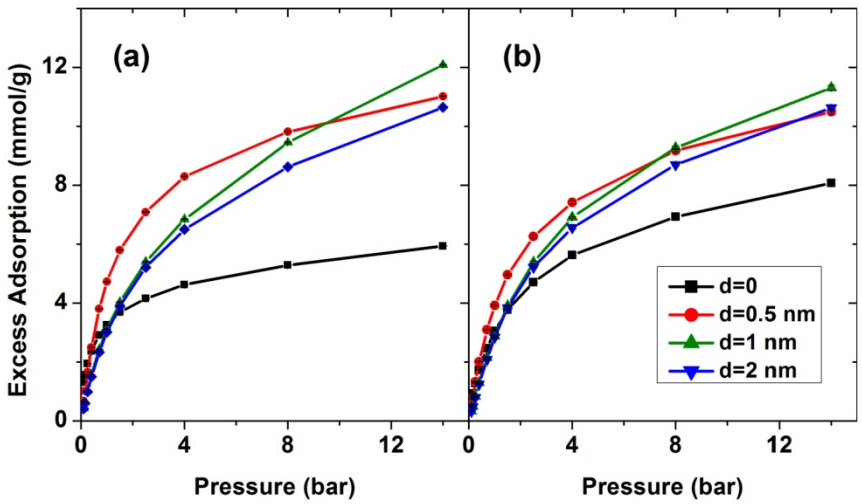

FIG. 4. Excess adsorption isotherms of CO_2 in double-walled carbon nanotube arrays, with inner tube diameter (a) $2r = 3$ nm, (b) $2r = 8$ nm and intertube distance $d = 0$-2 nm. $T = 303$ K. Error bars are smaller than the symbols.

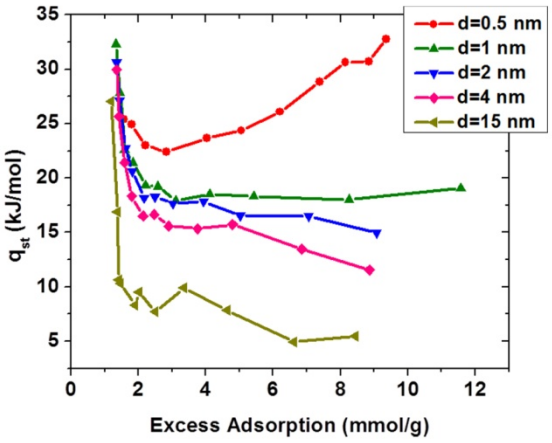

FIG. 6. Isosteric heat of adsorption of CO_2 in double-walled carbon nanotube arrays, with inner tube radius $2r = 1$ nm and intertube distance $d = 0$-15 nm. $T = 303$ K.

because of the reduction in its curvature. It is evident from Fig. 5 that CNT pore diameter has much less effect on the adsorption behavior as compared to the intertube distance (as seen in Figs. 3 and 4).

Fig. 6 presents the heat of adsorption of the systems with $2r = 1$ nm and $d = 0.5$-15 nm as a function of excess adsorption. The heat of adsorption of $d = 0$ is not shown since the excess adsorption of it is almost constant at ~40 kJ/mol. When $d = 0.5$ nm, the heat of adsorption decreases first with increasing excess adsorption until it reaches to a minimum and then it further increases. The initial decrease in q_{st} is due to the filling of grooves, which have a high carbon density. By filling the grooves, followed by the interstitial and the inner regions, which are all very low in volume, q_{st} starts increasing. For higher d, similar to $d = 0.5$ nm, a drastic decrease in q_{st} is seen first while grooves get filled. Subsequently, q_{st} continues to decrease though not dramatically. This is mainly attributed to the continuous filling process of the interstitial and inner volume until saturation. $d = 1$ nm case is an exception where q_{st} remains constant at 18 kJ/mol after the initial drop.

Having high adsorption is not the only main goal, since it is important to have low q_{st} for economically reusable adsorbent for CO_2. Moreover, an optimal CNT array depends on the pressure. For example, for $p = 1$ bar, $2r = 1$ nm and $d = 0.5$ nm is the best material which has the excess adsorption of 5.06 mmol/g (e.g., the excess adsorption is 2.5 and 4.7 mmol/g for $2r = 1$ nm, $d = 1$ nm and $2r = 3$ nm, $d = 0.5$ nm, respectively), though with a high q_{st} of 24 kJ/mol. The lowest q_{st}, 9.52 kJ/mol, belongs to the case with $2r = 1$ nm and $d = 15$ nm which has also the lowest amount of excess adsorption ($N_{ex} = 2.01$ mmol/g). At a higher pressure, e.g., $p = 14$ bars, the case with $2r = 3$ nm and $d = 1$ nm shows the highest adsorption ($N_{ex} = 12.08$ mmol/g) but with $q_{st} = 17.69$ kJ/mol, while the lowest q_{st} is 5.46 kJ/mol (belongs to the case with $2r = 1$ nm and $d = 15$ nm) but with 43% less in adsorption capacity. Hence, clearly there is a trade-off in the amount of adsorption and energy required for reusability.

C. Molecular simulation of SO_2 adsorption

SO_2 isotherms on DWCNT with $2r = 1$, 3, 5, 8 nm and $d = 0$-2 nm at $T = 303$ K are shown in Fig. 7. The system with

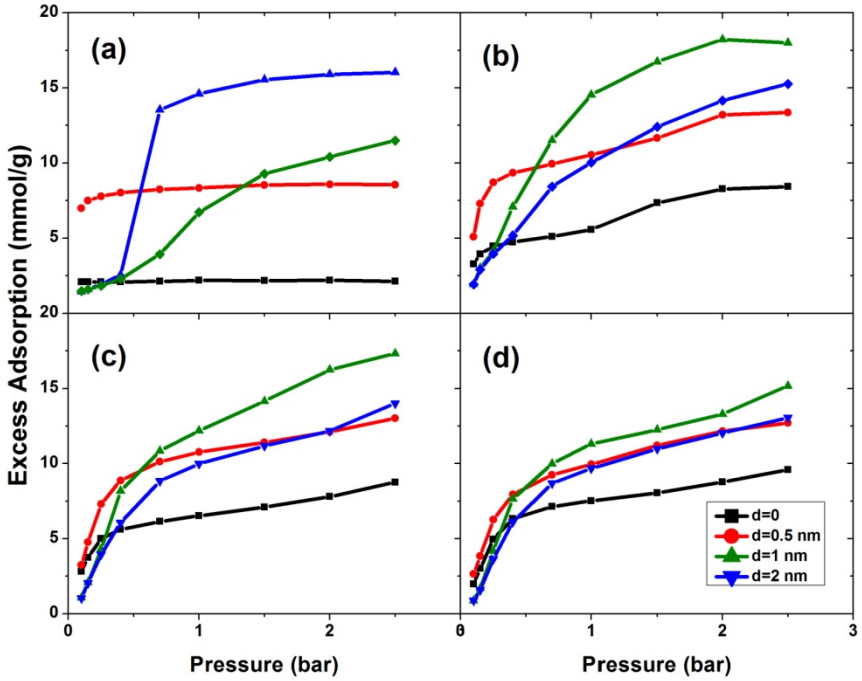

FIG. 7. Excess adsorption isotherms of SO_2 in double-walled carbon nanotube arrays, with inner tube diameter (a) $2r = 1$ nm, (b) $2r = 3$ nm, (c) $2r = 5$ nm, (d) $2r = 8$ nm and intertube distance $d = 0$-2 nm. $T = 303$ K. Error bars are smaller than the symbols.

$2r$ = 1 nm and d = 0 (Fig. 7(a)) shows a low constant excess adsorption in the whole pressure range, because of the limited volume both inside the CNTs and in the intertube region. The case of d = 0.5 nm shows a similar result but with higher amount of adsorption. For d = 1 nm, the amount of adsorption is less than that of d = 0.5 nm for $p < 0.5$ bars. However, at $p \sim 0.5$ bars, the system undergoes capillary condensation. Subsequently, at $p > 0.5$ bars, the amount of adsorption is above that of d = 0.5 nm. Further increase in d to 2 nm yields lower adsorption in the whole pressure range in comparison with d = 1 nm. Furthermore, capillary condensation is not observed for d = 2 nm up to p = 3 bars. Increasing the diameter to 3-8 nm does not change the optimal intertube distance for the highest adsorption capacity. So at very low pressures, $p < 0.5$ bars, d = 0.5 nm has the highest adsorption capacity while at higher pressures, $0.5 < p < 3$, d = 1 nm shows the maximum adsorption capacity. Nevertheless, the effect of d is more dramatic at low CNT diameter.

The optimum intertube distance for the maximum SO_2 adsorption is the same as that for CO_2. However, corresponding pressures are 9 bars and 0.5 bars for CO_2 and SO_2, respectively. Furthermore, the effect of intertube distance is stronger for SO_2 than CO_2. For the case of SO_2, increasing d from 0 to 0.5 nm at p = 1 bar increases the adsorption by 280%, 89%, 65%, and 32% for $2r$ = 1, 3, 5, and 8 nm, respectively. A similar dependence was seen at p = 4 bars for the case of CO_2. This is due to the stronger interaction of SO_2 molecules with the CNT and also with each other. Fig. S4[40] shows the CO_2 and SO_2 isotherms for $2r$ = 3 nm and d = 0-2 nm, which clearly indicate higher adsorption for SO_2 than that for CO_2 under the same condition.

In the case of $2r$ = 3 nm and d = 0 (Fig. 7(b)), a primary increase in the adsorption is seen, as the pressure is increased till p = 0.3 bars. Then, for 0.3 bars < p < 1 bar, the adsorption increases gradually. Further increase in pressure enhances the adsorption distinctly, as seen in the second increase in the adsorption curve between 1 bar and 2 bars. This can be explained due to the layering transition. The snapshots of the system are shown in Fig. 8. When d = 0, the groove and interstitial regions have very limited capacity and are saturated at a low pressure $p \sim 0.1$ bars. Inside the CNT, the first layer of adsorption is formed at $p \sim 0.2$ bars. By increasing the pressure to 1 bar, the first layer slowly saturates indicated by the slow increase in the adsorption isotherm. By further increase in pressure, the second layer starts to form. Formation of the second layer causes saturation in the inner space, which is reflected in the significant increase in the adsorption isotherm value. The same situation is found for d = 0.5 nm. For d = 1 nm, the inner and outer regions are saturated almost at the same pressure. Hence, the curve has a continuous increase in the whole pressure range, and the layering transition is not seen. The curve of d = 2 nm is similar to d = 1 nm because groove and interstitial regions are not completely filled below 3 bars. The adsorption isotherm displays no rapid increase

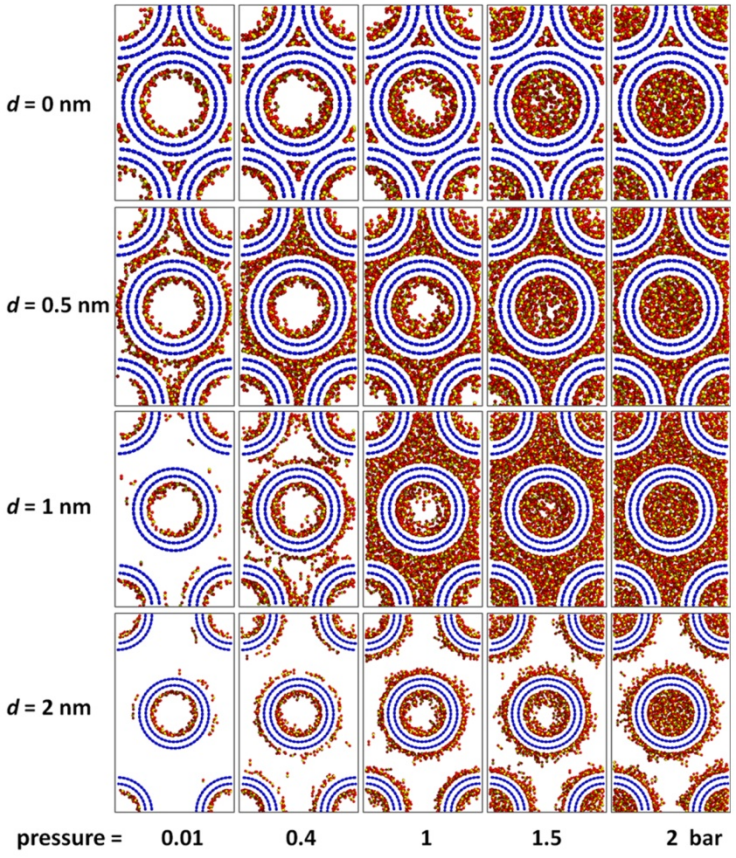

FIG. 8. Snapshots of SO_2 adsorption in double-walled carbon nanotube arrays, with inner tube diameter $2r$ = 3 nm and various intertube distances. T = 303 K.

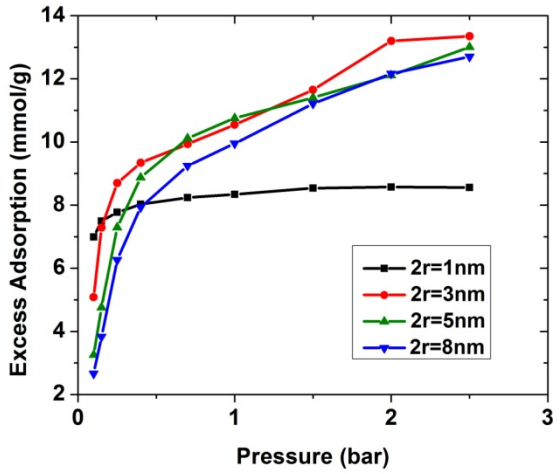

FIG. 9. Excess adsorption isotherms of SO_2 in double-walled carbon nanotube arrays, with intertube distance $d = 0.5$ nm and inner tube diameter $2r$ = 1-8 nm. $T = 303$ K. Error bars are smaller than the symbols.

change of curvature for thicker CNTs. The reason is possibly the larger available space inside the CNTs, for which the transition from first layer to second layer does not lead to saturation inside the CNT.

Fig. 9 presents SO_2 isotherm on double-walled CNT of varying diameters at a fixed intertube distance of $d = 0.5$ nm. As for CO_2, the effect of diameter is not as dramatic as that of the intertube distance. For $2r = 1$ nm, the adsorption is almost constant due to the limited available space, inside and outside of the CNT, in comparison with the SO_2 molecular size. The case with $2r = 3$ nm has the highest adsorption in the whole pressure range except 0.6 bars $< p <$ 1.2 bars. This exception is due to the layering transition explained above. Larger tube curvature leads to higher adsorption but at the same time having enough volume is an important factor too. In the studied pressure range, CNTs with $2r = 3$ nm are the best compromise of high curvature with sufficient volume at the same time.

Langmuir and Freundlich models have also been fitted to the SO_2 adsorption data of the system with $2r = 3$ nm and various d values. Table II summarizes the fitted model parameters. For the Langmuir model, $d = 1$ nm has the highest capacity for SO_2 adsorption so that N_{ex}^{max} of $d = 1$ nm is 100% and 19% more than that of $d = 0.5$ and 2 nm, respectively. For the Freundlich model, $d = 1$ nm shows a value of K of $d = 1$ nm 12% and 29% more than that of $d = 0.5$ and $d = 2$ nm, respectively. Similar to the case of CO_2, the optimal CNT intertube distance and diameter for SO_2 adsorption depend on the pressure. For instance, at $p = 1$ bar, the system with $2r = 1$ nm and $d = 1$ nm is found to have the highest adsorption while the case with $2r = 3$ nm and $d = 1$ nm leads to maximum adsorption at $p = 2.5$ bars.

TABLE II. Langmuir and Freundlich isotherm parameters obtained by fitting the SO_2 adsorption data on double-walled CNT with $2r = 3$ nm and d = 0-2 nm. R^2 is the coefficient of determination of fitting.

	Langmuir model			Freundlich model		
d	N_{ex}^{max}	b	R^2	K	n	R^2
0	8.37 ± 0.71	4.27 ± 1.40	0.78	6.33 ± 0.16	0.30 ± 0.03	0.94
0.5	13.25 ± 0.54	6.60 ± 1.21	0.96	10.89 ± 0.24	0.24 ± 0.02	0.94
1	27.16 ± 2.10	0.97 ± 0.17	0.98	12.25 ± 0.67	0.55 ± 0.67	0.93
2	22.65 ± 0.73	0.82 ± 0.06	0.99	9.46 ± 0.23	0.57 ± 0.031	0.99

V. CONCLUSION

In this work, molecular simulation and experiments were used to find a geometry for three-dimensionally aligned double-walled CNT arrays, which is optimum for having higher CO_2 and SO_2 adsorption at low pressures and T = 303 K. Experimental results for CO_2 adsorption on CNT with inner diameter of 8 nm show that reducing the intertube distance leads to increase in adsorption at $p = 1$ bar. Molecular simulation investigations were performed on double-walled CNTs with inner diameters 1-8 nm and intertube distances of 0-15 nm. The results show that for CO_2 adsorption at low pressure, $p < 9$ bars, the $d = 0.5$ nm system has the highest adsorption, while for the pressure range $9 < p < 14$ bars, the maximum adsorption is found for $d = 1$ nm. Reducing the intertube distance from $d = 2$ to $d = 0.5$ nm at $p = 1$ bar increases the adsorption capacity by 103, 57, 46, and 38% for $2r = 1$, 3, 5, and 8 nm, respectively. On the other hand, the experimental results of CO_2 adsorption show an increase of 34% and 57% for CNT architectures, which have been compacted by ethanol and water treatment, respectively, for $2r = 8$ nm at $p = 1$ bar. Although the experiments and simulation results do not give the same value, the results are in line with each other qualitatively.

For SO_2 adsorption, the optimal intertube distances are akin to those seen for CO_2; however, the pressure, where crossover occurs, is much lower at ~0.5 bars. Furthermore, it was found that the intertube distance has a much larger effect on gas adsorption than the tube diameter. As a result, the optimal CNT geometry depends on the operating pressure and the gas. For example, at $p = 1$ bar, DWCNTs with $2r = 1$ nm and $d = 0.5$ nm show the highest adsorption capacity for CO_2, while $2r = 3$ nm and $d = 1$ nm show the maximum adsorption capacity for SO_2.

ACKNOWLEDGMENTS

D.J.B. and J.J.S. would like to thank Silvio Heinschke for the N_2 adsorption measurement. M.R. would like to thank Jurek Schneider for his help in free volume calculations. This work was supported by the Priority Programme 1570 *Porous media with well-defined pore structure in chemical engineering: Modelling, application, synthesis* of Deutsche Forschungsgemeinschaft. J.K.S. gratefully acknowledges the support of the Alexander von Humboldt Foundation, and the Ministry of Earth Sciences, India.

[1]R. K. Pachauri, M. R. Allen, V. R. Barros, J. Broome, W. Cramer, R. Christ, J. A. Church, L. Clarke, Q. Dahe, P. Dasgupta, N. K. Dubash, O. Edenhofer, I. Elgizouli, C. B. Field, P. Forster, P. Friedlingstein, J. Fuglestvedt, L. Gomez-Echeverri, S. Hallegatte, G. Hegerl, M. Howden, K. Jiang, B. Jimenez Cisneros, V. Kattsov, H. Lee, K. J. Mach, J. Marotzke, M. D. Mastrandrea, L. Meyer, J. Minx, Y. Mulugetta, K. O'Brien, M. Oppenheimer, J. J. Pereira,

R. Pichs-Madruga, G.-K. Plattner, H.-O. Pörtner, S. B. Power, B. Preston, N. H. Ravindranath, A. Reisinger, K. Riahi, M. Rusticucci, R. Scholes, K. Seyboth, Y. Sokona, R. Stavins, T. F. Stocker, P. Tschakert, D. van Vuuren, and J.-P. van Ypersele, IPCC, 2014: *Climate Change 2014: Synthesis Report. Contribution of Working Groups I, II and III to the Fifth Assessment Report of the Intergovernmental Panel on Climate Change*, edited by R. Pachauri and L. Meyer (IPCC, Geneva, Switzerland), 151 pp., http://hdl.handle.net/10013/epic.45156.

[2]D. M. D'Alessandro, B. Smit, and J. R. Long, "Carbon dioxide capture: Prospects for new materials," Angew. Chem., Int. Ed. **49**, 6058–6082 (2010).

[3]A. D. Ellerman, *Markets for Clean Air: The U.S. Acid Rain Program* (Cambridge University Press, 2000).

[4]F. L. Darkrim, P. Malbrunot, and G. P. Tartaglia, "Review of hydrogen storage by adsorption in carbon nanotubes," Int. J. Hydrogen Energy **27**, 193–202 (2002).

[5]M. J. O'Connell, *Carbon Nanotubes: Properties and Applications* (CRC Press, 2006).

[6]X. Ren, C. Chen, M. Nagatsu, and X. Wang, "Carbon nanotubes as adsorbents in environmental pollution management: A review," Chem. Eng. J. **170**, 395–410 (2011).

[7]E. J. Bottani and J. M. D. Tascón, *Adsorption by Carbons: Novel Carbon Adsorbents* (Elsevier, 2011).

[8]A. V. Eletskii, "Sorption properties of carbon nanostructures," Phys.-Usp. **47**, 1119–1154 (2004).

[9]L. Liu and S. K. Bhatia, "Molecular simulation of CO_2 adsorption in the presence of water in single-walled carbon nanotubes," J. Phys. Chem. C **117**, 13479–13491 (2013).

[10]X. Peng, D. Cao, and W. Wang, "Adsorption and separation of $CH_4/CO_2/N_2/H_2/CO$ mixtures in hexagonally ordered carbon nanopipes CMK-5," Chem. Eng. Sci. **66**, 2266–2276 (2011).

[11]P. Kowalczyk, S. Furmaniak, P. A. Gauden, and A. P. Terzyk, "Optimal single-walled carbon nanotube vessels for short-term reversible storage of carbon dioxide at ambient temperatures," J. Phys. Chem. C **114**, 21465–21473 (2010).

[12]A. Cao, H. Zhu, X. Zhang, X. Li, D. Ruan, C. Xu, B. Wei, J. Liang, and D. Wu, "Hydrogen storage of dense-aligned carbon nanotubes," Chem. Phys. Lett. **342**, 510–514 (2001).

[13]D. Zilli, P. R. Bonelli, and A. L. Cukierman, "Effect of alignment on adsorption characteristics of self-oriented multi-walled carbon nanotube arrays," Nanotechnology **17**, 5136–5141 (2006).

[14]S. Agnihotri, J. P. B. Mota, M. Rostam-Abadi, and M. J. Rood, "Structural characterization of single-walled carbon nanotube bundles by experiment and molecular simulation," Langmuir **21**, 896–904 (2005).

[15]F. J. A. L. Cruz, I. A. A. C. Esteves, and J. P. B. Mota, "Adsorption of light alkanes and alkenes onto single-walled carbon nanotube bundles: Langmuirian analysis and molecular simulations," Colloids Surf., A **357**, 43–52 (2010).

[16]W. Shi and J. Johnson, "Gas adsorption on heterogeneous single-walled carbon nanotube bundles," Phys. Rev. Lett. **91**, 015504 (2003).

[17]S. Agnihotri, J. P. B. Mota, M. Rostam-Abadi, and M. J. Rood, "Adsorption site analysis of impurity embedded single-walled carbon nanotube bundles," Carbon **44**, 2376–2383 (2006).

[18]F. J. A. L. Cruz, I. A. A. C. Esteves, S. Agnihotri, and J. P. B. Mota, "Adsorption equilibria of light organics on single-walled carbon nanotube heterogeneous bundles: Thermodynamical aspects," J. Phys. Chem. C **115**, 2622–2629 (2011).

[19]J. J. Cannon, T. J. H. Vlugt, D. Dubbeldam, S. Maruyama, and J. Shiomi, "Simulation study on the adsorption properties of linear alkanes on closed nanotube bundles," J. Phys. Chem. B **116**, 9812–9819 (2012).

[20]F. Cruz and J. Mota, "Thermodynamics of adsorption of light alkanes and alkenes in single-walled carbon nanotube bundles," Phys. Rev. B **79**, 165426 (2009).

[21]M. Rahimi, J. K. Singh, D. J. Babu, J. J. Schneider, and F. Müller-Plathe, "Understanding carbon dioxide adsorption in carbon nanotube arrays: Molecular simulation and adsorption measurements," J. Phys. Chem. C **117**, 13492–13501 (2013).

[22]D. J. Babu, M. Lange, G. Cherkashinin, A. Issanin, R. Staudt, and J. J. Schneider, "Gas adsorption studies of CO_2 and N_2 in spatially aligned double-walled carbon nanotube arrays," Carbon **61**, 616–623 (2013).

[23]R. Joshi, J. Engstler, L. Houben, M. B. Sadan, A. Weidenkaff, P. Mandaliev, A. Issanin, and J. J. Schneider, "Catalyst composition, morphology and reaction pathway in the growth of 'super-long' carbon nanotubes," ChemCatChem **2**, 1069–1073 (2010).

[24]J. G. Harris and K. H. Yung, "Carbon dioxide's liquid-vapor coexistence curve and critical properties as predicted by a simple molecular model," J. Phys. Chem. **99**, 12021–12024 (1995).

[25]M. H. Ketko, G. Kamath, and J. J. Potoff, "Development of an optimized intermolecular potential for sulfur dioxide," J. Phys. Chem. B **115**, 4949–4954 (2011).

[26]W. D. Cornell, P. Cieplak, C. I. Bayly, I. R. Gould, K. M. Merz, D. M. Ferguson, D. C. Spellmeyer, T. Fox, J. W. Caldwell, and P. A. Kollman, "A second generation force field for the simulation of proteins, nucleic acids, and organic molecules," J. Am. Chem. Soc. **117**, 5179–5197 (1995).

[27]U. Essmann, L. Perera, M. L. Berkowitz, T. Darden, H. Lee, and L. G. Pedersen, "A smooth particle mesh Ewald method," J. Chem. Phys. **103**, 8577 (1995).

[28]M. L. Greenfield and D. N. Theodorou, "Geometric analysis of diffusion pathways in glassy and melt atactic polypropylene," Macromolecules **26**, 5461–5472 (1993).

[29]J. Jiang and S. I. Sandler, "Separation of CO_2 and N_2 by adsorption in C_{168} schwarzite: A combination of quantum mechanics and molecular simulation study," J. Am. Chem. Soc. **127**, 11989–11997 (2005).

[30]R. Babarao, Z. Hu, J. Jiang, S. Chempath, and S. I. Sandler, "Storage and separation of CO_2 and CH_4 in silicalite, C_{168} schwarzite, and IRMOF-1: A comparative study from Monte Carlo simulation," Langmuir **23**, 659–666 (2007).

[31]D. J. Babu, S. Yadav, T. Heinlein, G. Cherkashinin, and J. J. Schneider, "Carbon dioxide plasma as a versatile medium for purification and functionalization of vertically aligned carbon nanotubes," J. Phys. Chem. C **118**, 12028–12034 (2014).

[32]D. J. Babu, S. N. Varanakkottu, A. Eifert, D. de Koning, G. Cherkashinin, S. Hardt, and J. J. Schneider, "Inscribing wettability gradients onto superhydrophobic carbon nanotube surfaces," Adv. Mater. Interfaces **1**, 1300049 (2014).

[33]T. Yamada, T. Namai, K. Hata, D. N. Futaba, K. Mizuno, J. Fan, M. Yudasaka, M. Yumura, and S. Iijima, "Size-selective growth of double-walled carbon nanotube forests from engineered iron catalysts," Nat. Nanotechnol. **1**, 131–136 (2006).

[34]B. Zhao, D. N. Futaba, S. Yasuda, M. Akoshima, T. Yamada, and K. Hata, "Exploring advantages of diverse carbon nanotube forests with tailored structures synthesized by supergrowth from engineered catalysts," ACS Nano **3**, 108–114 (2009).

[35]M. De Volder and A. J. Hart, "Engineering hierarchical nanostructures by elastocapillary self-assembly," Angew. Chem., Int. Ed. **52**, 2412–2425 (2013).

[36]D. N. Futaba, K. Hata, T. Yamada, T. Hiraoka, Y. Hayamizu, Y. Kakudate, O. Tanaike, H. Hatori, M. Yumura, and S. Iijima, "Shape-engineerable and highly densely packed single-walled carbon nanotubes and their application as super-capacitor electrodes," Nat. Mater. **5**, 987–994 (2006).

[37]H.-J. Butt, K. Graf, and M. Kappl, *Physics and Chemistry of Interfaces* (John Wiley & Sons, 2006).

[38]I. Langmuir, "The adsorption of gases on plane surfaces of glass, mica and platinum," J. Am. Chem. Soc. **40**, 1361–1403 (1918).

[39]H. Freundlich, *Kapillarchemie* (Akademische Verlagsgesellschaft, Wiesbaden, Germany, 1909).

[40]See supplementary material at http://dx.doi.org/10.1063/1.4929609 for the simulation data, best, and worst fits of Langmuir and Freundlich of excess adsorption isotherms of CO_2 in double-walled carbon nanotube arrays.

5 Adsorption and Separation of Binary Mixtures of SO_2, CO_2 and N_2 by Ordered Carbon Nanotube Arrays: Grand-canonical Monte Carlo Simulations

Mahshid Rahimi[1], Jayant K. Singh[1,2] and Florian Müller-Plathe[1]

1. Technische Universität Darmstadt, Eduard-Zintl-Institut für Anorganische und Physikalische Chemie, Alarich-Weiss-Str. 4, D-64287 Darmstadt, Germany

2. Department of Chemical Engineering, Indian Institute of Technology Kanpur, Kanpur-208016, India

Corresponding Author:

*mahshid.rahimi@theo.chemie.tu-darmstadt.de

5.1 Abstract

The adsorption and separation behavior of SO_2-CO_2, SO_2-N_2 and CO_2-N_2 binary mixtures in bundles of aligned double-walled carbon nanotubes are investigated using the grand-canonical Monte Carlo (GCMC) method and ideal adsorbed solution theory. The simulations were performed at 303 K with nanotubes of inner diameter 3 nm and various intertube distance. The results showed that the packing with intertube distance d=0 has the highest selectivity for SO_2-N_2 and CO_2-N_2 binary mixtures. For the SO_2-CO_2 case, the optimum intertube distance for having the maximum selectivity depends on the applied pressure, so that at p < 0.8 bar d=0 shows the highest selectivity and at 0.8 bar < p < 2.5 bar, the highest selectivity belongs to d=0.5 nm. Ideal adsorbed solution theory cannot predict the adsorption of the binary systems containing SO_2, especially when d=0. As the intertube distance is increased, the ideal adsorbed solution theory based predictions become closer to that of GCMC simulations. However, in the case of CO_2-N_2, simulations and ideal adsorbed solution theory are in good agreement.

5.2 Introduction

In the last decade carbon nanotubes (CNTs) were studied widely as an adsorbent of different gases such as H_2, N_2, CO_2, SO_2, alkanes and noble gases.[1,2] This great interest in using CNTs for gas adsorption and separation is mainly due to their hollow cylindrical geometry, low mass density and large specific area.[3,4] In many studies, CNTs were compared with other gas sorbents and found to have higher gas adsorption and separation. Lu. *et al.* studied CO_2 capture experimentally and showed that CNTs are better adsorbents in terms of capacity per mass, compared with other sorbent such as zeolites and activated carbon.[5] Diffusivities of light gases (H_2 and CH_4) in carbon nanotubes and zeolites with comparable pore sizes were studied by molecular dynamic simulation. It was found that diffusivity of H_2 and CH_4 in carbon nanotubes is orders of magnitude faster than in zeolites.[6] Using grand canonical Monte Carlo (GCMC) simulation for CO_2 and CH_4 adsorption, Huang *et al*. showed that CNTs have a higher selectivity for CO_2/CH_4 separation than that reported for activated carbons, zeolite 13X and metal organic frameworks (MOFs).[7]

The important role of carbon porosity was revealed by simulated SO_2 adsorption isotherms on activated carbon.[8] This role is more important in the case of CNTs because of their well-defined structure and arrangement. Accordingly, optimizing the geometrical properties like tube diameter and intertube distance has always been a question. Jakobtorweihen *et al*.[9] employed GCMC simulations to investigate the adsorption of linear alkanes and alkenes on CNTs with different tube diameters. Narrower pores were found to have higher adsorption at low pressure ($p < 2$ bar) and lower adsorption at high pressure (2 bar $< p <$ 1000 bar). Kowalczyk and coworkers[10] used GCMC to measure the amount of CO_2 adsorption on CNTs and showed that the optimum diameter for having the highest adsorption depends on the applied pressure. This result was confirmed by a recent study about SO_2 adsorption on CNTs.[11] The same method is used to measure the adsorption of CO_2 and SO_2 molecules on single-walled CNT (SWCNT).[12] The contribution of inner and outer adsorption was studied and it was found out that for both molecules, the inside adsorption is higher at low pressures. The outside adsorption becomes larger above 10 and 2 bar for CO_2 and SO_2, respectively.

In CNTs bundles, the intertube distance is a second geometrical parameter that can be tuned[13] and is also claimed to have an important effect on adsorption.[14,15] Agnihotri *et al*.[16] combined experiment and simulation to analyze the adsorption sites in CNT bundles. They showed that grooves are the most favorable sites. They are completely filled already at very low pressure. In order to measure the adsorption locally, Bienfait and coworkers[17] used neutron diffraction measurement of different gases on CNTs. They also found grooves as the best adsorption sites.

The ideal adsorbed solution theory (IAST) developed by Myers and Prausnitz[18] is a technique to calculate multi-component adsorption equilibria based on single-component adsorption isotherms. The agreement of IAST and GCMC simulation for the adsorption of binary mixtures of $CO_2/CH_4/H_2/N_2$ on various materials, like MOFs and CNTs, was confirmed by various groups.[19–21] Cannon and coworkers[22] used GCMC to study adsorption and selectivity of linear alkanes on closed nanotube bundles. They found that the adsorption of alkane mixture agrees between IAST and simulation. Peng *et al.*[23] showed that the IAST prediction of CO_2 and CH_4 adsorption in ordered carbon nanopipes is in good agreement with experiment. Using molecular simulation and IAST, the selectivity of nanoporous carbon materials for the mixture of CO_2 and H_2 was studied by Kumar and Rodriguez-Reinoso.[24] To investigate the effects of nanopores structure, carbon nanotubes, slit-shaped pore carbon form and a carbon model with disordered pore structure were considered. The results showed that CNTs have the highest selectivity towards CO_2.

Among all the adsorption and separation studies, there are few investigations of SO_2 and its mixture with CO_2. Wang and coworkers[25] used GCMC to calculate SO_2-CO_2 and SO_2-N_2 mixtures in CNT bundles with different tube diameters. They found that among the studied diameters, 1.09 nm and 0.81 nm show the highest selectivity for SO_2-CO_2 and SO_2-N_2 respectively. Furthermore, they showed a decrease of selectivity with increasing temperature. The observations of these authors were still based on bundles of single walled CNTs (SWCNTs) with fixed intertube distance. However, it is not known if such behavior also occurs for double or multi-walled CNT bundles. Moreover, the effect of intertube distance was not investigated. Finally, it would be helpful for experimental studies to know if IAST can be used for the adsorption of SO_2-CO_2 mixture in bundles of CNTs.

In this study, we investigate the adsorption and selectivity of binary mixtures (SO_2-CO_2, CO_2-N_2 and SO_2-N_2) in bundles of double-walled carbon nanotubes (DWCNTs) by the GCMC method. Since the influence of tube diameter has been reported, the intertube distances of DWCNT arrays are varied in order to find the optimum geometry for each adsorption/separation situation. The simulation results are compared with IAST.

5.3 Model and Method

Following our previous works,[14,15,26] the location of DWCNTs in the simulation box are arranged on a hexagonal lattice and periodic boundary conditions are used in all three directions (cf. Figure 1 of ref. 14). In the present study, DWCNTs with a inner tube diameter of $2R$=2.98 nm, which was found to be optimum for single gas adsorption,[26] and a length of 7.38 nm are used. The intertube distance (surface to surface distance) is varied (d = 0 to 2 nm), since it has a

stronger effect compared to the tube diameter, and since its optimum value depends on the applied pressure.[11] The simulation box length in the direction of the CNT axes is equal to CNT length; the simulation box lengths in the other two directions are adjusted to the intertube distance. In total, there are 11760 carbon atoms in the simulation box.

The DWCNTs are considered as rigid structure with a C–C bond length of 0.142 nm. The Lennard-Jones potential as in the AMBER96 force field[27] is used to describe DWCNTs. It has been used also in similar work.[11,28] The EPM2 model of Harris and Yung[29] is used to describe CO_2. In this model, CO_2 is considered as a 3-site rigid molecule with Lennard-Jones potential (σ_{C-C}=0.2757 nm, ε_{C-C}=0.23388 kJ/mol, σ_{O-O}=0.3033 nm, ε_{O-O}=0.66837 kJ/mol) plus a set of partial point charges (q_C=0.6512e), fixed bond length (l_{C-O}=0.1149 nm) and fixed angle (θ_{O-C-O}=180°). Ketko *et al*.[30] developed an optimized intermolecular potential for SO_2 to calculate accurately the vapor-liquid equilibria, critical properties, vapor pressure, and heats of vaporization. This model, which is used in the present study, is described SO_2 with Lennard-Jones interaction and partial charges (σ_{S-S}=0.339 nm, ε_{C-C}=0.61361 kJ/mol, σ_{O-O}=0.305 nm, ε_{O-O}=0.65684 kJ/mol, l_{S-O}=0.1432 nm, θ_{O-S-O}=119.3°). The N_2 molecules are also modeled as a 3-site Lennard-Jones potential plus a set of partial point charges, fixed bond length and fixed angle.[31] Dissimilar non-bonded interactions are calculated using the Lorentz-Berthelot combining rules. The electrostatic interactions are calculated by the smooth-particle-mesh Ewald (SPME) method.[32]

The grand canonical Monte Carlo method at a constant chemical potential μ, volume V and temperature T is used to calculate adsorption and separation coefficient of gases. Three Monte Carlo moves, displace, rotate, insert/delete, with the probability of 0.2, 0.1 and 0.7, respectively are implemented. The temperature is fixed at 303 K and the atomic cutoff is 1 nm. In order to account for the non ideality of gases, the fugacities of the components in the bulk phase is calculated using Peng-Robinson equation of state (PR EOS) for mixtures.[33] For all simulation runs, 1×10^7 Monte Carlo steps are used for equilibration and another 1×10^7 Monte Carlo steps for collection. The output of the simulation is the total number of gas molecules of each component, which is converted to a common unit for adsorption, mmol of gas per gram of adsorbent and is denoted as n_i for the component i. Adsorption selectivity of component i relative to component j in a binary system is calculated by

$$S_{i/j} = \left(\frac{x_i}{y_i}\right)/\left(\frac{x_j}{y_j}\right) \quad (1)$$

where x_i and y_i are the mole fractions of component i in the adsorbed and bulk gas phases, respectively.

The composition of flue gas depends strongly on the type of fuel and the combustion conditions. For instance, the flue gas from coal-fired consists of 7 to 15 % mole CO_2.[34,35] In this work, we use the mole ratio of 5:95, 1:99 and 15:85 in the bulk phase for the binary mixtures of SO_2-CO_2, SO_2-N_2, CO_2-N_2, respectively.[25,36–38]

The ideal adsorbed solution theory (IAST) predicts multi-component equilibria from single-component isotherms.[18] According to IAST, the following equation holds for each component of the studied mixture based on an analogy with Raoult's law:

$$py_i = x_i p_i(\pi) \tag{2}$$

where p is the total pressure in the bulk gas phase, p_i is the bulk pressure of component i that corresponds to the spreading pressure π of the binary mixture; x_i and y_i are have been explained above (equation 1). Since the mole fractions the adsorbed phase sum to one, equation 2 can be written

$$\frac{py_1}{p_1} + \frac{py_2}{p_2} = 1 \tag{3}$$

for each component, p_i and π are related through

$$\frac{\pi A}{RT} = \int_0^{p_i} \frac{n_i(p)}{p} dp \tag{4}$$

where A is the surface area of the adsorbent, R is the universal gas constant, T denotes temperature, and $n_i(p)$ is the amount adsorbed at pressure p.

Levan and Vermeulen used the equations 2-4 and together with the single-component Langmuir isotherms to derive an explicit and thermodynamically consistent binary Langmuir isotherm.[39,40] The adsorption isotherm of each pure component is simulated individually using GCMC. Then it is fitted using the Langmuir isotherm

$$n_i^0 = \frac{n_{i,max}^0 K_i p}{1 + K_i p} \tag{5}$$

where $n_{i,max}^0$ is the monolayer capacity, K_i is the constant in Langmuir isotherm and n_i^0 is the adsorbed amount of component i in a single-component system. The fitted parameters and equations 2-4 are used to calculate the adsorption of component i, n_i, in a binary mixture

$$n_1 = \frac{QP_1^*}{1+P_1^*+P_2^*} + \left(n_{1,max}^0 - n_{2,max}^0\right)\frac{P_1^* P_2^*}{(P_1^*+P_2^*)^2}\ln(1 + P_1^* + P_2^*) \tag{6}$$

$$n_2 = \frac{QP_2^*}{1+P_1^*+P_2^*} + \left(n_{2,max}^0 - n_{1,max}^0\right)\frac{P_1^* P_2^*}{(P_1^*+P_2^*)^2}\ln(1 + P_1^* + P_2^*) \tag{7}$$

The dimensionless parameters, P_i^* is defined as $P_i^* = K_i p_i$, Q is the weighted monolayer capacity and can be calculated by

$$Q = \frac{n_{1,max}^0 P_1^* + n_{2,max}^0 P_2^*}{P_1^* + P_2^*} \quad (8)$$

5.4 Results and Discussion

5.4.1 SO_2 - CO_2 Mixture

Figure 1 shows the adsorption isotherms of a mixture of SO_2 and CO_2 with mole ratio of 5:95 on a bundle of 3-nm diameter DWCNT as a function of the total bulk pressure. For CO_2 (Figure 1-a), the system with d=0.5 nm shows the highest adsorption in the studied pressure range. The reason is the direct relationship between d and adsorption energy, and the inverse relationship between d and accessible volume. The competitive effects of adsorption energy and adsorption space volume cause d=0.5 nm to be the optimum intertube distance for having the maximum adsorption in this pressure range (0.1 bar < p < 2.5 bar). The bulk partial pressure of CO_2 (p_{CO2}) varies with the total pressure of the particle reservoir. It is in the range 0.095 bar to 2.375 bar. The optimum intertube distance, within this partial pressure range, for maximum adsorption amount is similar to that of pure CO_2.[26] For SO_2 (figure 1-b) at low pressure p < 0.5 bar, d=0 has the highest adsorption because there is a strong interaction between SO_2 molecules and CNT walls in the interstitial and groove regions when d=0. Since the partial pressure of SO_2 is very low (0.005 bar < p_{SO2} < 0.025 bar), these regions have enough volume to accommodate the SO_2 molecules. As the pressure increases to ~0.5 bar (partial pressure of SO_2 is ~0.025 bar), the intertube volume is saturated and optimal inertube distance is slightly shifted up to d=0.5 nm. This trend continues to the highest studied pressure in the present work (p=2.5 bar) and CNT arrays with d=0.5 nm have the highest adsorption between 0.5 bar and 2.5 bar. It is expected however, that a further increase of pressure will shift the optimal intertube distance to even higher values as it was seen in earlier works for the adsorption of pure SO_2.[11] Moreover, it was found in the earlier works[11,26] for pure SO_2 system, that the maximum adsorption is achieved for d=0.3[11] and d=0.5[26] nm at low pressure. Our result does not contradict these foundings since the lowest pressure studied in the former studies was p_{SO2}~0.1 bar, but not the very low pressure region (0.005 bar < p_{SO2} < 0.125 bar) of this work. Furthermore, our results confirm the previous foundings that the optimum intertube distance depends on the applied pressure and the optimum d is shifts to higher values with increasing pressure.[11]

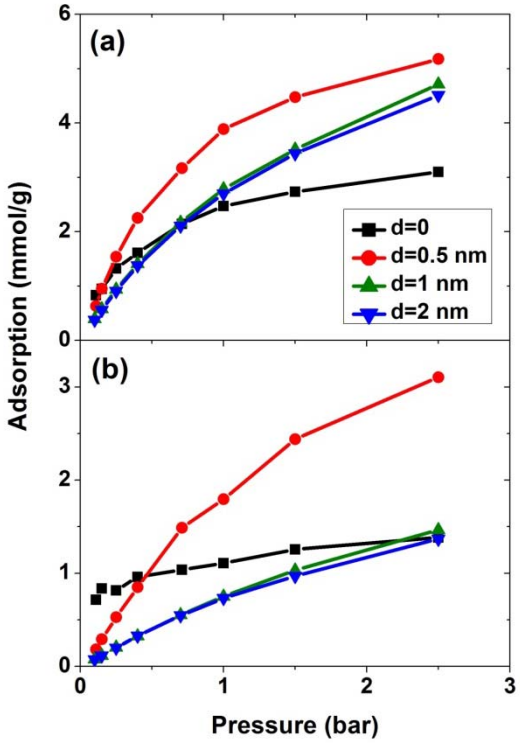

Figure 1. Excess adsorption isotherms of a) SO_2 and b) CO_2 in SO_2-CO_2 (5:95) binary mixture system on double-walled carbon nanotube arrays, with inner tube diameter $2R$=3 nm and intertube distance d=0-2 nm. T= 303 K. Pressure refers to the total pressure of the SO_2-CO_2 mixture.

As expected, for all cases CO_2 has a higher adsorption than SO_2 due to its higher bulk concentration (95 mol %). However, the selectivity of SO_2 over CO_2 shows a non-uniform behavior (figure 2). When d=0, the system shows the highest selectivity ($S_{SO2/CO2}$=16) at very low pressure, since molecules perfectly fit to the narrow intertube pores of DWCNTs. Increasing the pressure to p=0.7 bar, leads to a decrease of the selectivity to around 8. With further increase of the pressure, the selectivity remains almost constant ($S_{SO2/CO2} \sim 8$). The situation for the intertube distance of d=0.5 nm is almost reversed. The selectivity increases strongly with pressure up to p=0.7 bar, then it continues increasing but very smoothly. As a result, the two curves cross at p~0.8 bar. The two systems with d=1 nm and 2 nm show qualitatively behavior similar to d=0.5 nm. The selectivity increases smoothly over the whole studied pressure region. However, the selectivity does not exceed 6. Consequently, at lower pressure (p < 0.8 bar) d=0 has the highest selectivity, while the highest selectivity at higher pressure (0.8 bar < p < 2.5 bar) is found for the system with d=0.5 nm. The selectivity found by Wang *et a.l*[25] for SWCNTs with similar inner diameter ($2R$=2.71 nm) varies from ~10 to ~20 at different pressure and it is obviously higher than that found in the present study for DWCNTs. This is most likely due to the higher outer diameter of our DWCNTs ($2R_{out}$=3.66 nm) and consequently, their larger intertube volume which leads to a decrease in adsorption energy. Besides, it was also reported that for the

case of single-component systems, SWCNTs show higher adsorption than DWCNTs.[41] However, SWCNTs are still expensive and difficult to synthesis.[42] Moreover, the selectivity value is found to range from 4 to 16, indicating optimizing pore size can increase the selectivity 4 times. Thus DWCNTs are still attractive from an application view point.

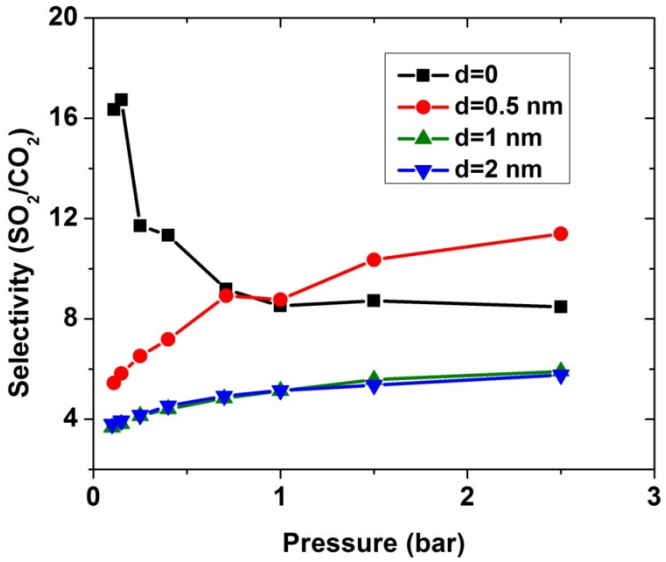

Figure 2. Selectivity of SO_2 over CO_2, computed from GCMC method, in SO_2-CO_2 (5:95) binary mixture on double-walled carbon nanotube arrays, with inner tube diameter $2R$=3 nm and intertube distance d=0-2 nm. T = 303 K.

At low pressure, CO_2 and SO_2 may adsorb separately without interfering with each other.[43] In order to verify this assertion, separate simulations are performed for pure SO_2 and CO_2 with the pressure the same as the partial pressure in the binary mixture. Figure 3 shows the SO_2 and CO_2 adsorption as a function of their partial pressure in three different situations: single-component system, binary system and IAST prediction. When d=0, the IAST prediction does not agree with the simulation data neither for CO_2 nor for SO_2. It means that in the adsorbed phase SO_2-CO_2, the molecules do not behave as ideal mixture because of their density in the low intertube space volume of this geometry. The GCMC results show higher SO_2 adsorption and lower CO_2 adsorption than IAST prediction, reflecting the high selectivity for SO_2 of this system (figure 2). Furthermore, the adsorption of single gases deviate markedly from the adsorption of each component in the binary mixture. Thus, the assumption that each gas is adsorbed separately without interfering with the other, is evidently not true in the CNT arrays with d=0. There are also deviations between IAST predictions and the GCMC adsorption isotherms of single gases because the IAST predicts that each component occupies a certain amount of volume and as a result, the accessible volume in the IAST prediction for the other component is less than for single gas systems. With increasing intertube distance, IAST predictions for the adsorption

isotherms move closer to the simulation results, so that for d=2 nm, the difference between adsorbed amounts predicted by IAST and simulation is less than 5 % for CO_2 at p_{CO2}=2.375 bar and also for SO_2 at p_{SO2}=0.125 bar. This is due to the reduction of the gas density with increasing intertube distance. Adsorption isotherms of binary system and that of single-component systems show the same trend with increasing d. For instance, at p_{CO2}=0.66 bar, the deviations between adsorption of CO_2 in the binary system and single-component system are 13%, 8% and 7% for d=0.5 nm, 1 nm and 2 nm, respectively. Moreover, for d > 0, there is only a small deviation between the adsorption isotherms of binary system and that of single-component system at low pressure (e. g. for CO_2, d=2 nm, at p_{CO2}=0.38 bar the deviations is ~5%). Increasing the pressure enhances the deviation so that for d=2 nm, at p_{CO2}=2.375 bar, the difference between adsorption in binary system and single-component system is ~13%. It means that, at very low pressure, the two gases behave independently. However, at higher pressure, each gas occupies a considerable amount of volume and reduces the accessible volume for the other one and hence, the presence of one gas has a detrimental effect on the adsorption of the other.

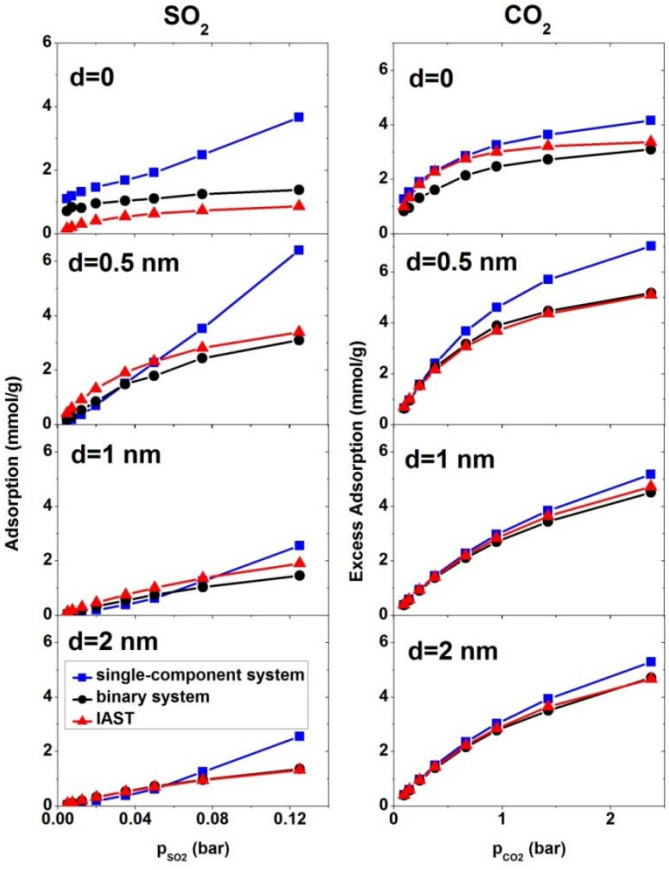

Figure 3. Comparison of different methods in calculating the adsorption of SO_2 (left column) and CO_2 (right column) in a binary mixture system on double-walled carbon nanotube arrays, with inner tube diameter 2R=3 nm and intertube distance d=0-2 nm. T= 303 K.

Figure 4 represents the density profile of CO_2 and SO_2 in systems with different d and p. The density profile inside the CNT is indifferent to d, as has been observed before for pure CO_2 and SO_2 adsorption.[14,11] In all systems, a layer of CO_2 and SO_2 forms at low pressure (p=0.4 bar). This layer grows in density with increasing the pressure. Outside the CNT when d=0, the density of SO_2 is higher than that of CO_2 at low pressure. As the pressure increases, the density of SO_2 remains almost the same but the density of CO_2 increases, confirming what has been observed for selectivity in figure 2. The reduction in selectivity is owed to the outer intertube volume being small and SO_2 being a large molecule. Therefore, the intertube volume saturates soon. The CO_2 molecules are smaller and they can fit themselves in the remaining space. For d=0.5 nm, the density of both CO_2 and SO_2 increases with pressure. The increase is larger for in SO_2 than for CO_2, because the intertube space is larger, and SO_2 molecules interact strongly with CNT carbon molecules than CO_2. A similar behavior is observed for the case of d=1 nm.

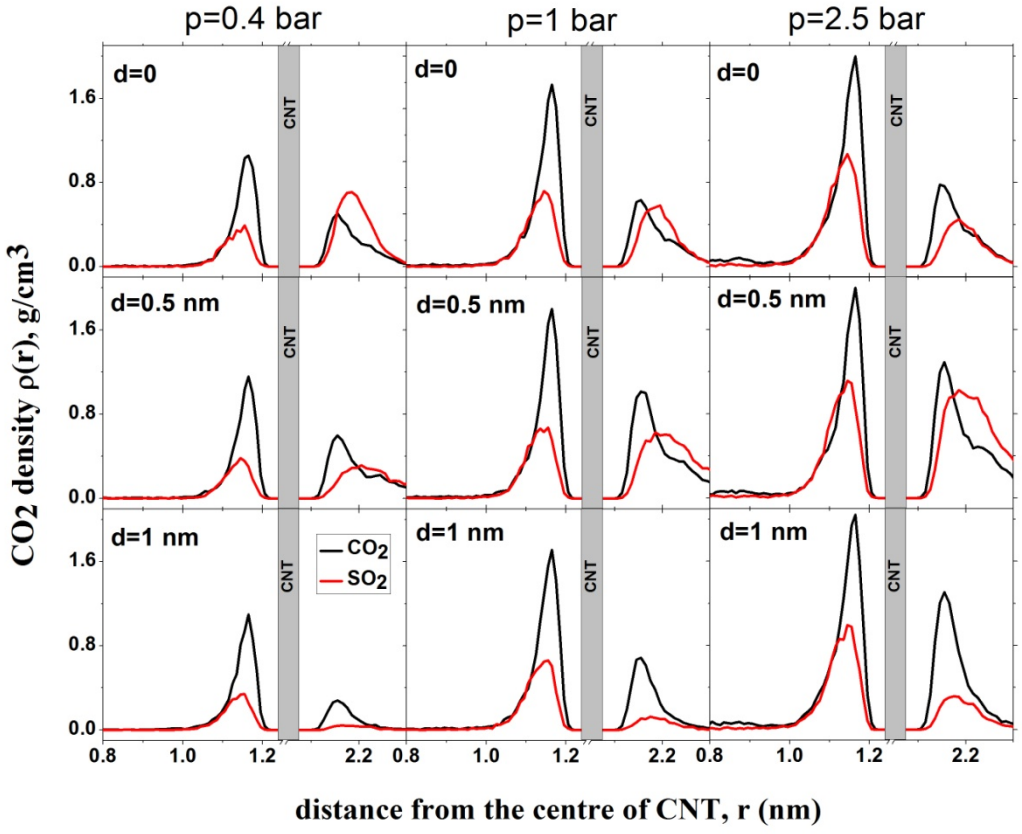

Figure 4. Density profile for SO_2 (red) and CO_2 (black) adsorption in a binary mixture (5:95) on double-walled carbon nanotube, with tube radius 2R=3 nm and intertube distance d=0-1 nm, at fixed pressure (p=0.4, 1 bar and p=2.5 bar, left to right). T = 300 K.

5.4.2 SO_2 - N_2 Mixture

Figure 5 presents SO_2 and N_2 adsorption isotherms in SO_2-N_2 (1:99) system. When d=0, a remarkable increase of SO_2 in adsorption can be seen until p~0.4 bar. Beyond, the adsorption approaches saturation with a lower rate. Increasing d leads to a drastic reduction in SO_2 adsorption and, hence, d=0 has the highest adsorption in the studied pressure region. This due to the strong interaction between SO_2 molecules and CNTs walls in the intertube space and also very low partial pressure of SO_2 (p_{SO2} < 0.025 bar) which causes the limited intertube space to be large enough to accommodate the few SO_2 molecules. This result is in line with SO_2 adsorption isotherms in SO_2-CO_2 system (figure 1), where d=0, also has the maximum adsorption at low partial pressure (p_{SO2} < 0.025 bar).

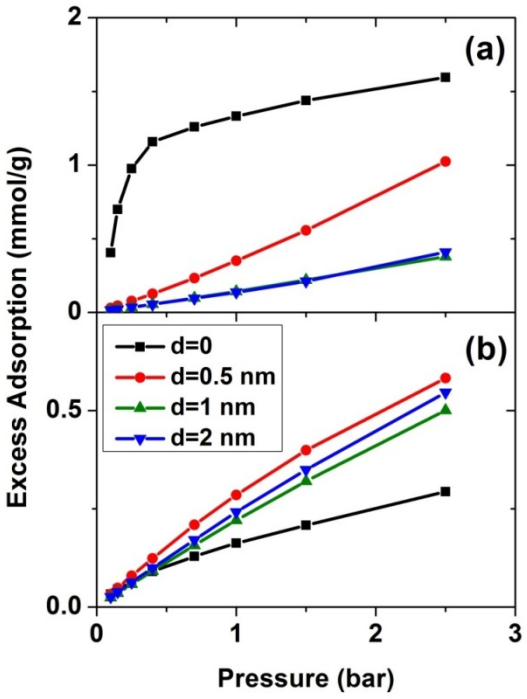

Figure 5. Excess adsorption isotherms of a) SO_2 and b) N_2 in a binary mixture (1:99) on double-walled carbon nanotube arrays, with inner tube diameter 2R=3 nm and intertube distance d=0-2 nm. T= 303 K.

In the case of N_2 adsorption, d=0 shows the lowest adsorption because most of the available volume, especially in the groove and interstitial regions, is filled with SO_2 molecules which have stronger interaction with CNTs. However, N_2 adsorption increases uniformly with pressure since N_2 molecules are smaller than SO_2 and they fit in the accessible space between SO_2 molecules. Increasing the intertube distance slightly to 0.5 nm has two important consequences. Firstly, the intertube volume increases and secondly, the density of SO_2 molecules decreases. As a result, there is more space accessible for N_2 molecules. Therefore, N_2 adsorption is notably higher at

d=0.5 nm than *d*=0. Further increase in the intertube distance, reduces the interaction between N_2 molecules and DWCNT carbons which causes a decrease in adsorption of N_2.

The adsorption for N_2 is generally less than for SO_2 in all systems, although the bulk concentration of N_2 is much higher than SO_2. To investigate the reason we calculate the minimum energy of one single SO_2, CO_2 and N_2 molecule inside the CNT. For this purpose the probability of the Monte Carlo moves, displace, rotate, insert/delete, is changed to 0.7, 0.3 and 0.0, respectively and the simulation is carried out at low temperature (5 K). The minimum adsorption energies are -13 kJ/mol, -22.6 kJ/mol and -27.4 kJ/mol for one N_2, CO_2 and SO_2 molecule, respectively. Thus, the observed selectivity for SO_2 (figure 6) is mainly caused by the interaction of individual molecules with the CNT. The selectivity for the system with *d*=0 increases initially with pressure, reaching a maximum of more than 1600 at *p*=0.25 bar. Further increase in pressure leads to a decrease in selectivity, but at *p*=2.5 bar it is still ~400. This is due to the fact that SO_2 is a large molecule with a strong interaction with CNT. Therefore, SO_2 molecules fill the intertube space soon at low pressure (p < 0.4 bar) and saturate the system. On the other hand, the small N_2 molecules can be accommodated between SO_2 molecules and thus, N_2 adsorption shows a monotonic increase as a function of pressure. The selectivities of the other systems are almost constant ($S_{SO2/N2}$ ~100, ~55, ~45 for d=0.5 nm, 1 nm and 2 nm, respectively) in the studied pressure region.

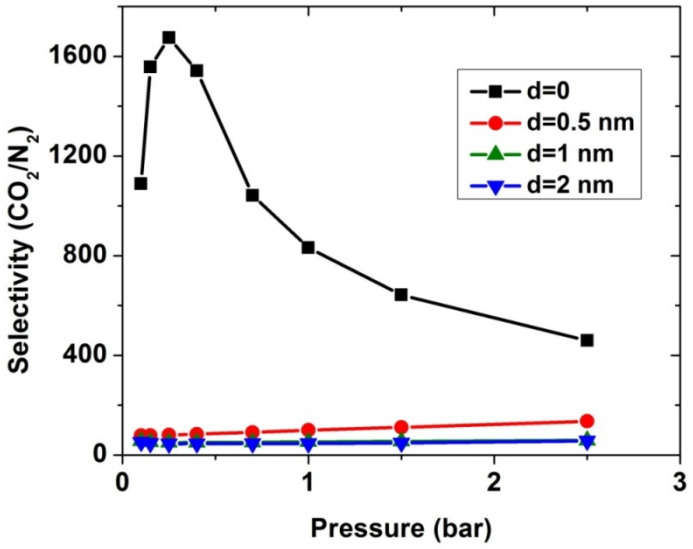

Figure 6. Selectivity of SO_2 over N_2, computed from GCMC simulations, in a binary mixture (1:99) on double-walled carbon nanotube arrays, with inner tube diameter 2*R*=3 nm and intertube distance *d*=0-2 nm. *T* = 303 K.

A comparison between GCMC simulation and IAST prediction in SO_2-N_2 system is shown in figure 7. As for the SO_2-CO_2 system, IAST cannot predict the adsorption very well for *d*=0.

Because of the high density in the intertube space, the behavior of the gases is far from the ideal. For lager *d*, the gas density decreases and as a consequence the IAST predictions becomes more similar to the adsorption calculated by simulation. Furthermore, the IAST predictions and GCMC results of the SO_2-N_2 mixture agree better than that of the SO_2-CO_2 mixture because of the weaker interaction of N_2 with either SO_2 or CNT carbons than that of CO_2.

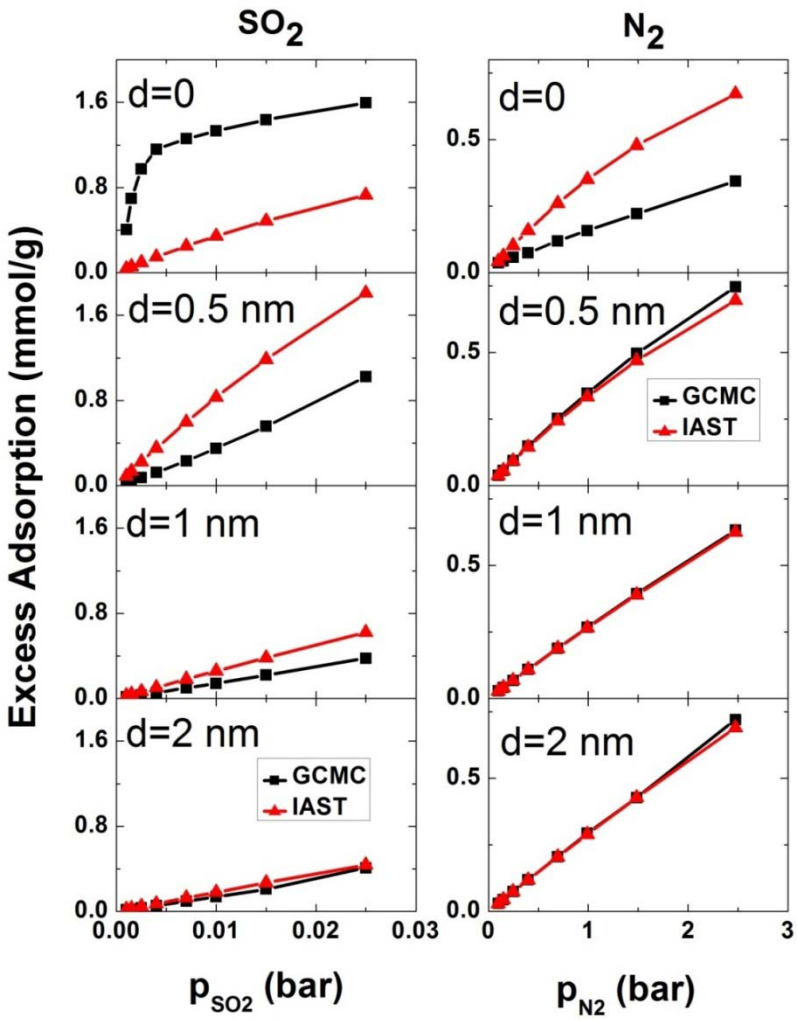

Figure 7. Comparison of excess adsorption data from IAST and GCMC simulations: SO_2 (left column) and N_2 (right column) in a binary mixture (1:99) on double-walled carbon nanotube arrays, with inner tube diameter 2*R*=3 nm and intertube distance *d*=0-2 nm. *T* = 303 K.

5.4.3 CO_2 - N_2 Mixture

Figure 8 shows the CO_2-N_2 (15:85) adsorption calculated by the GCMC method and IAST predictions. When *d*=0, there is an obvious deviation between IAST predictions and GCMC simulation but it is much less than what is observed in SO_2-CO_2 and SO_2-N_2 mixtures. Like the previous mixtures, in the systems with $d > 0$, the deviation between IAST and GCMC is less than

that of d=0. At p=2.5 bar, the maximum deviation is less than 7% and 3% for CO_2 and N_2 respectively. In short, IAST can predict CO_2-N_2 mixture better that SO_2-CO_2 and SO_2-N_2 mixtures. This result is in line with previous works.[19,21]

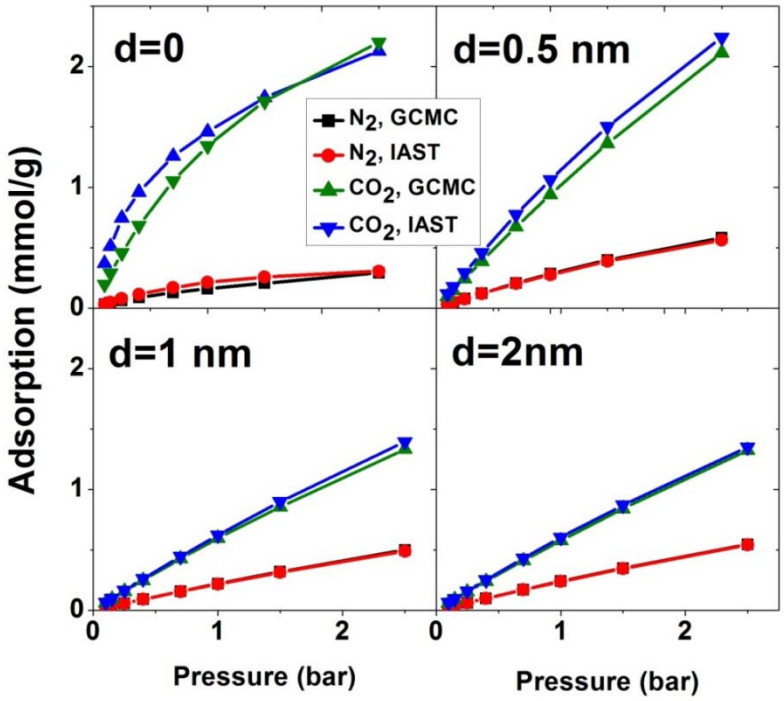

Figure 8. Excess adsorption isotherms of CO_2 and N_2 in a binary mixture system on double-walled carbon nanotube arrays, with inner tube diameter 2R=3 nm and intertube distance a) d=0, b) d=0.5 nm, c) d=1 nm and d) d=2 nm. T = 303 K.

Similar to SO_2-N_2 mixture, in all 4 CNT arrays, CO_2 shows higher adsorption than N_2 although in the bulk, there is more N_2 than CO_2. This is due to the stronger interaction between CO_2 and CNT (cf. Section 3.2). Moreover, d=0 shows the highest difference between the N_2 and CO_2 adsorption. The selectivity highlights this difference (Figure 9). The system with d=0 has the highest selectivity due to the strong interaction between CO_2 molecules and CNT carbons in the intertube space. With increasing pressure, the limited adsorption space in this region causes the selectivity to decrease from around 70 to around 40 at p=2.5 bar, which is still high. Unlike for d=0, an increase in the pressure enhances the selectivity of CNTs with d=0.5 nm. Nevertheless, the selectivity of this system is much lower (~20) than that with d=0. For larger d, the system shows an almost constant selectivity (~15 and ~13 for d=1 nm and 2 nm, respectively) in the studied pressure range and it is lower than for the two shorter intertube distances. Moreover, the observed selectivity of CO_2 over N_2 for an optimized DWCNTs is higher than what has been reported for zeolites (between ~10 and ~30 depends on the type of zeolites and the pressure) and MOFs (between ~5 and ~40 depends on the type of MOFs and the pressure).[36,44]

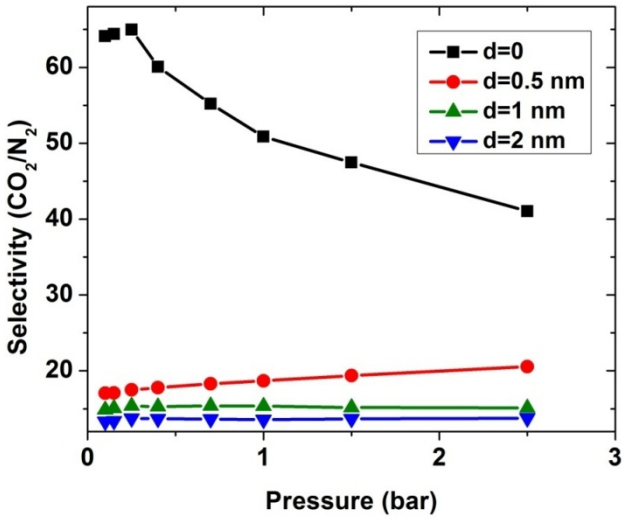

Figure 9. Selectivity of CO_2 over N_2 (15:85), computed from GCMC method, in a binary mixture system on double-walled carbon nanotube arrays, with inner tube diameter $2R$=3 nm and intertube distance d=0-2 nm. T = 303 K.

5.5 Conclusion

In this work, we used grand-canonical Monte Carlo simulation to study the adsorption and separation properties of aligned DWCNTs against flue gas mixture components (e.g. SO_2, CO_2, N_2) at 303 K. Bundles of DWCNT with a constant inner diameter of $2R$=3 nm but different intertube distances of d=0-2 nm were studied.

The quantity and quality of the selectivity for each system depend on the type of adsorbate molecules and also on the adsorbent structure. For SO_2-CO_2 mixtures, the adsorption of CO_2 and SO_2 is characterized by non-linear behavior as a function of intertube distance. As a result, at low pressures p < 0.8 bar, bundles whose tubes touch each other (d=0) show the highest selectivity towards SO_2. For higher pressures, bundles with a finite but short intertube distance (d=0.5 nm) show the highest selectivity. For SO_2-N_2 and CO_2-N_2 on the other hand, no such pressure dependence is found and close-packed CNT bundles (d=0) have the maximum selectivity towards SO_2 and CO_2 respectively over the whole studied pressure range. The selectivity relates directly to the difference in the strength of interaction between each component and CNT. The highest difference and consequently, the highest selectivity is observed between SO_2 and N_2, followed by CO_2 and N_2 and finally SO_2 and CO_2. The lowest and highest observed selectivities are 4 and 16 for SO_2-CO_2, 50 and 1600 for SO_2-N_2, and 10 and 70 for CO_2-N_2, respectively. These results indicate that first, DWCNTs are excellent materials for gas purification and second, optimizing the pore structure is very important to achieve the highest selectivity. Fortunately, close-packed bundles are easy to obtain[45] and show the highest selectivity in most cases.

The IAST predictions failed in predicting the adsorption for mixtures involving SO_2, in particular when *d*=0. Increasing *d* reduces the deviation between IAST and GCMC in SO_2-CO_2 and SO_2-N_2 binary mixtures. Nevertheless, the results are still not in agreement, indicating that IAST is not suitable for the systems containing SO_2. In the case of CO_2-N_2, the IAST and GCMC are in good agreement and like the two other systems, as *d* increases, the deviation between GCMC and IAST reduces.

5.6 Acknowledgements

MR would like to thank Sadanandam Namsani for valuable comments and discussion. JKS thanks the Alexander von Humboldt foundation and the Ministry of Earth Sciences, GOI, for financial support. This work was supported by the Priority Programme 1570 *Porous media with well-defined pore structure in chemical engineering: Modeling, application, synthesis* of Deutsche Forschungsgemeinschaft.

References

1 F. L. Darkrim, P. Malbrunot and G. P. Tartaglia, *Int. J. Hydrogen Energy*, 2002, **27**, 193–202.

2 J. Zhao, A. Buldum, J. Han and J. P. Lu, *Nanotechnology*, 2002, **13**, 195–200.

3 X. Ren, C. Chen, M. Nagatsu and X. Wang, *Chem. Eng. J.*, 2011, **170**, 395–410.

4 M. J. O'Connell, *Carbon Nanotubes: Properties and Applications*, CRC Taylor & Francis, Boca Raton, FL, 2006.

5 C. Lu, H. Bai, B. Wu, F. Su and J. F. Hwang, *Energy & Fuels*, 2008, **22**, 3050–3056.

6 A. I. Skoulidas, D. M. Ackerman, J. K. Johnson and D. S. Sholl, *Phys. Rev. Lett.*, 2002, **89**, 185901.

7 L. Huang, L. Zhang, Q. Shao, L. Lu, X. Lu, S. Jiang and W. Shen, *J. Phys. Chem. C*, 2007, **111**, 11912–11920.

8 S. Furmaniak, A. P. Terzyk, P. A. Gauden, P. Kowalczyk and G. S. Szymański, *Chem. Phys. Lett.*, 2013, **578**, 85–91.

9 S. Jakobtorweihen and F. J. Keil, *Mol. Simul.*, 2009, **35**, 90–99.

10 P. Kowalczyk, S. Furmaniak, P. a. Gauden and A. P. Terzyk, *J. Phys. Chem. C*, 2010, **114**, 21465–21473.

11 Y. Yang, M. Rahimi, J. K. Singh, M. C. Böhm and F. Müller-Plathe, *J. Phys. Chem. C*. (submitted)

12 Z. Nickmand, S. F. Aghamiri, M. R. Talaie Khozanie and H. Sabzyan, *Sep. Sci. Technol.*, 2014, **49**, 499–505.

13 D. N. Futaba, K. Hata, T. Yamada, T. Hiraoka, Y. Hayamizu, Y. Kakudate, O. Tanaike, H. Hatori, M. Yumura and S. Iijima, *Nat. Mater.*, 2006, **5**, 987–94.

14 M. Rahimi, J. K. Singh, D. J. Babu, J. J. Schneider and F. Müller-Plathe, *J. Phys. Chem. C*, 2013, **117**, 13492–13501.

15 M. Rahimi, J. K. Singh and F. Müller-Plathe, *J. Phys. Chem. C*, 2015, **119**, 15232–15239.

16 S. Agnihotri, J. P. B. Mota, M. Rostam-Abadi and M. J. Rood, *Carbon* , 2006, **44**, 2376–2383.

17 M. Bienfait, P. Zeppenfeld, N. Dupont-Pavlovsky, M. Muris, M. Johnson, T. Wilson, M. DePies and O. Vilches, *Phys. Rev. B*, 2004, **70**, 035410.

18 A. L. Myers and J. M. Prausnitz, *AIChE J.*, 1965, **11**, 121–127.

19 X. Peng, X. Cheng and D. Cao, *J. Mater. Chem.*, 2011, **21**, 11259–11270.

20 R. Babarao, Z. Hu, J. Jiang, S. Chempath and S. I. Sandler, *Langmuir*, 2007, **23**, 659–66.

21 P. Kowalczyk, *Phys. Chem. Chem. Phys.*, 2012, **14**, 2784–90.

22 J. J. Cannon, T. J. H. Vlugt, D. Dubbeldam, S. Maruyama and J. Shiomi, *J. Phys. Chem. B*, 2012, **116**, 9812–9.

23 X. Peng, D. Cao and W. Wang, *Chem. Eng. Sci.*, 2011, **66**, 2266–2276.

24 K. Vasanth Kumar and F. Rodríguez-Reinoso, *RSC Adv.*, 2012, **2**, 9671.

25 W. Wang, X. Peng and D. Cao, *Environ. Sci. Technol.*, 2011, **45**, 4832–8.

26 M. Rahimi, D. J. Babu, J. K. Singh, Y.-B. Yang, J. J. Schneider and F. Müller-Plathe, *J. Chem. Phys.*, 2015, 143, 124701.

27 W. D. Cornell, P. Cieplak, C. I. Bayly, I. R. Gould, K. M. Merz, D. M. Ferguson, D. C. Spellmeyer, T. Fox, J. W. Caldwell and P. A. Kollman, *J. Am. Chem. Soc.*, 1995, **117**, 5179–5197.

28 G. Hummer, J. C. Rasaiah and J. P. Noworyta, *Nature*, 2001, **414**, 188–90.

29 J. G. Harris and K. H. Yung, *J. Phys. Chem.*, 1995, 12021–12024.

30 M. H. Ketko, G. Kamath and J. J. Potoff, *J. Phys. Chem. B*, 2011, **115**, 4949–4954.

31 J.-C. Neyt, A. Wender, V. Lachet and P. Malfreyt, *J. Phys. Chem. B*, 2011, **115**, 9421–9430.

32 U. Essmann, L. Perera, M. L. Berkowitz, T. Darden, H. Lee and L. G. Pedersen, *J. Chem. Phys.*, 1995, **103**, 8577.

33 D.-Y. Peng and D. B. Robinson, *Ind. Eng. Chem. Fundam.*, 1976, **15**, 59–64.

34 P. Wattanaphan, T. Sema, R. Idem, Z. Liang and P. Tontiwachwuthikul, *Int. J. Greenh. Gas Control*, 2013, **19**, 340–349.

35 A. Chakma, *Energy Convers. Manag.*, 1995, **36**, 427–430.

36 B. Liu and B. Smit, *J. Phys. Chem. C*, 2010, **114**, 8515–8522.

37 W. Sun, L.-C. Lin, X. Peng and B. Smit, *AIChE J.*, 2014, **60**, 2314–2323.

38 X. Xu, C. Song, R. Wincek, J. M. Andresen, B. G. Miller and A. W. Scaroni, *Fuel Chem. Div. Prepr.*, 2003, **48**, 162–163.

39 M. D. LeVan and T. Vermeulen, *J. Phys. Chem.*, 1981, **85**, 3247–3250.

40 A. Sharma, S. Namsani and J. K. Singh, *Mol. Simul.*, 2014, **41**, 414–422.

41 D. D. Do, H. D. Do, A. Wongkoblap and D. Nicholson, *Phys. Chem. Chem. Phys.*, 2008, **10**, 7293–303.

42 A. Aqel, K. M. M. A. El-Nour, R. A. A. Ammar and A. Al-Warthan, *Arab. J. Chem.*, 2012, **5**, 1–23.

43 P. Kowalczyk, *Phys. Chem. Chem. Phys.*, 2012, **14**, 2784–90.

44 B. Liu and B. Smit, *Langmuir*, 2009, **25**, 5918–26.

45 D. J. Babu, M. Lange, G. Cherkashinin, A. Issanin, R. Staudt and J. J. Schneider, *Carbon*, 2013, **61**, 616–623.

6 Conclusion and Outlook

In this work, we used grand-canonical Monte Carlo simulations to understand the adsorption and separation of CO_2 and SO_2 onto ordered carbon nanotube arrays. The geometrical properties of the CNT arrays, *i.e.* tube diameter and intertube distance, as well as structural properties such as chirality were considered in order to maximize the sorption capacity of the material. We also investigated how the adsorption changes when the CNT arrays are positively or negatively charged, as electrically contacted CNT arrays are a possible functional material for electric swing adsorption devices.

Partial adsorption isotherms of CO_2, *i.e*. only inner tube volume, only interstices between tubes, and unrestricted, were calculated in order to analyze the experimental results and study the contributions of different regions. It was shown that more than 40% of the CNTs in the experiment were closed. Beside, the unrestricted adsorption isotherm was found to be quantitatively equivalent to the sum of inner and outer adsorption, indicating no significant interference between inner and outer regions.

For a fixed tube diameter, the intertube distance dramatically affects the adsorption capacity because changing the intertube distance changes the mechanism of adsorption. As the loading increases, the adsorption procedure for $d \leq 0.5$ nm is as follows: grooves and inner surface adsorption→ fill interstitial region→ fill inner region. At higher distances, $d > 0.5$ nm, the sequence changes to: inner surface adsorption + partial outer surface adsorption→ complete outer surface adsorption→ fill interstitial, groove, inner adsorption. This change in the mechanism of adsorption is clearly reflected in the behavior of the heat of adsorption and adsorption isotherms. As a result, excess adsorption displays a non-linear behavior with *d*. Decreasing the intertube distance up to 1 nm can increase the adsorption up to ~40% depending on the system and pressure. This is in agreement with the experimental results and shows the importance of optimizing intertube distance to maximize the adsorption. Further diminution in *d,* leads to opposite effect in low and high pressure. So that, for high pressure, further reduction in *d*, decreases the adsorption, while for low pressures, the adsorption continues increasing with decreasing the intertube distance down to 0.5 nm. Thus, for low pressure, the highest adsorption occurs at d=0.5 nm. Changing the tube diameter does not change this trend.

For a fixed intertube distance at d=0.5 nm and $p < 4$ bar, the excess adsorption of the CNT with the tube diameter of 1 nm is slightly more than that of 3 nm-diameter CNT (the maximum difference is 0.4 mmol/g at p=1.5 bar). Hence, in this pressure range the CNT with the diameter of 1 nm has the highest adsorption. With increasing the pressure, the optimum tube diameter to

achieve the highest adsorption shifts up to 3 nm. Further increase in the inner diameter decreases the excess adsorption marginally. Moreover, the role of the intertube distance ismore important than that of the CNT diameter.

For the adsorption of SO_2, the effect of intertube distance is similar to that observed for CO_2. However, the pressure that the optimum intertube distance shifts to higher value is much lower (~0.5 bar). In other words, at $p < 0.5$ bar, the highest amount of adsorption belongs to the CNTs with d=0.5 nm, while at $p > 0.5$ bar, it is the CNT with d=1 nm which shows the highest adsorption. Furthermore, similar to the CO_2 results, it was found that diameter has much less effect on the adsorption behavior as compared to the intertube distance.

The adsorption and orientational ordering of CO_2 molecules on parallel bundles of charged as well as uncharged carbon nanotubes were investigated. In order to observe the charge effect, a fixed charge of 0.02 *e* was placed on each carbon atom of the CNTs. The results show that having positive charge on CNTs, increases the adsorption significantly (up to 15% at a pressure of 1.88 bar), while a negative charge causes the adsorption to decrease, compared to neutral CNT arrays. Furthermore, the tube chirality does not play any role in the adsorption in both charged and uncharged states. Charging the nanotubes, changes the potential energy for the interaction between the individual CO_2 molecule and the nanotube and leads to the increase or decrease of adsorption.

The structure of the adsorbed layers at different pressures and charge states were studied. We found that the higher adsorption on positively charged nanotubes leads to thicker adsorbed layers, followed by neutral CNTs and finally negatively charged CNT. The difference in thickness of the layers causes different orientational order of the adsorbed molecules, so that the positively charged nanotubes have the most orientational disorder among the adsorbed CO_2 molecules. At constant pressure of 1.88 bar, charging the CNT positively to a charge per carbon atom of +0.04 *e*, increases the excess adsorption by one third, while charging it negatively to q = –0.04 *e* reduces it by about 1/6. This indicates that CNTs can be used as a functional material for electric swing adsorption and that rapid adsorption and desorption of CO_2 could technically be driven by applying and removing electrical charges on the sorbent.

We have also investigated the separation properties of bundles of CNTs against flue gas mixture components (e.g. SO_2, CO_2, N_2). Various intertube distances were used and the results confirm the key role of intertube distance in selectivity as well. For SO_2-CO_2 binary system, CNTs with d=0 show the highest selectivity towards SO_2 at $p < 0.8$ bar, while the maximum selectivity belongs to the CNTs with d=0.5 nm at 0.8 bar < p < 2.5 bar. For SO_2-N_2 and CO_2-N_2 binary mixtures, close-packed CNT bundles (d=0) show the highest selectivity towards SO_2 and CO_2 respectively, in

studied pressure range. The lowest and highest observed selectivities are 4 and 16 for SO_2-CO_2, 50 and 1600 for SO_2-N_2, and 10 and 70 for CO_2-N_2, respectively, indicating that optimizing the pore structure is very important to achieve the highest selectivity. Moreover, they confirm that DWCNTs are excellent materials for gas purification.

The IAST predictions failed in predicting the adsorption of the systems containing SO_2, especially for lower *d.* With increasing *d*, the deviation between IAST and GCMC reduces, however the results are still not in coincidence. In the case of CO_2-N_2, simulations and ideal adsorbed solution theory are in good agreement when $d > 0$.

CO_2 and SO_2 are not the only harmful gases which should be removed from flue gases. Hence, it would also be interesting to study adsorption and separation behavior of bundles of CNTs among other gases like CH_4, H_2S, NO_2, NH_3, *etc*. The investigations of the adsorption of mixed fluids can be continued, but in the presence of water, since water is always one of the components of flue gases. Thus, interference or noninterference of humidity on the adsorption of gases can be observed. Using simulations as a prescreening method the experiments can be focused on pressure and temperature regimes of particular interest.

One may think to examine the adsorption of gases like SO_2 and H_2S on charged CNTs, since having charge on CNTs are more effective for the gases with dipole moment. Furthermore, simulation of chemically modified CNT arrays is of great interest. Simulations can be targeted at modified CNT arrays (oxidation products, surface groups, defects) in order to elucidate their role in gas adsorption. Calculations will therefore fall in the concluding phase of the project and might well extend beyond its end.

Mahshid Rahimi

Ingelheimerstrasse 1

64295 Darmstadt

Erklärung

Ich erkläre hiermit, dass ich meine Dessertation selbstständig und nur mit den angegebenen Hilfsmitteln angefertigt habe.

Kapitel vier meiner Thesis ist aus einer Zusammenarbeit mit der Arbeitsgruppe von Prof. J. J. Schneider (Eduard-Zintl-Institut für Anorganische Chemie, Technische Universität Darmstadt) entstanden. Die experimentellen Daten wurden von Deepu J. Babu, einem Doktorranden aus der Arbeitsgruppe von Prof. J. J. Schneider, aufgezeichnet, worauf hiermit ausdrücklich hingewiesen wird.

Darmstadt, den 6. November 2015

Mahshid Rahimi

Mahshid Rahimi

Ingelheimerstrasse 1

64295 Darmstadt

Erklärung

Ich erkläre hiermit, noch keine Promotionsversuch unternohmen zu haben.

Darmstadt, den 6. November 2015

Mahshid Rahimi